N78-29503

COLLEGE OF ENGINEERING

VPI-E-78-14 July, 1978

Theoretical-Experimental Correlation for Buckling of Composite Cylinders under Combined Compression and Torsion

by

Carl T. Herakovich

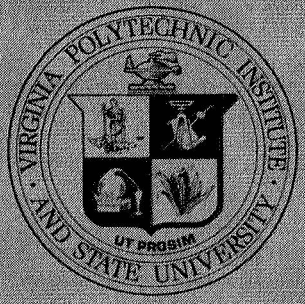

VIRGINIA POLYTECHNIC INSTITUTE AND STATE UNIVERSITY
BLACKSBURG, VIRGINIA

College of Engineering
Virginia Polytechnic Institute and State University
Blacksburg, VA. 24061

VPI-E-78-14 July, 1978

Theoretical-Experimental Correlation for Buckling of Composite Cylinders under Combined Compression and Torsion

by

Carl T. Herakovich

Department of Engineering Science and Mechanics

Final Report - NASA Contract NAS1-13175 Task Auth. #17

Prepared for: Materials Application Branch
National Aeronautics & Space Administration
Langley Research Center
Hampton, VA. 23665

FOREWORD

This report documents the work which was performed under NASA Contract NAS1-13175 Task Authorization #17 during the period January 1, 1976 through June 30, 1978. VPI&SU personnel who made significant contributions to this work include:

Mr. David A. O'Brien	Dr. Peter W. Hsu
Mr. Gary L. Farley	Mr. David A. Danello
Mr. Willard L. Unkenholz	Mr. George G. Lough
Mr. Paul R. Frosell, Jr.	Ms. Frances Carter

Some of the test results were obtained at Langley Research Center by Mr. H. Benson Dexter with assistance from Mr. James J. Kiss. Mr. Dexter also served as the NASA contract monitor.

ABSTRACT

Comparisons between theory and experiment for buckling of laminated graphite-epoxy and boron-epoxy cylinders under combined compression and torsion are presented. The experimental results are compared to a theory by Wu. It is shown that there is excellent agreement between theory and experiment for pure torsional loading (positive and negative), experimental buckling loads for pure compression are well below the predicted values, and good correlation is exhibited between theory and experiment for buckling under combined loading when compared in the form of normalized buckling interaction diagrams in axial-torsional load space.

TABLE OF CONTENTS

LIST OF TABLES

LIST OF FIGURES

LIST OF FIGURES (continued)

LIST OF FIGURES (continued)

1.0 INTRODUCTION

As advanced composite materials become more widely accepted, they will naturally be used in a wide variety of applications and loading environments. Thus it is important that engineers have a fundamental understanding of the behavior of these materials in complex as well as simple loading conditions. This requires that theoretical work be done to accurately predict the load carrying capacity of structural elements under various loading configurations and that there be experimental verification of the theory.

This investigation was undertaken for the expressed purpose of conducting a series of combined load buckling tests on composite cylinders and comparing the experimental results to the theoretical predictions of Wu [1]. The test cylinders were fabricated from boron-epoxy and graphite-epoxy and the loading consisted of a series of combined axial and torsional loads. The theoretical predictions for buckling loads are presented in the form of buckling interaction diagrams in axial-torsional load space; experimental results are shown on these interaction diagrams for comparison between theory and experiment. Five boron-epoxy and four graphite-epoxy laminates were tested. The boron-epoxy laminates were: $[0]$, $[\pm 45]_s$, $[-45_2/45_2]_s$, $[0/\pm 45/90]_s$ and [-82.5/30/20/-82.5]; the graphite-epoxy laminates were: $[\pm 45]_s$, $[-45_2/45_2]_s$, $[0/\pm 45/90]_s$ and [-82.5/30/20/-82.5]. A complete listing of specimens is presented in Table 1.

Previous works on buckling of composite cylinders include those of Marlowe, Sushinsky and Dexter [2] on torsional buckling of composite and composite-reinforced aluminum cylinders, Wilkins and Love [3] on

combined compression-torsion buckling of graphite-epoxy cyclinders, and Tennyson [4] on combined axial-torsional buckling of glass/epoxy cylinders. The latter paper also presents a rather extensive list of references on buckling of laminated composite cylinders.

2.0 BUCKLING ANALYSIS

2.1 Introduction

This chapter presents a rather brief summary of the analysis used to predict the buckling loads of laminated fibrous composite cylinders (modeled as anisotropic materials) under combined radial pressure, axial compression and torsion. The method is taken directly from Wu [1], and a computer program which he supplied to LaRC was used to obtain results for combined axial compression and torsional loading.

The geometry of the laminated shell is shown in Fig. 1a where the left hand coordinate system $x\theta z$ is employed. The origin is located at the mid-section of the cylinder and in the midplane of the shell thickness. Equilibrated loads are applied at the ends of the cylinder.

Following the isotropic theory of Flügge [5], the basic assumptions adopted in the present analysis are

(a) the shell is thin, $h/r \ll 1$

(b) the deflections of the shell are small

(c) the transverse normal stress $\sigma_z \simeq 0$

(d) normals to the reference surface remain normal to it and undergo no change in length during deformation, $\varepsilon_z = \gamma_{xz} = \gamma_{\theta z} \simeq 0$

2.2 Fundamental Equations

2.2.1 Stress-strain relations

For thin shells of anisotropic materials the elastic stress-strain relations reduce to

$$\begin{Bmatrix} \sigma_x \\ \sigma_\theta \\ \tau_{x\theta} \end{Bmatrix} = \begin{bmatrix} C_{11} & C_{12} & C_{16} \\ C_{12} & C_{22} & C_{26} \\ C_{16} & C_{26} & C_{66} \end{bmatrix} \begin{Bmatrix} \varepsilon_x \\ \varepsilon_\theta \\ \gamma_{x\theta} \end{Bmatrix} \qquad (1)$$

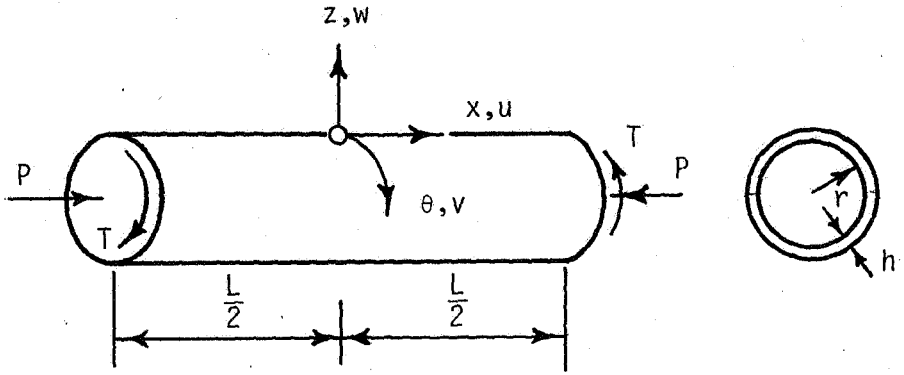

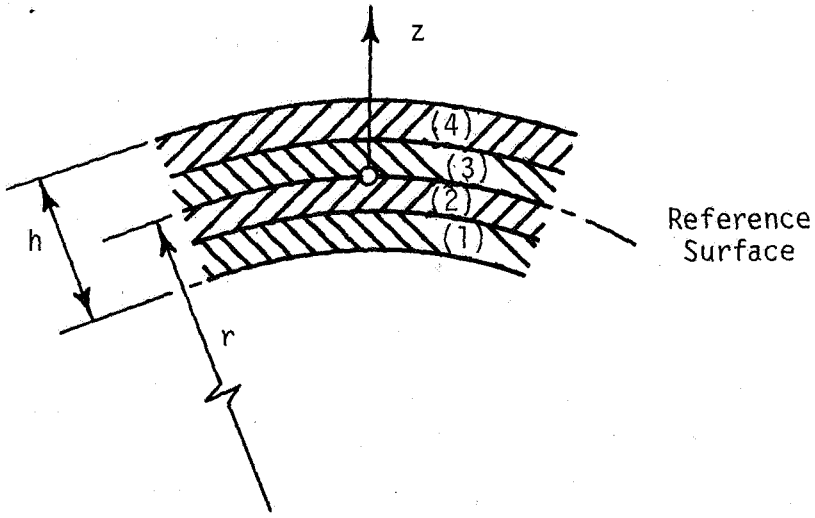

Fig. 1a. Shell Geometry

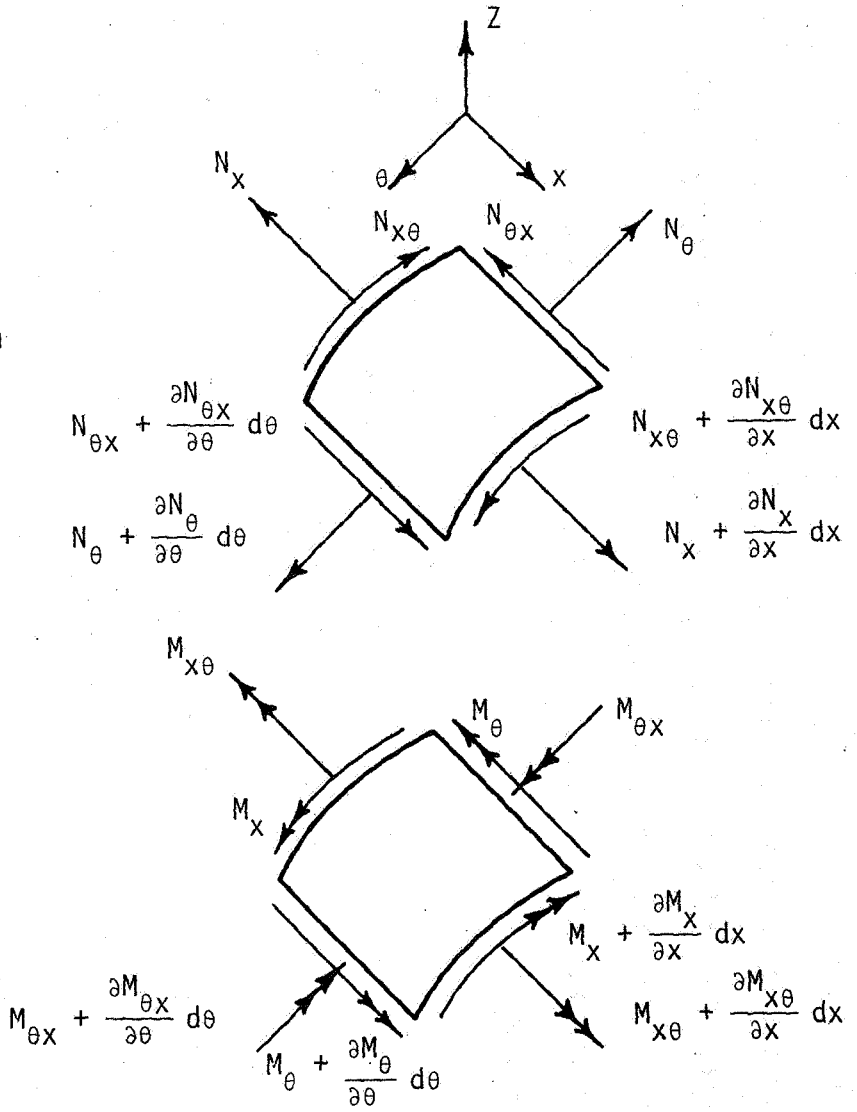

Fig. 1b. Stress Resultants

Fig. 1. Analytical Model

2.2.2 Strain-displacement relations

The strains at any point of the shell can be expressed in terms of the membrane strains ε_x°, ε_θ°, $\gamma_{x\theta}^\circ$ and curvatures κ_x, κ_θ, $\kappa_{x\theta}$ as

$$\varepsilon_x = \varepsilon_x^\circ + z\kappa_x$$

$$\varepsilon_\theta = \varepsilon_\theta^\circ + z(1 - \frac{z}{r})\kappa_\theta \qquad (2)$$

$$\gamma_{x\theta} = (1 + \frac{z^2}{2r^2})\gamma_{x\theta}^\circ + z(1 - \frac{z}{2r})\kappa_{x\theta}$$

where

$$\varepsilon_x^\circ = \frac{\partial u}{\partial x}$$

$$\varepsilon_\theta^\circ = \frac{1}{r}(\frac{\partial v}{\partial \theta} + w)$$

$$\gamma_{x\theta}^\circ = \frac{1}{r}\frac{\partial u}{\partial \theta} + \frac{\partial v}{\partial x}$$

$$\kappa_x = -\frac{\partial^2 w}{\partial x^2}$$

$$\kappa_\theta = -\frac{1}{r^2}(\frac{\partial^2 w}{\partial \theta^2} + w)$$

$$\kappa_{x\theta} = -(\frac{2}{r}\frac{\partial^2 w}{\partial x \partial \theta} + \frac{1}{r^2}\frac{\partial u}{\partial \theta} - \frac{1}{r}\frac{\partial v}{\partial x})$$

and the approximation

$$\frac{r}{r+z} \simeq 1 - \frac{z}{r} + (\frac{z}{r})^2 \quad \text{has been used.}$$

2.2.3 Force-displacement relations

The stresses on the shell element (Fig. 1b) are replaced by the stress resultants and stress couples per unit length defined by

$$\begin{Bmatrix} N_x \\ N_{x\theta} \end{Bmatrix} = \int_{-\frac{h}{2}}^{\frac{h}{2}} \begin{Bmatrix} \sigma_x \\ \tau_{x\theta} \end{Bmatrix} (1 + \frac{z}{r})\, dz$$

$$\begin{Bmatrix} N_\theta \\ N_{\theta x} \end{Bmatrix} = \int_{-\frac{h}{2}}^{\frac{h}{2}} \begin{Bmatrix} \sigma_\theta \\ \tau_{\theta x} \end{Bmatrix} dz \qquad (3)$$

$$\begin{Bmatrix} M_x \\ M_{x\theta} \end{Bmatrix} = \int_{-\frac{h}{2}}^{\frac{h}{2}} \begin{Bmatrix} \sigma_x \\ \tau_{x\theta} \end{Bmatrix} (1 + \frac{z}{r})\, z\, dz$$

$$\begin{Bmatrix} M_\theta \\ M_{\theta x} \end{Bmatrix} = \int_{-\frac{h}{2}}^{\frac{h}{2}} \begin{Bmatrix} \sigma_\theta \\ \tau_{\theta x} \end{Bmatrix} z\, dz$$

2.2.4 Linear buckling equations

In Flügge's theory, the following linear equilibrium equations were derived:

$$\frac{\partial N_x}{\partial x} + \frac{1}{r}\frac{\partial N_{\theta x}}{\partial \theta} - p\left(\frac{1}{r}\frac{\partial^2 u}{\partial \theta^2} - \frac{\partial w}{\partial x}\right) - p\frac{\partial^2 u}{\partial x^2} - 2T\frac{1}{r}\frac{\partial^2 u}{\partial x \partial \theta} = 0$$

$$\frac{1}{r}\frac{\partial N_\theta}{\partial \theta} + \frac{\partial N_{x\theta}}{\partial x} + \frac{1}{r^2}\frac{\partial M_\theta}{\partial \theta} + \frac{1}{r}\frac{\partial M_{x\theta}}{\partial x} - \frac{p}{r}\left(\frac{\partial^2 v}{\partial \theta^2} + \frac{\partial w}{\partial \theta}\right) - p\frac{\partial^2 v}{\partial x^2} - \frac{2T}{r}\left(\frac{\partial^2 v}{\partial x \partial \theta} + \frac{\partial w}{\partial x}\right) = 0 \qquad (4)$$

$$\frac{1}{r^2}\frac{\partial^2 M_\theta}{\partial \theta^2} + \frac{1}{r}\left(\frac{\partial^2 M_{x\theta}}{\partial x \partial \theta} + \frac{\partial^2 M_{\theta x}}{\partial x \partial \theta}\right) + \frac{\partial^2 M_x}{\partial x^2} - \frac{N_\theta}{r} - p\left(\frac{\partial u}{\partial x} - \frac{1}{r}\frac{\partial v}{\partial \theta} + \frac{1}{r}\frac{\partial^2 w}{\partial \theta^2}\right)$$

$$-p\frac{\partial^2 w}{\partial x^2} + \frac{2T}{r}\left(\frac{\partial v}{\partial x} - \frac{\partial^2 w}{\partial x \partial \theta}\right) = 0$$

where the positive values of p, P and T are, respectively, the external radial pressure, the axial compression per unit length, and the shear force per unit length.

Substituting Equations (1) and (2) into (3), making use of $(z/r)^3 << 1$, and then substituting the resulting equations into Equation (4) leads to the following equilibrium equations for cylindrical shells made of anisotropic materials and loaded with any combination or radial pressure, axial compression, and torsion.

$$\left(A_{11} + \frac{B_{11}}{r} - P\right) \frac{\partial^2 u}{\partial x^2} + \frac{2}{r}\left(A_{16} - T\right) \frac{\partial^2 u}{\partial x \partial \theta} + \left(\frac{A_{66}}{r^2} - \frac{B_{66}}{r^3} + \frac{D_{66}}{r^4} - \frac{p}{r}\right) \frac{\partial^2 u}{\partial \theta^2}$$

$$+ \left(A_{16} + \frac{2B_{16}}{r} + \frac{D_{16}}{r^2}\right) \frac{\partial^2 v}{\partial x^2} + \left(\frac{A_{12}}{r} + \frac{A_{66}}{r} + \frac{B_{12}}{r^2} + \frac{B_{66}}{r^2}\right) \frac{\partial^2 v}{\partial x \partial \theta} + \frac{A_{26}}{r^2} \frac{\partial^2 v}{\partial \theta^2}$$

$$- \left(B_{11} + \frac{D_{11}}{r}\right) \frac{\partial^3 w}{\partial x^3} - \left(\frac{3B_{16}}{r} + \frac{D_{16}}{r^2}\right) \frac{\partial^3 w}{\partial x^2 \partial \theta} - \left(\frac{B_{12}}{r^2} + \frac{2B_{66}}{r^2} - \frac{D_{66}}{r^3}\right) \frac{\partial^3 w}{\partial x \partial \theta^2}$$

$$- \left(\frac{B_{26}}{r^3} - \frac{D_{26}}{r^4}\right) \frac{\partial^3 w}{\partial \theta^3} + \left(\frac{A_{12}}{r} + p\right) \frac{\partial w}{\partial x} + \left(\frac{A_{26}}{r^2} - \frac{B_{26}}{r^3} + \frac{D_{26}}{r^4}\right) \frac{\partial w}{\partial \theta} = 0 \qquad (5a)$$

$$\left(A_{16} + \frac{2B_{16}}{r} + \frac{D_{16}}{r^2}\right) \frac{\partial^2 u}{\partial x^2} + \left(\frac{A_{12}}{r} + \frac{A_{66}}{r} + \frac{B_{12}}{r^2} + \frac{B_{66}}{r^2}\right) \frac{\partial^2 u}{\partial x \partial \theta} + \frac{A_{26}}{r^2} \frac{\partial^2 u}{\partial \theta^2}$$

$$+ \left(A_{66} + \frac{3B_{66}}{r} + \frac{3D_{66}}{r^2} - P\right) \frac{\partial^2 v}{\partial x^2} + \left(\frac{2A_{26}}{r} + \frac{4B_{26}}{r^2} + \frac{2D_{26}}{r^3} - \frac{2T}{r}\right) \frac{\partial^2 v}{\partial x \partial \theta}$$

$$+ \left(\frac{A_{22}}{r^2} + \frac{B_{22}}{r^3} - \frac{p}{r}\right) \frac{\partial^2 v}{\partial \theta^2} - \left(B_{16} + \frac{2D_{16}}{r}\right) \frac{\partial^3 w}{\partial x^3} - \left(\frac{B_{12}}{r} + \frac{2B_{66}}{r} + \frac{D_{12}}{r^2}\right.$$

$$\left. + \frac{3D_{66}}{r^2}\right) \frac{\partial^3 w}{\partial x^2 \partial \theta} - \left(\frac{3B_{26}}{r^2} + \frac{2D_{26}}{r^3}\right) \frac{\partial^3 w}{\partial x \partial \theta^2} - \frac{B_{22}}{r^3} \frac{\partial^3 w}{\partial \theta^3} + \left(\frac{A_{26}}{r} + \frac{B_{26}}{r^2} - \frac{2T}{r}\right) \qquad (5b)$$

$$\frac{\partial w}{\partial x} + \left(\frac{A_{22}}{r^2} - \frac{p}{r}\right) \frac{\partial w}{\partial \theta} = 0$$

$$\left(B_{11} + \frac{D_{11}}{r}\right) \frac{\partial^3 u}{\partial x^3} + \left(\frac{3B_{16}}{r} + \frac{D_{16}}{r^2}\right) \frac{\partial^3 u}{\partial x^2 \partial \theta} + \left(\frac{B_{12}}{r^2} + \frac{2B_{66}}{r^2} - \frac{D_{66}}{r^3}\right) \frac{\partial^3 u}{\partial x \partial \theta^2}$$

$$+ \left(\frac{B_{26}}{r^3} - \frac{D_{26}}{r^4}\right) \frac{\partial^3 u}{\partial \theta^3} - \left(\frac{A_{12}}{r} + p\right) \frac{\partial u}{\partial x} + \left(-\frac{A_{26}}{r^2} + \frac{B_{26}}{r^3} - \frac{D_{26}}{r^4}\right) \frac{\partial u}{\partial \theta} + \left(B_{16}\right.$$

$$\left. + \frac{2D_{16}}{r}\right) \frac{\partial^3 v}{\partial x^3} + \left(\frac{B_{12}}{r} + \frac{2B_{66}}{r} + \frac{D_{12}}{r^2} + \frac{3D_{66}}{r^2}\right) \frac{\partial^3 v}{\partial x^2 \partial \theta} + \left(\frac{3B_{26}}{r^2} + \frac{2D_{26}}{r^3}\right) \frac{\partial^3 v}{\partial x \partial \theta^2} \qquad (5c)$$

$$+ \frac{B_{22}}{r^3} \frac{\partial^3 y}{\partial \theta^3} + \left(-\frac{A_{26}}{r} - \frac{B_{26}}{r^2} + \frac{2T}{r}\right) \frac{\partial v}{\partial x} + \left(-\frac{A_{22}}{r^2} + \frac{p}{r}\right) \frac{\partial v}{\partial \theta} - D_{11} \frac{\partial^4 w}{\partial x^4}$$

$$- \frac{4D_{16}}{r} \frac{\partial^4 w}{\partial x^3 \partial \theta} - \left(\frac{2D_{12}}{r^2} + \frac{4D_{66}}{r^2}\right) \frac{\partial^4 w}{\partial x^2 \partial \theta^2} - \frac{4D_{26}}{r^3} \frac{\partial^4 w}{\partial x \partial \theta^3} - \frac{D_{22}}{r^4} \frac{\partial^4 w}{\partial \theta^4} + \left(\frac{2B_{12}}{r}\right.$$

$$\left. - p\right) \frac{\partial^2 w}{\partial x^2} + \left(\frac{4B_{26}}{r^2} - \frac{2D_{26}}{r^3} - \frac{2T}{r}\right) \frac{\partial^2 w}{\partial x \partial \theta} + \left(\frac{2B_{22}}{r^3} - \frac{2D_{22}}{r^4} - \frac{p}{r}\right) \frac{\partial^2 w}{\partial \theta^2} + \left(-\frac{A_{22}}{r^2}\right.$$

$$\left. + \frac{B_{22}}{r^3} - \frac{D_{22}}{r^4}\right) w = 0$$

where A_{ij}, B_{ij} and D_{ij} are defined by lamination theory [7].

2.2.5 Boundary conditions

2.2.5.1 Simply supported boundary conditions:

$$S1: \quad w = M_x = N_x + \frac{T}{r} \frac{\partial u}{\partial \theta} = T_x + P \frac{\partial v}{\partial x} = 0 \qquad (6)$$

$$S2: \quad w = M_x = u = v = 0$$

$$S3: \quad w = M_x = u = T_x + P\frac{\partial v}{\partial x} = 0$$

$$S4: \quad w = M_x = N_x + \frac{T}{r}\frac{\partial u}{\partial \theta} = v = 0$$

2.2.5.2 Clamped boundary conditions:

$$C1: \quad w = \frac{\partial w}{\partial x} = N_x + \frac{T}{r}\frac{\partial u}{\partial \theta} = T_x + P\frac{\partial v}{\partial x} = 0$$

$$C2: \quad w = \frac{\partial w}{\partial x} = u = v = 0$$

$$C3: \quad w = \frac{\partial w}{\partial x} = u = T_x + P\frac{\partial v}{\partial x} = 0 \qquad (7)$$

$$C4: \quad w = \frac{\partial w}{\partial x} = N_x + \frac{T}{r}\frac{\partial u}{\partial \theta} = v = 0$$

where $T_x = N_{x\theta} + \frac{M_{x\theta}}{r}$ is the Kirchhoff boundary shear.

2.3 Method of Solution

The problem is viewed as an eigenvalue problem in which it is desired to find a set of displacement modes which satisfy the equilibrium equations (5) and a given set of boundary conditions. The method of solution uses a set of displacement modes (with undetermined coefficients) which satisfy the equilibrium equations identically, and solves for the undetermined coefficients by forcing satisfaction of the boundary conditions to obtain a boundary determinant. The buckling load is then the minimum load which satisfied both equilibrium equations and the boundary determinant.

The set of displacement modes is assumed in the form

$$u = U \sin\left(\frac{\lambda x}{r} + n\theta\right)$$

$$v = V \sin\left(\frac{\lambda x}{r} + n\theta\right) \qquad (8)$$

$$w = W \cos \left(\frac{\lambda x}{r} + n\theta\right)$$

where n is the number of waves in the circumferential direction, and U, V, and W are undetermined coefficients. Substituting these functions into the equilibrium equations (5) and setting the determinant of the coefficient matrix to zero leads to an eighth degree polynomial in terms of λ:

$$a_8\lambda^8 + a_7\lambda^7 + a_6\lambda^6 + a_5\lambda^5 + a_4\lambda^4 + a_3\lambda^3 + a_2\lambda^2 + a_1\lambda + a_0 = 0 \qquad (9)$$

where a's are coefficients in terms of A_{ij}, B_{ij}, D_{ij}, n, p, P, and T. The characteristic roots of Equation (9) are complex numbers in general. However, since, the a_i of (9) are real constants, the complex roots form conjugate pairs. Hence Equation (8) is generalized to

$$u = \sum_{k=1}^{8} U_k \sin \left(\frac{\lambda_k x}{r} + n\theta\right)$$

$$v = \sum_{k=1}^{8} V_k \sin \left(\frac{\lambda_k x}{r} + n\theta\right) \qquad (10)$$

$$w = \sum_{k=1}^{8} W_k \cos \left(\frac{\lambda_k x}{r} + n\theta\right)$$

The displacement modes (10) do not in general satisfy the boundary conditions. However, the complex conjugate nature of λ_k, U_k, V_k and W_k may be utilized to eliminate the imaginary parts in Equations (10). As a result, the displacement modes contain only the real quantities as follows:

$$u = \sum_{k=1,3}^{7} \left[\left(U_{crk}\omega_k + U_{cik+1}\omega_{k+1}\right) \cos n\theta + \left(U_{srk}\omega_k + U_{sik+1}\omega_{k+1}\right) \sin n\theta\right]$$

$$v = \sum_{k=1,3}^{7} [(V_{crk}\omega_k + V_{cik+1}\omega_{k+1}) \cos n\theta + (V_{srk}\omega_k + V_{sik+1}\omega_{k+1}) \sin n\theta]$$

$$w = \sum_{k=1,3}^{7} [(W_{crk}\omega_k + W_{cik+1}\omega_{k+1}) \cos n\theta + (W_{srk}\omega_k + W_{sik+1}\omega_{k+1}) \sin n\theta] \quad (11)$$

where U_{crk}, U_{srk}, W_k, ... etc. are defined in Reference [1].

Using Equations (11) the boundary conditions ((6) and (7)) may now be expressed in terms of the unknown ω's as a set of homogeneous algebraic equations. The nontrivial solutions further require that these "boundary determinants" vanish. The buckling load for the given length, geometry, and materials properties is then the minimum load which satisfied both the Equation (9) and the boundary determinant corresponding to each K. The reader may refer to Reference [1] for the special cases of n = 0 and 1 wherein the characteristic equation (9) is reduced and special treatment must be taken.

3.0 THEORETICAL PREDICTIONS

3.1 Theoretical Buckling Loads

The computer program developed by Wu [1] was used to predict the buckling loads of the cylinders used in the experimental investigation. The results were obtained in the form of specific buckling loads for a series of axial/torsional load ratios. A buckling interaction diagram was then determined by plotting these buckling loads in normalized axial-torsional load space. Axial loads were normalized with respect to the buckling load in pure compression (P*) and torsional loads were normalized with respect to the buckling load for positive pure torsion (T*). Interaction diagrams (both line and point plots) are presented in the Results Section. The line plots were obtained using cubic spline interpolation. The experimental results are shown on the line plots as individual data points. A complete listing of all theoretical buckling loads is presented in Appendix A.

3.2 Input Data for the Wu Program

The Wu program requires geometric, material, boundary condition and loading input data. The geometric properties were determined from measurements on each cylinder and the loading data was preselected to sufficiently determine the interaction diagram. The material property data for the two material systems investigated were obtained from the literature for typical fiber volume fractions (Table 2). The modulus in the fiber direction (E_{11}) was then corrected for the specific fiber volume fraction present in each specimen. These fiber volume fractions were determined from thickness measurements, the known number of plies, and assumed nominal ply thickness and fiber volume fraction. The

modified moduli are presented in Tables 3 and 4. A summary of variable input properties for the actual cylinders is presented in Table 5. All other required material properties were taken from Table 2. All theoretical results are for the type C3 clamped boundary conditions defined in equ. 7.

3.3 Modulus Predictions

Lamination theory [7] was used to predict Young's modulus E_x along the axis of each cylinder and the shear modulus $G_{x\theta}$ in the plane of the laminate. The assumed material properties for these calculations are presented in Tables 5 and 6, and comparisons between theory and experiment are presented in Table 7. These comparisons which were made as part of the assessment of the quality control on the specimens will be discussed in the Results Section.

TABLE 1

BASIC DATA FOR COMPOSITE CYLINDERS

Spec. No.	Material	Laminate	Length (in)	Thickness (in)	t/ply (in)	Avg. Radius (in)	X-Sectional Area (in^2)	Number Tests
1	B/E	$[\mp 45]_s$	19.875	0.022	0.0055	2.987	0.413	3
2	B/E	$[0_8]$	14.0	0.0371	0.0046	2.967	0.692	4
3	B/E	[-82.5/30/20/-82.5]	20.0	0.0208	0.0052	3.002	0.392	0
4	B/E	"	20.03	0.0215	0.0054	3.002	0.406	13
5	B/E	"	20.25	0.0211	0.0053	3.003	0.398	1
6	B/E	$[-45_2/45_2]_s$	19.97	0.0440	0.0055	3.015	0.834	14
7	Gr/E	[-82.5/30/20/-82.5]	14.875	0.0214	0.0054	3.006	0.402	0
8	Gr/E	"	20.03	0.0228	0.0057	3.007	0.431	16
9	Gr/E	"	20.03	0.0213	0.0053	3.005	0.402	2
10	Gr/E	"	18.5	0.0224	0.0056	3.005	0.423	13
11	Gr/E	$[\mp 45]_s$	13.125	0.026	0.0065	2.987	0.488	7
12	B/E	[-82.5/30/20/-82.5]	20.0	0.0210	0.0053	2.984	0.394	3
13	B/E	$[0/\pm 45/90]_s$	20.0	0.040	0.0050	2.976	0.748	13

TABLE 1 BASIC DATA FOR COMPOSITE CYLINDERS (continued)

Spec. No.	Material	Laminate	Length (in)	Thickness (in)	t/ply (in)	Avg. Radius (in)	X-Sectional Area (in^2)	Number Tests
14	Gr/E	$[-45_2/45_2]_s$	20.0	0.050	0.0063	2.976	0.935	23
15	Gr/E	$[0/\pm45/90]_s$	20.0	0.040	0.0050	2.976	0.748	4
16	Gr/E	$[\mp45]_s$	18.0	0.025	0.0062	2.988	0.469	0
17	B/E	[-82.5/30/20/-82.5]	20.125	0.021	0.0052	2.986	0.394	13
18	Gr/E	$[-45_2/45_2]_s$	20.0	0.054	0.0067	2.976	1.01	2
19	B/E	"	20.0	0.038	0.0047	2.978	0.711	2
20	Gr/E	"	20.0	0.052	0.0065	2.975	0.972	2
21	Gr/E	"	20.0	0.040	0.0051	2.976	0.748	20
22	Gr/E	$[0/\pm45/90]_s$	16.875	0.051	0.0064	2.974	0.953	3
23	B/E	"	19.0	0.038	0.0047	2.977	0.711	2
A	Gr/E	"	20.062	0.041	0.0051	2.970	0.765	0
B	Gr/E	"	20.062	0.041	0.0051	2.970	0.765	9

TABLE 2

TYPICAL MATERIAL PROPERTIES FOR INPUT TO WU PROGRAM

Boron-Epoxy (AVCO 5505/4)

$E_{11} = 30 \times 10^6$ psi $\qquad E_{22} = 2.7 \times 10^6$ psi

$G_{12} = 1.0 \times 10^6$ psi $\qquad \nu_{12} = 0.21$

Graphite-Epoxy (Modmor I fibers, Narmco 5208 resin)

$E_{11} = 30 \times 10^6$ psi $\qquad E_{22} = 1.7 \times 10^6$ psi

$G_{12} - 1.0 \times 10^6$ psi $\qquad \nu_{12} = 0.21$

TABLE 3

MODULUS VALUES CORRECTED FOR FIBER VOLUME FRACTION
(BORON-EPOXY AVCO 5505/4)

Laminate	Spec No.	V_f	E_{11} (corrected) ($\times 10^{-6}$psi)
$[0_8]$	2	0.57	31.56
$[0/\pm45/90]_s$	13	0.52	28.84
"	23	0.55	30.47
$[\pm45]_s$	1	0.473	26.27
"	3	0.50	27.75
[-82.5/30/20/-82.5]	4	0.483	26.82
"	5	0.492	27.31
"	12	0.495	27.47
"	17	0.495	27.47
$[-45_2/45_2]_s$	6	0.473	26.27
"	19	0.547	30.31

Assumed Constituent Properties:

$E_m = 0.49 \times 10^6$psi $\qquad E_f = 55 \times 10^6$psi

Nominal ply thickness = 0.0046"

TABLE 4

MODULUS VALUES CORRECTED FOR FIBER VOLUME FRACTION
(MODMOR I, 5208 GRAPHITE-EPOXY)

Laminate	Spec No.	V_f	E_{11} (corrected) ($\times 10^{-6}$psi)
[-82.5/30/20/-82.5]	7	0.56	18.72
"	8	0.53	17.72
"	9	0.56	18.72
"	10	0.54	17.90
$[\mp 45]_s$	11	0.46	15.50
"	16	0.48	16.09
$[-45_2/45_2]_s$	14	0.48	16.09
"	18	0.44	14.94
"	20	0.46	15.50
"	21	0.47	15.79
$[0/\pm 45/90]_s$	15	0.60	20.0
"	22	0.60	20.0
"	A	0.59	19.52
"	B	0.59	19.52

Assumptions:

$E_f = 33 \times 10^6$psi $E_m = 0.49 \times 10^6$psi

Nominal ply thickness = 0.0050"

TABLE 5

VARIABLE WU INPUT DATA FOR ACTUAL TUBES

Laminate	Spec No.	L/R	R (in)	E_{11} ($\times 10^{-6}$ psi)	t/ply (in)
Boron-Epoxy					
$[\mp 45]_s$	1	6.65383	2.987	26.27	0.0055
[0]	2	4.71857	2.967	31.56	0.0046
[-82.5/30/20/-82.5]	3	6.66223	3.002	27.75	0.0052
"	4	6.67222	3.002	26.82	0.0054
"	5	6.74326	3.003	27.31	0.0053
"	12	6.70241	2.984	27.47	0.0053
"	17	6.73979	2.986	27.47	0.00525
$[-45_2/45_2]_s$	6	6.62355	3.015	26.27	0.0055
"	19	6.71592	2.978	30.31	0.0047
$[0/\pm 45/90]_s$	13	6.72043	2.976	28.84	0.0050
"	23	6.38226	2.977	30.47	0.0047
Graphite-Epoxy					
[-82.5/30/20/-82.5]	7	4.94844	3.006	18.72	0.00535
"	8	6.6578	3.007	17.72	0.0057
"	9	6.66556	3.005	18.72	0.005325
"	10	6.15641	3.005	17.90	0.0056
$[\mp 45]_s$	11	4.39404	2.987	15.50	0.0065
"	16	6.0241	2.988	16.09	0.00625
$[-45_2/45_2]_s$	14	6.72043	2.976	16.09	0.00625
"	18	6.72043	2.976	14.94	0.00675
"	20	6.72269	2.975	15.50	0.0065
"	21	5.67418	2.974	15.79	0.006375
$[0/\pm 45/90]_s$	15	6.72043	2.976	20.0	0.0050
"	22	6.72043	2.976	20.0	0.0050
"	a	6.75488	2.970	19.52	0.005125
"	b	6.75488	2.970	19.52	0.005125

NOTE: See Table 2 for other material properties

TABLE 6

ASSUMED PROPERTIES FOR INPUT TO LAMINATION THEORY

Boron-Epoxy

E_{11}: See Table 5* $E_{22} = 2.7 \times 10^6$ psi

$G_{12} = 1.26 \times 10^6$ psi $\nu_{12} = 0.21$

Ply thickness: See Table 5*

Graphite-Epoxy

E_{11}: See Table 5* $E_{22} = 1.7 \times 10^6$ psi

$G_{12} = 1.0 \times 10^6$ psi $\nu_{12} = 0.3$

Ply thickness: See Table 5*

*Variable depending on actual tube thickness

4.0 EXPERIMENTAL PROGRAM

4.1 Specimens

The specimens used in this investigation were thin-walled cylinders made from either boron-epoxy or graphite-epoxy composite laminates. The boron-epoxy was 4 mil fibers in AVCO 5505 resin and the graphite-epoxy was Modmor I fibers in Narmco 5208 resin. All cylinders were approximately 6 inches in diameter and most were approximately 20 inches in length. Wall thickness varied with the number of plies in the laminate ranging from a low of 0.021 inches to a high of 0.054 inches. A detailed listing of specimen geometries is given in Table 1 and a typical specimen is shown in Fig. 2. Twenty foil-type strain gages were bonded to each specimen in the pattern shown in Fig. 3. Load was introduced through aluminum plugs which were bonded to the ends of the specimens (Fig. 2).

4.2 Data Acquisition

Load and strain were acquired using a variety of data acquisition devices during the course of the investigation. Load was monitored using strip charts, oscilloscopes, the CB^2 data acquisition system [6], and a commercially available data acquisition system. Strain was monitored using strip charts, the CB^2 system, oscilloscopes, and the commercial data acquisition system. Figure 4 shows some of the data acquisition equipment used during a typical test at VPI&SU. For the tests conducted at Langley, all data was acquired and stored using their automatic data acquisition system. Load and strain were also monitored on oscilloscopes during the tests.

4.3 Loading

The great majority of the tests were conducted at VPI&SU on an MTS

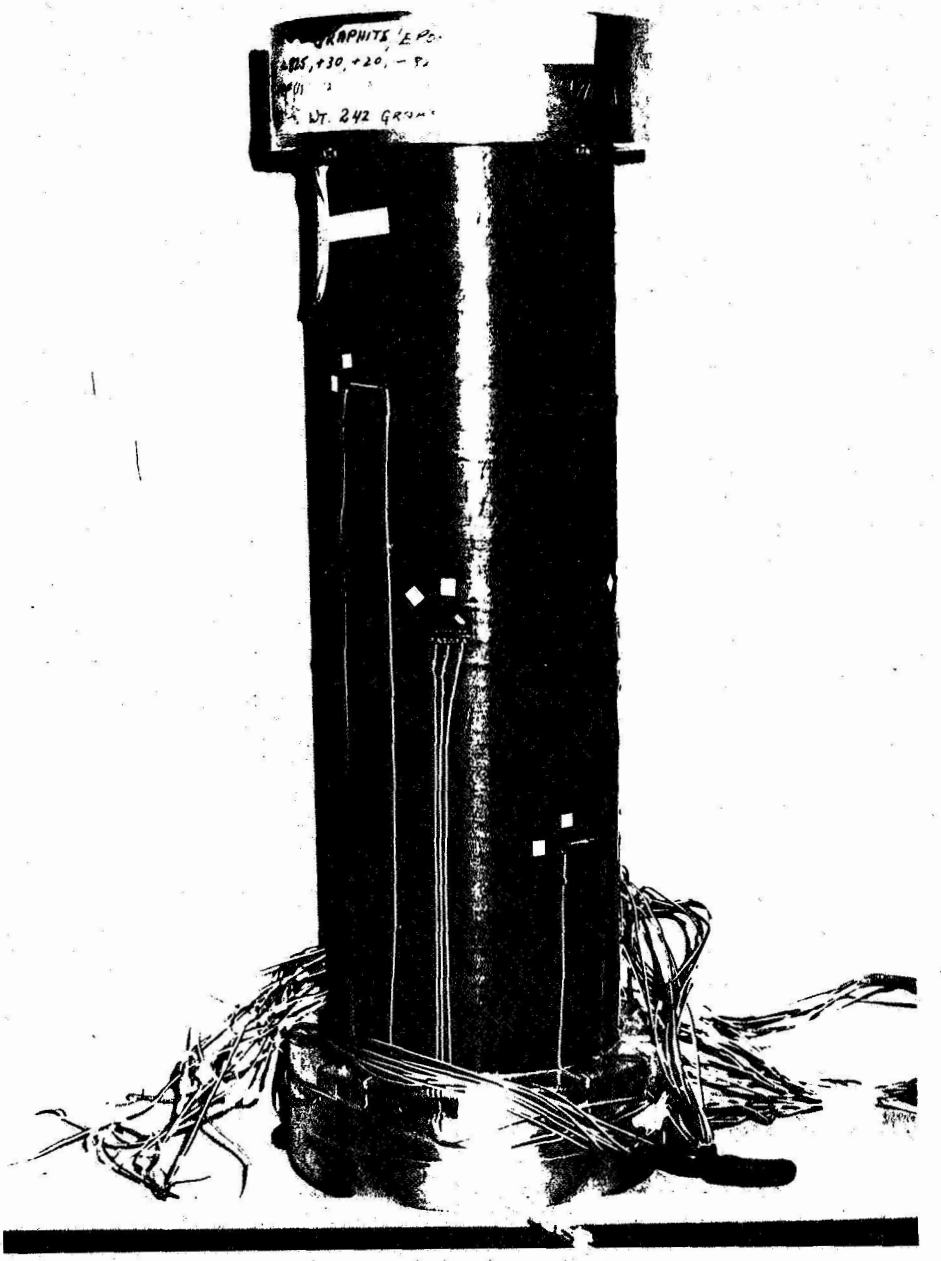

Fig. 2. Typical Composite Cylinder with End Plugs

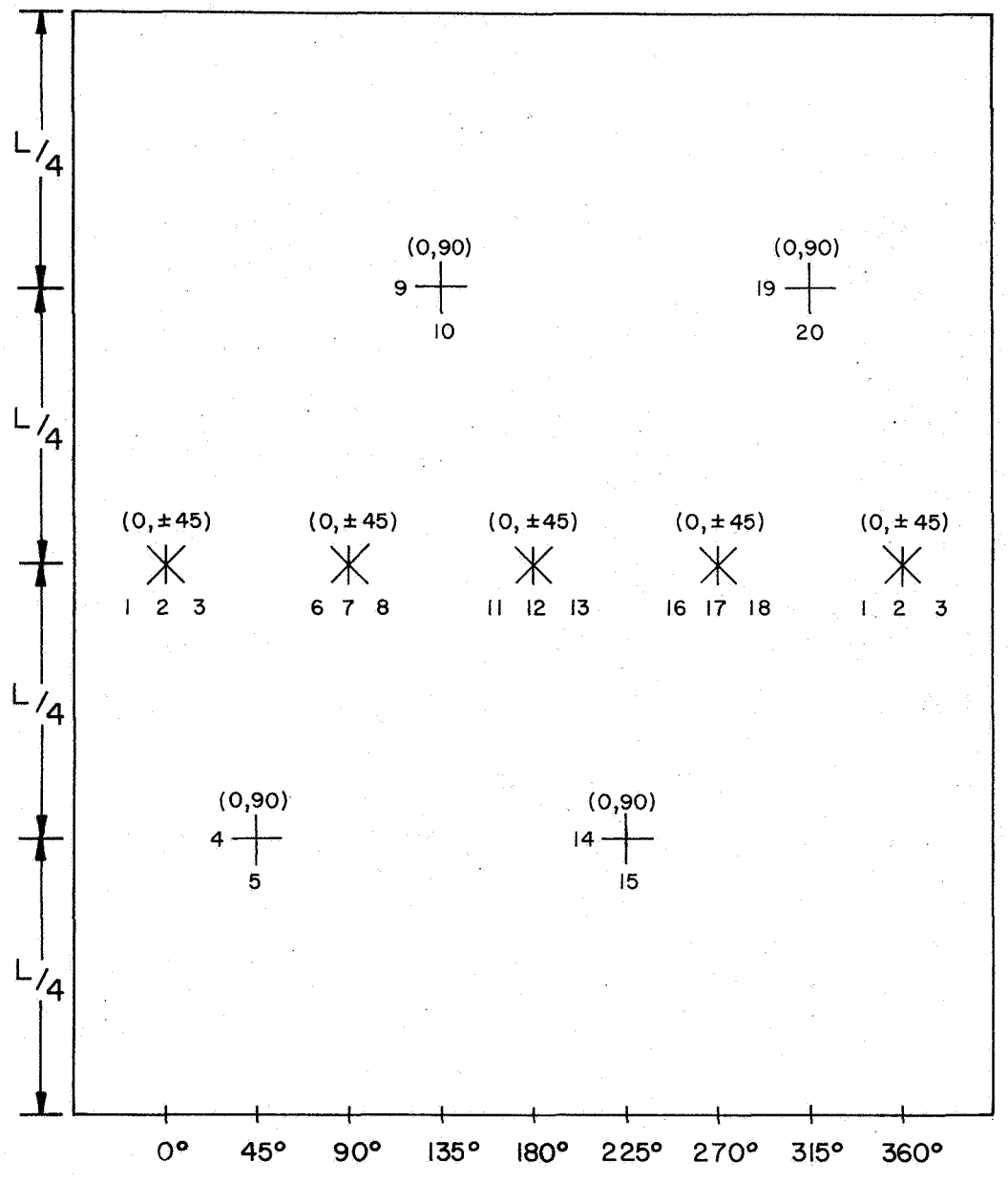

Fig. 3. Strain Gage Pattern

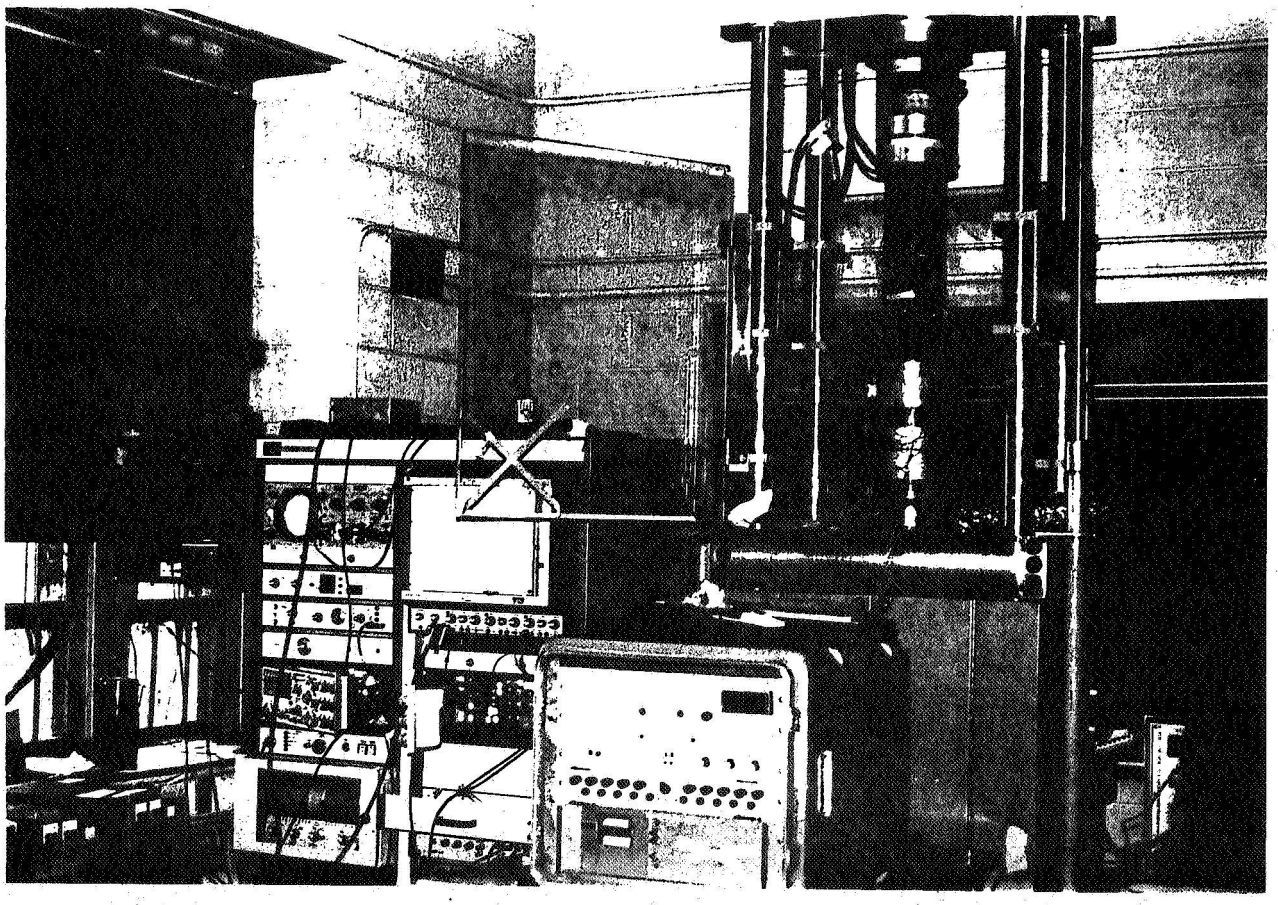

Fig. 4. Experimental Setup

axial-torsional combined loader. The other tests were conducted at Langley Research Center on two different machines, one being pure torsion and the other a combined axial-torsional loader. The VPI machine had the capability to function under load or displacement control with each mode independent of the other. Considerable difficulty was encountered with this machine. It was rated at 50 Kips axial and ±20 Kip-in torsional, but did not provide the rated torsional capacity in both directions. The maximums attainable were +20 Kip-in and -17.5 Kip-in.* Early tests were run under load control in order to a priori establish the load ratios for the test. This proved to be an unsatisfactory manner in which to run buckling tests without failing the specimen. Because of the automatic loading nature of the machine, the load continued to increase at the specified loading rate as the buckling point was approached and as a result the specimen failed before unloading could be accomplished. Subsequent tests were run under displacement control or a combination of displacement and load control. Displacement control on both loading modes was used for all tests except the pure compression and pure torsion tests on cylinders which were made from unsymmetric laminates. The latter tests were run under a combination of load and stroke control in order to insure that undesired loads were not introduced due to the coupling between in-plane forces and bending moments associated with unsymmetric laminates. These two loading methods (displacement control, and combined displacement and load control) proved to be more satisfactory for determining the buckling point without failing the specimen.

---

*Pure torsion results for cylinders with buckling loads in excess of the maximum attainables at VPI&SU were obtained at Langley Research Center.

The complete series of tests on each cylinder consisted of pure compression, pure (positive and negative) torsion, and several combined compression-torsion loads. The complete series was not conducted for all cylinders since some specimens failed before the series was completed and others were duplicate specimens.

4.4 Test Procedures and Determination of the Buckling Point

The specimens used in this investigation were very expensive and, therefore, it was necessary to conduct as many tests as possible with each cylinder in order to obtain a good spectrum of loading combinations at a reasonable cost. This required that each specimen be loaded under a particular loading configuration up to the buckling point and then unloaded before any permanent damage had occurred. It was desired to repeat this procedure many times with each specimen with only the loading configuration being changed. This proved to be a particularly troublesome task throughout the entire testing program. Buckling the cylinders under pure torsion was a fairly stable event and the deformation at the buckling torque could usually be controlled without damaging the specimen. In addition, the torsional buckling load was quite predictable and this was extremely helpful when testing. Buckling under pure compression was very unpredictable and usually a much more dynamic event. Thus, it was difficult to obtain buckling loads at or near the pure compression configuration without damaging the specimen. (The response was of course also dependent upon the laminate being studied.) As a result of the difficulty in obtaining a buckle without damaging the specimen, a very conservative approach was adopted during the experimental program. Subsequent analysis of the experimental data indicated that in many

cases the test was stopped prior to attainment of the buckling load. Such data points are not plotted on the buckling interaction diagrams, but they are listed in Table 9. Even with the conservative approach fourteen of twenty-five specimens were failed during the course of the investigation.

A particularly good example of torsional buckling response is shown in Fig. 5a which is an oscilloscope trace of torque vs. strain for four strain gages mounted at +45° on a $[-45_2/45_2]_s$ graphite-epoxy cylinder. Nonlinear response and strain reversal are clear evidence that the cylinder has buckled. Fig. 5b is another example of a pure torsion tests conducted at Langley Research Center. The specimen is a quasi-isotropic $[0/\pm45/90]_s$ graphite-epoxy cylinder and the gages are all at 45° to the axis of the cylinder. In this example the test was stopped as soon as the initiation of buckling was evident.

Figure 6 shows two examples of oscilloscope traces for axial load vs. strain for pure compression loading. The traces in Fig. 6a are from a test conducted at Langley and those in Fig. 6b are from a test conducted at VPI&SU. The NASA test provided a much clearer indication of buckling than did the VPI test. The NASA test was for a $[0/\pm45/90]_s$ graphite-epoxy cylinder with all strain gages along the axis of the cylinder and the VPI test was for a $[0/\pm45/90]_s$ boron-epoxy cylinder with the strain gages at 0°, ±45° and 90°. Initiation of buckling is evident in only the 0° gage of the VPI test.

Two examples of oscilloscope traces for combined compression-torsion loading are shown in Fig. 7. The results in Fig. 7a are from a Langley test on the same $[0/\pm45/90]_s$ graphite-epoxy cylinder as

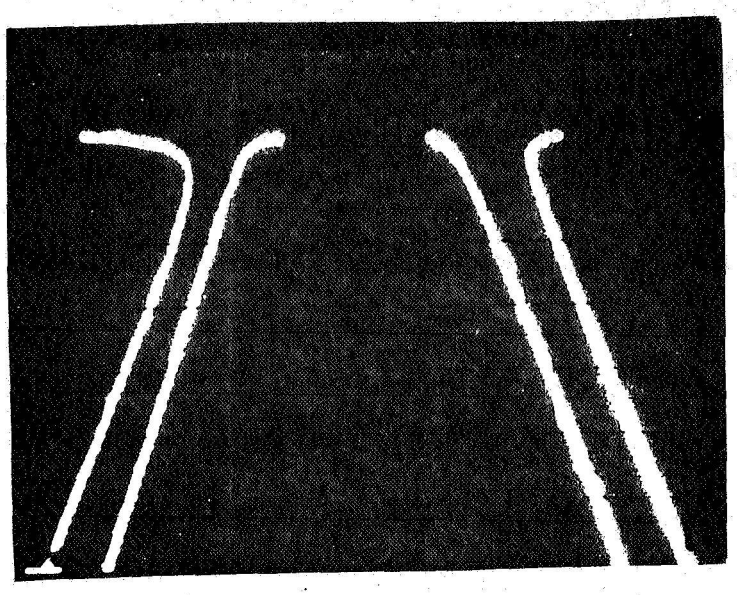

Fig. 5a. $[-45_2/45_2]_s$ Graphite-Epoxy

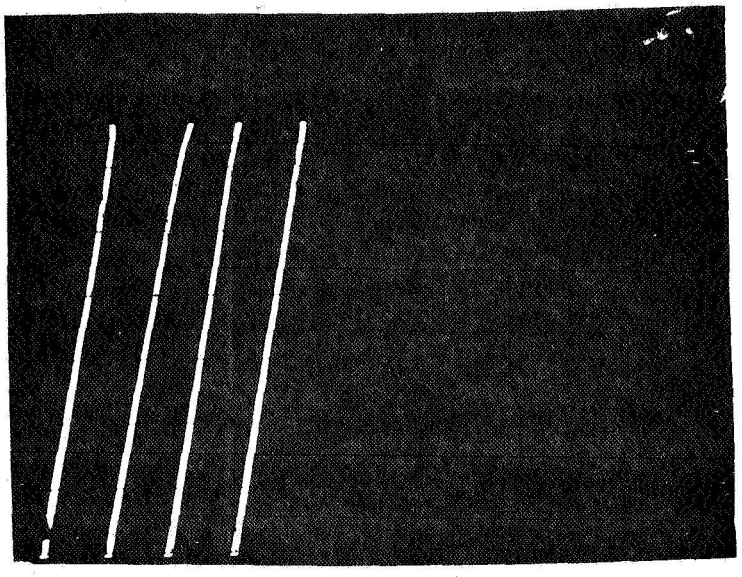

Fig. 5b. $[0/\pm45/90]_s$ Graphite-Epoxy

Fig. 5. Load-Strain Histories for Pure Torsion

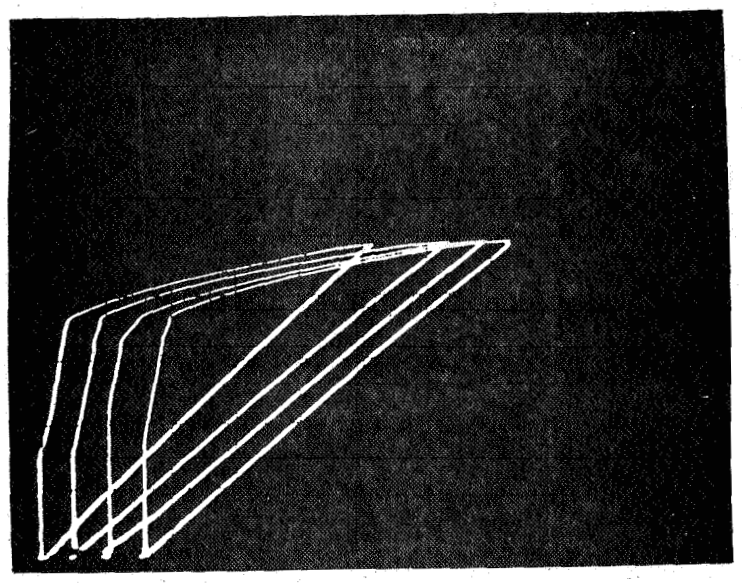

Fig. 6a. $[0/\pm45/90]_s$ Graphite-Epoxy

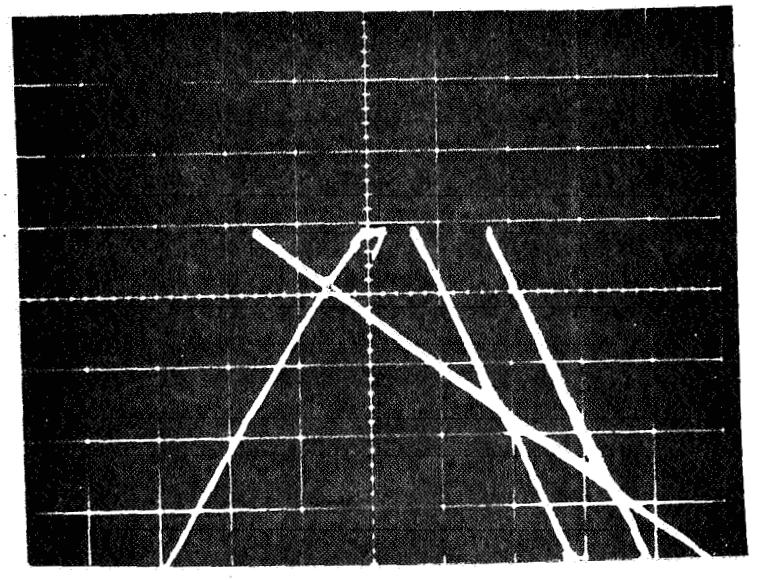

Fig. 6b. $[0/\pm45/90]_s$ Boron-Epoxy

Fig. 6. Load-Strain Histories for Pure Compression

shown in Fig. 7b. The strains which are from gages at +45° and -45° to the cylinder axis clearly show the initiation of buckling. Fig. 7b shows results obtained at VPI&SU on the same $[0/\pm45/90]_s$ boron-epoxy cylinder as shown in Fig. 6b. This figure also clearly shows the initiation of buckling as indicated by the strain at 0°, +45°, -45° and 90°. In general it can be stated that it was more difficult to ascertain the initiation of buckling (without failure) in the combined loading mode. Also, greater control of the deformation of the specimen near the buckling load was attainable in the tests conducted at Langley. The tests conducted at VPI&SU were plagued by occasional surges in the loading.

Another aspect of the testing program which had a profound influence on the conduct of the tests was the frequent audible sounds which were emitted by the specimen during loading. These cracking sounds usually were more frequent at higher load levels. Although the source of the cracking noises could not be ascertained, tests were often stopped because of them. It is interesting to note that cylinders which were tested further after emitting loud noises often exhibited good buckling behavior under a different loading configuration. The cracking noises could be attributed to debonding between the specimen and the end plug as well as formation of cracks in the specimen. Visual inspection of the specimens did not exhibit cracks unless failure was evident.

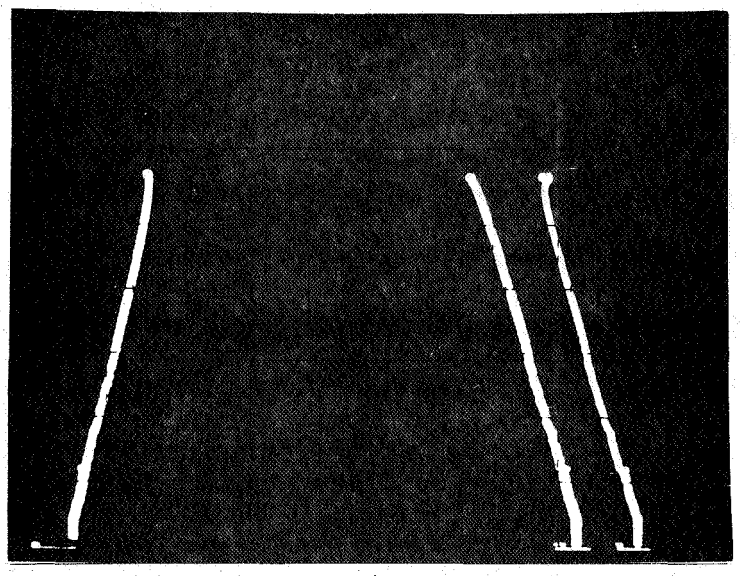

Fig. 7a. $[0/\pm45/90]_s$ Graphite-Epoxy

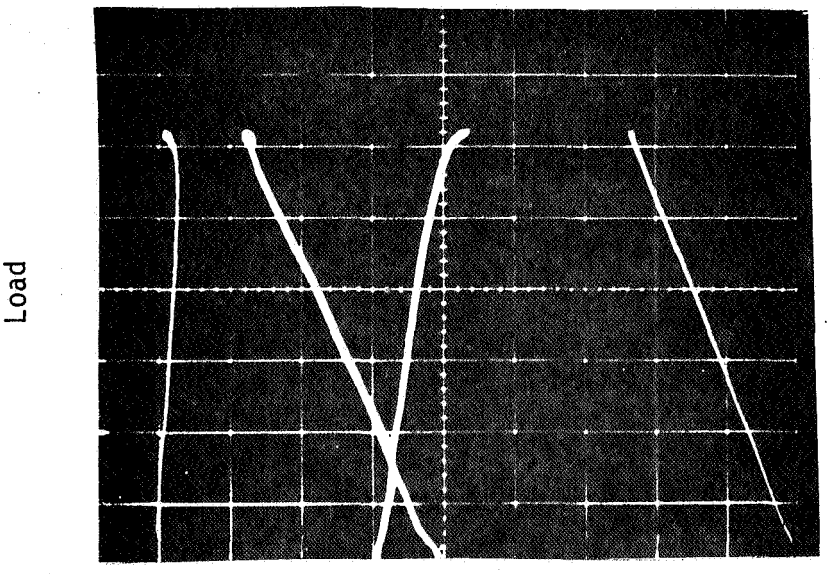

Fig. 7b. $[0/\pm45/90]_s$ Boron-Epoxy

Fig. 7. Load-Strain Histories for Combined Compression-Torsion

5.0 RESULTS

5.1 Modulus Values

Comparisons between theoretical and experimental modulus values are presented in Table 7. The table shows results for the Young's modulus in the direction of the cylinder axis (E_x) and the shear modulus in the plane of the laminate ($G_{x\theta}$). The theoretical results are based upon lamination theory [7]. The assumed material properties for input to lamination theory are listed in Table 6. The input for the theory was taken from the literature and the only unidirectional specimen available for testing. The data were modified for thickness (fiber volume fraction) as discussed previously. Since most of the input data for these calculations were taken from typical properties in the literature, the laminate predictions can only be considered approximate values. Close examination of Table 7 indicates that there is fairly good agreement between theory and experiment with the percent difference ranging from a low of five percent to a high of 38 percent. In view of all of the unknown factors such as fiber volume fraction, fiber alignment and unidirectional material properties, this difference is not surprising. In fact, in many cases the agreement is quite good.

5.2 Pure Compression and Pure Torsion

A comparison between the theoretical buckling loads for pure compression and pure torsion as predicted by the Wu program and the experimental results are presented in Table 8. These results generally show that there is excellent agreement between the theoretical and experimental buckling loads for positive and negative torsion, but the experimental results for pure compression are well below the

TABLE 7

THEORETICAL AND EXPERIMENTAL MODULUS VALUES

Laminate	Spec No.	Experimental E_x ($\times 10^{-6}$ psi)	Experimental $G_{x\theta}$ ($\times 10^{-6}$ psi)	Lamination Theory E_x ($\times 10^{-6}$ psi)	Lamination Theory $G_{x\theta}$ ($\times 10^{-6}$ psi)
Boron-Epoxy					
$[\mp 45]_s$	1	-	7.03	4.32	6.99
[0]	2	31.30	1.26	31.56	1.26
[-82.5/30/20/-82.5]	3	-	-	6.22	1.85
"	4	5.02	1.59	6.16	1.84
"	5	-	1.66	6.19	1.85
"	12	-	1.40	6.20	1.85
"	17	6.38	1.52	6.20	1.85
$[-45_2/45_2]_s$	6	3.33	7.02	4.32	6.99
"	19	-	9.15	4.39	8.00
$[0/\pm 45/90]_s$	13	10.98	4.85	11.53	4.45
"	23	-	-	11.84	4.56
Graphite-Epoxy					
[-82.5/30/20/-82.5]	7	-	-	4.52	1.39
"	8	4.11	1.28	4.44	1.38
"	9	-	-	4.52	1.39
"	10	3.36	1.06	4.46	1.38
$[\mp 45]_s$	11	2.28	5.46	3.28	4.09
"	16	-	-	3.30	4.23
$[-45_2/45_2]_s$	14	2.06	4.43	3.30	4.23
"	18	-	4.50	3.27	3.95
"	20	-	5.86	3.29	4.09
"	21	-	5.20	3.29	4.16
$[0/\pm 45/90]_s$	15	-	4.09	8.06	3.10
"	22	9.89	4.76	8.06	3.10
"	A&B	9.03	4.05	7.89	3.05

* See Table 6 for input properties.

TABLE 8

THEORETICAL AND EXPERIMENTAL BUCKLING LOADS

Laminate	Spec No.	Experimental			Theoretical		
		P (Kips)	T+ (K-in)	T- (K-in)	P (Kips)	T+ (K-in)	T- (K-in)
Boron-Epoxy							
$[\mp 45]_s$	1	-	4.0	-	9.5	4.3	-7.3
[0]	2	12.5	-	-8.9	27.2	13.7	-13.7
[-82.5/30/20/-82.5]	3	-	-	-	8.9	7.3	-12.8
"	4	5.8	6.3	-14.3	9.8	7.7	-13.6
"	5	-	7.0	-	9.2	7.6	-13.1
"	12	-	5.0	-	9.4	7.5	-13.1
"	17	6.1	7.9	-7.5	9.1	7.3	-12.8
$[-45_2/45_2]_s$	6	13.85	20.85	-34.8	38.2	22.7	-37.6
"	19	-	16.8	-27.7	29.6	16.6	-27.7
$[0/\pm 45/90]_s$	13	30.75	-	-19.8	46.5	25.2	-21.3
"	23	19.25	20.2	-15.3	42.9	23.4	-19.8
Graphite-Epoxy							
[-82.5/30/20/-82.5]	7	-	-	-	6.8	6.1	-10.9
"	8	4.52	5.6	-11.5	7.8	6.1	-10.2
"	9	-	-	-	6.7	5.4	-9.2
"	10	-	5.1	-7.2	7.4	6.1	-10.4
$[\mp 45]_s$	11	4.1	5.22	-9.45	9.3	5.7	-9.6
"	16	-	-	-	8.9	4.5	-7.1
$[-45_2/45_2]_s$	14	12.2	17.6	-32.0	35.0	20.4	-33.0
"	18	-	19.4	-35.4	40.4	23.7	-37.8
"	20	-	18.0	-33.3	37.2	21.9	-35.2
"	21	-	19.8	-33.2	37.3	22.9	-38.1
$[0/\pm 45/90]_s$	15	-	20.4	-16.5	32.2	17.7	-14.7
"	22	22.5	17.9	-17.0	32.2	17.6	-14.6
"	A	19.25	20.2	-15.3	33.3	18.3	-15.0

theoretical values. The actual compressional buckling loads are 35-70 percent of the predicted values. Although these low values may be due in part to the conservative approach adopted during the experiments, this would not account for all the difference. In some cases, such as that shown in Fig. 6a, buckling is clearly evident at a load well below the predicted value. Thus, the results show that actual compressional buckling loads are considerably less than the theoretical values with a knock-down factor of 35-70 percent.

The results in Table 8 also show that the pure torsional buckling load of a given cylinder is very dependent upon the direction of loading. Both theoretical and experimental results show that the positive and negative values may differ by as much as a factor of 2.0. This behavior is directly related to the fiber orientation and location of the individual layers of the cylinder. If the fibers are in tension they will resist buckling, and the outmost layer has the most influence on the torsional buckling behavior of the cylinder. It is also apparent from Table 8 that some of the experimental torsional buckling loads are greater than the theoretical prediction. This is believed to be the result of inaccurate specification of the actual specimen and not a true indicator that the actual buckling load is greater than the predicted.

5.3 Combined Compression and Torsion

The results for combined loading are presented in Figs. 8-55 in the form of normalized buckling interaction diagrams. Axial loads have been normalized with respect to the experimental value P* for the buckling load under pure compression and torsional loads have been normalized with respect to the torsional buckling load T* for positive torsion. These values are listed in Table 9 along with all experimental

buckling loads. Estimated values for P* and T* were used whenever experimental values were not available. They are so indicated in Table 9.

The results are grouped by material and laminate configuration. Two figures are presented for each specimen. The first figure shows the experimental results superimposed on a cubic spline curve fit of the buckling loads predicted by the Wu program. The individual data points from the Wu program are shown in the second figure associated with each specimen. Experimental points are numbered according to the particular test number. Whenever more than one specimen of a particular configuration was tested, all experimental results for that type of specimen are shown on the first figure for that group. Close examination of the figures shows that the Wu predictions for a particular type of specimen will vary somewhat with the variable input data (Table 5). However, when plotted in normalized load space this variation is small. This is also true for laminates with the same fiber orientations, but different materials.

5.3.1 Boron-Epoxy Cylinders

5.3.1.1 The $[\bar{+}45]_S$ Laminate

The results for this specimen are shown in Figs. 8 and 9. Only three data points were obtained and it was necessary to estimate P*. The experimental results are in fairly good agreement with the theory. These results could be shifted up or down depending upon the actual value for P*. For this particular laminate, the value for negative torsion is predicted to be 1.7 times the positive value. The specimen failed during the third test. This was one of the early tests and the machine was being operated under load control. As discussed

previously this proved to be an unsatisfactory manner in which to run the tests.

5.3.1.2 The [0] Laminate

Figures 10 and 11 show the results for this laminate. Only two data points were obtained as the cylinder cracked parallel to the fibers during the pure compession test. The predicted positive and negative torsional buckling loads differ only in sign.

5.3.1.3 The [-82.5/30/20/-82.5] Laminate

This specimen is an example of a laminate which is neither balanced nor symmetric. Thus there is coupling between in-plane forces and bending moments, and also between normal and shear response. Pure compression and pure torsion were introduced to such specimens through a combination of load and stroke control. Early tests had clearly shown if the tests were run with both loading modes in stroke control the coupling effect introduced undesired loads. Figures 12 through 21 show the results for this type of specimen. The experimental results in Figure 12 represent tests on four different cylinders of this type. The line plot is from specimen No. 3 which was not tested. As indicated in the figure, there is very good agreement between theory and experiment in normalized load space. The difference in positive and negative torsion is clearly exhibited by both theory and experiment. The experimental results for individual specimens are shown in Figs. 14, 16, 18 and 20. The results shown in Fig. 18 (Specimen No. 17) were plagued by machine malfunctions which most likely account for the differences in theory and experiment. The shape of the experimental interaction diagram does, however, appear to be very similar to the predicted curve. Thus, the results may be in error by a constant factor.

5.3.1.4 The $[-45_2/45_2]_s$ Laminate

The results for this specimen are shown in Figs. 22 through 25. Only seven experimental points were obtained, and only two of these were for combined loading. Data point #8 exhibits good comparison with theory, but data point #5 indicates that the test was apparently stopped before the cylinder buckled. Analysis of numerous other tests on this specimen indicated that many tests had been stopped prior to buckling. These results are shown in Table 9. Both theory and experiment indicate a significant difference in positive and negative torsional buckling.

5.3.1.5 The $[0/\pm45/90]_s$ Laminate

Results for this quasi-isotropic laminate are shown in Figs. 26-29. As indicated in the figures there is very good agreement between theory and experiment for the normalized buckling interaction diagram. Because of the quasi-isotropic configuration of this laminate, the positive and negative torsional buckling loads are nearly the same.

5.3.2 Graphite-Epoxy Cylinders

5.3.2.1 The [-82.5/30/20/-82.5] Laminate

The results for this type of specimen are shown in Figs. 30-37. With the exception of specimen No. 10, there is good agreement between theory and experiment. Specimen No. 10 exhibited cracking and failure at relatively low loads. This may have been the result of a poor quality specimen. The theoretical buckling interaction diagram for this quasi-isotropic laminate is very similar to the curve for the quasi-isotropic boron-epoxy laminate.

5.3.2.2 The $[\mp45]_s$ Laminate

Theoretical predictions for this type of specimen are shown in Figs.

38-41. Only one specimen was tested and those results are shown in Fig. 38. Again, the correlation between theory and experiment is quite good.

5.3.2.3 The $[-45_2/45_2]_s$ Laminate

The results for this laminate are shown in Figs. 42-49. All four specimens were tested in positive and negative torsion, but only one specimen was tested under combined loading. All experimental results compare very well with the theoretical predictions.

5.3.2.4 The $[0/\pm45/90]_s$ Laminate

The results for this laminate are shown in Figs. 50-55. The results for specimens A and B are shown on one figure as these tests were conducted at Langley Research Center before any tests were conducted at VPI&SU. The composite of all experimental results in Fig. 50 indicates good comparison between theroy and experiment.

6. CONCLUSIONS

The following conclusions can be drawn from the investigation of the correlation between theoretical and experimental buckling loads for composite cylinders under compression, torsion, and combined compression-torsion:

1. The Wu theory gives very accurate predictions of the torsional buckling loads for both positive and negative torsion.
2. The pure torsional buckling load is a function of the loading direction and may vary by as much as a factor of 2.0.
3. The Wu theory overestimates the buckling load for pure compression; the knock-down factor for the specimens tested ranged from 35-70 percent.
4. The Wu theory compares very favorably with experimental results for buckling under combined compression-torsion when compared in normalized load space.

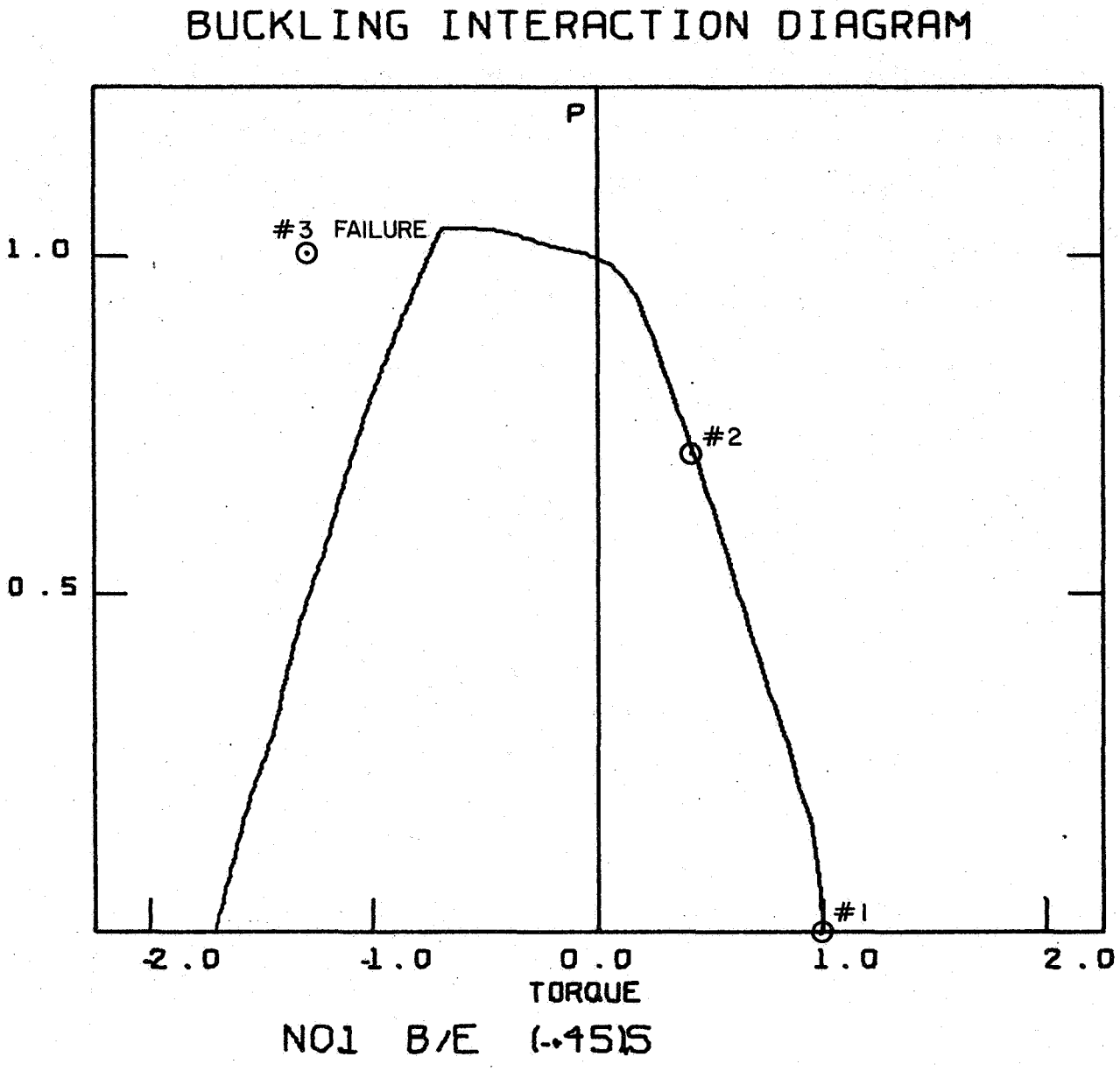

MAX TORQUE/COMPRESSION VALUES

T (+)		T (-)		P	
1271.9	LB-IN	-7289.4	LB-IN	9506.0	LB
182.6	N-M	-823.5	N-M	42284.9	N

Fig. 8. Line Interaction Diagram - Spec. #1 $[\mp 45]_S$ B/E

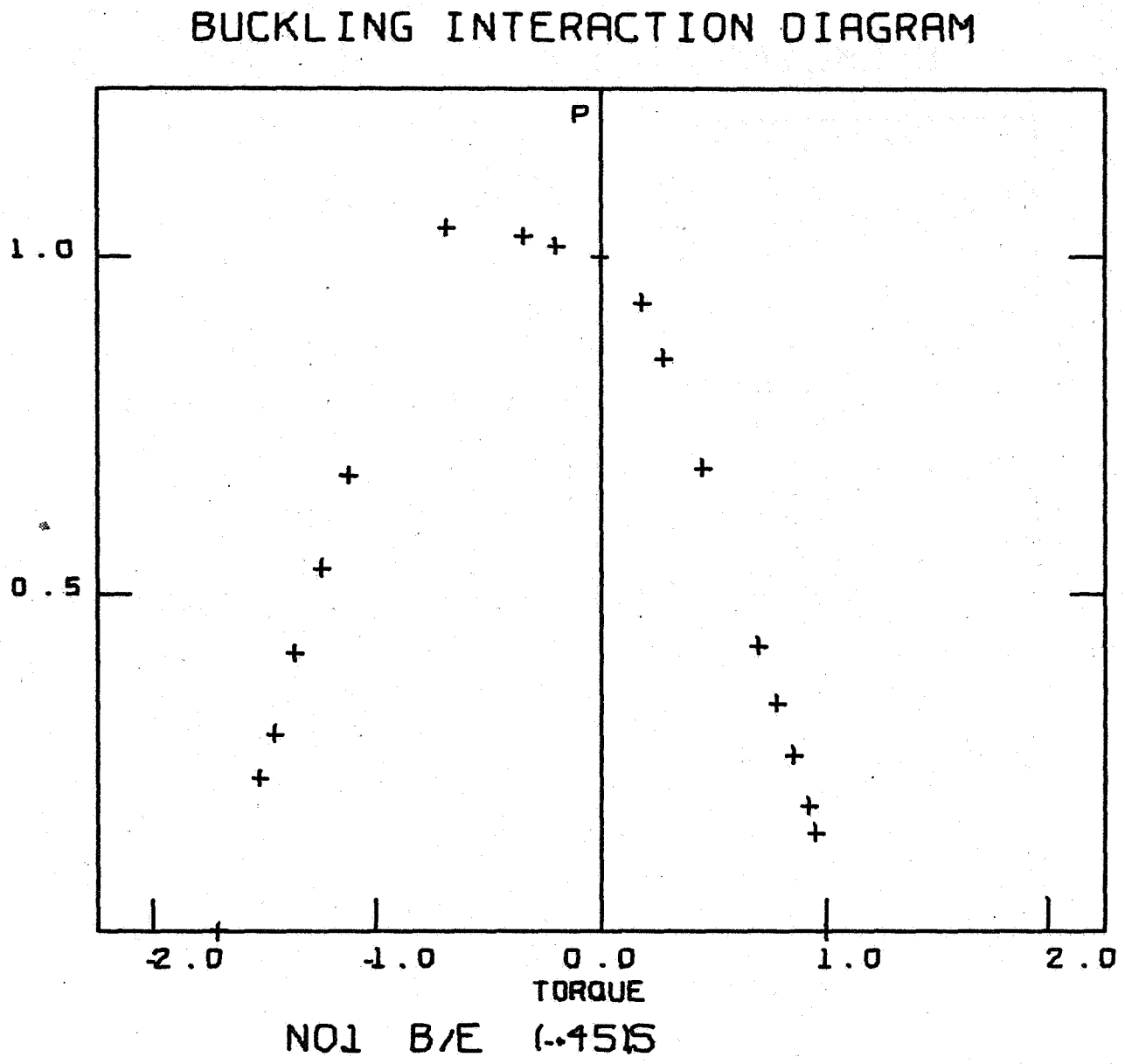

MAX TORQUE/COMPRESSION VALUES

T (+)		T (-)		P	
4271.9	LB-IN	-7289.4	LB-IN	9506.0	LB
482.6	N-M	-823.5	N-M	42284.9	N

Fig. 9. Point Interaction Diagram - Spec. #1 $[\mp 45]_S$ B/E

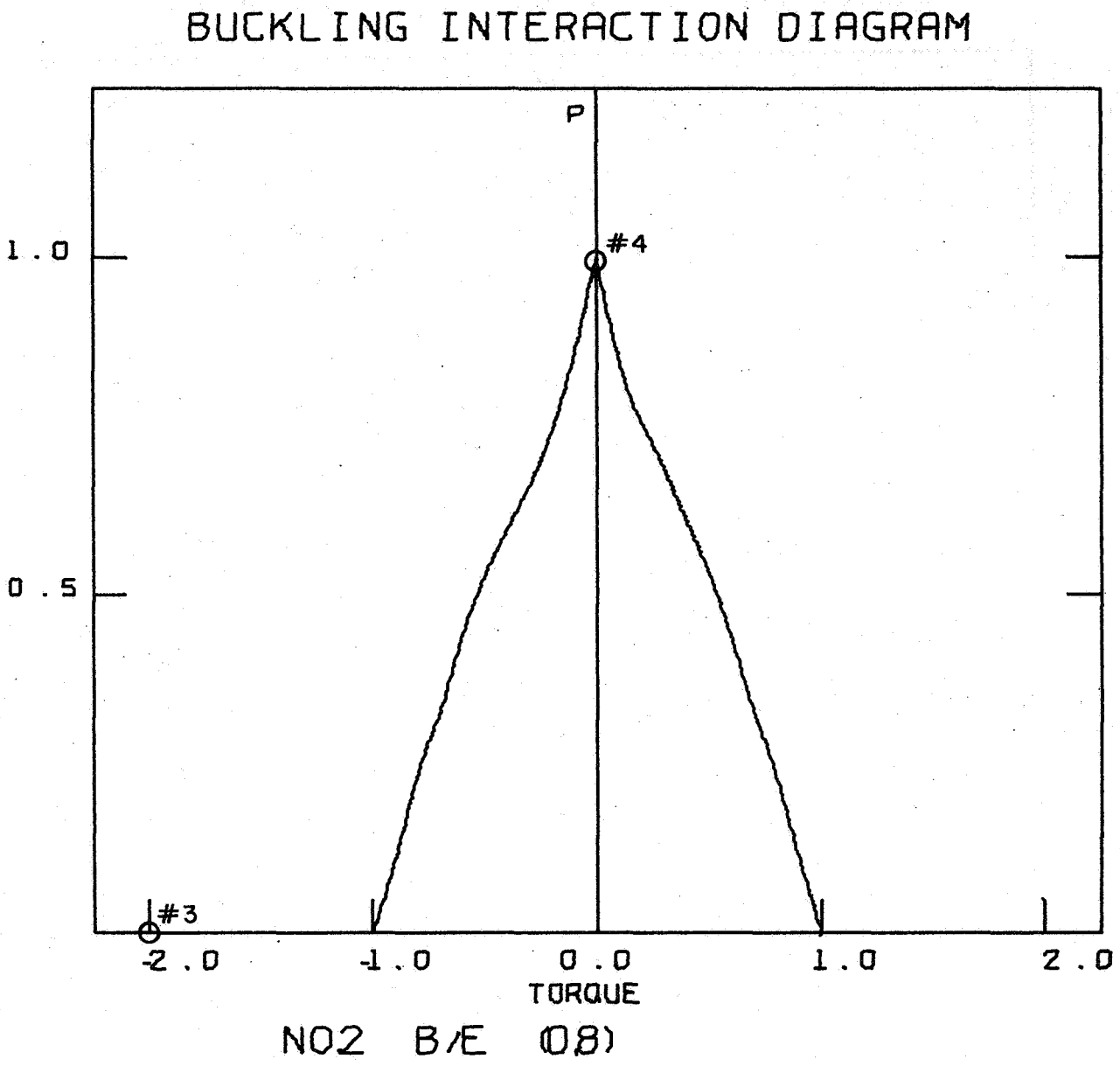

MAX TORQUE/COMPRESSION VALUES

T (+)		T (-)		P	
13679.6	LB-IN	-13679.6	LB-IN	27208.2	LB
1545.5	N-M	-1545.5	N-M	121028.4	N

Fig. 10. Line Interaction Diagram - Spec. #2 [0_8] B/E

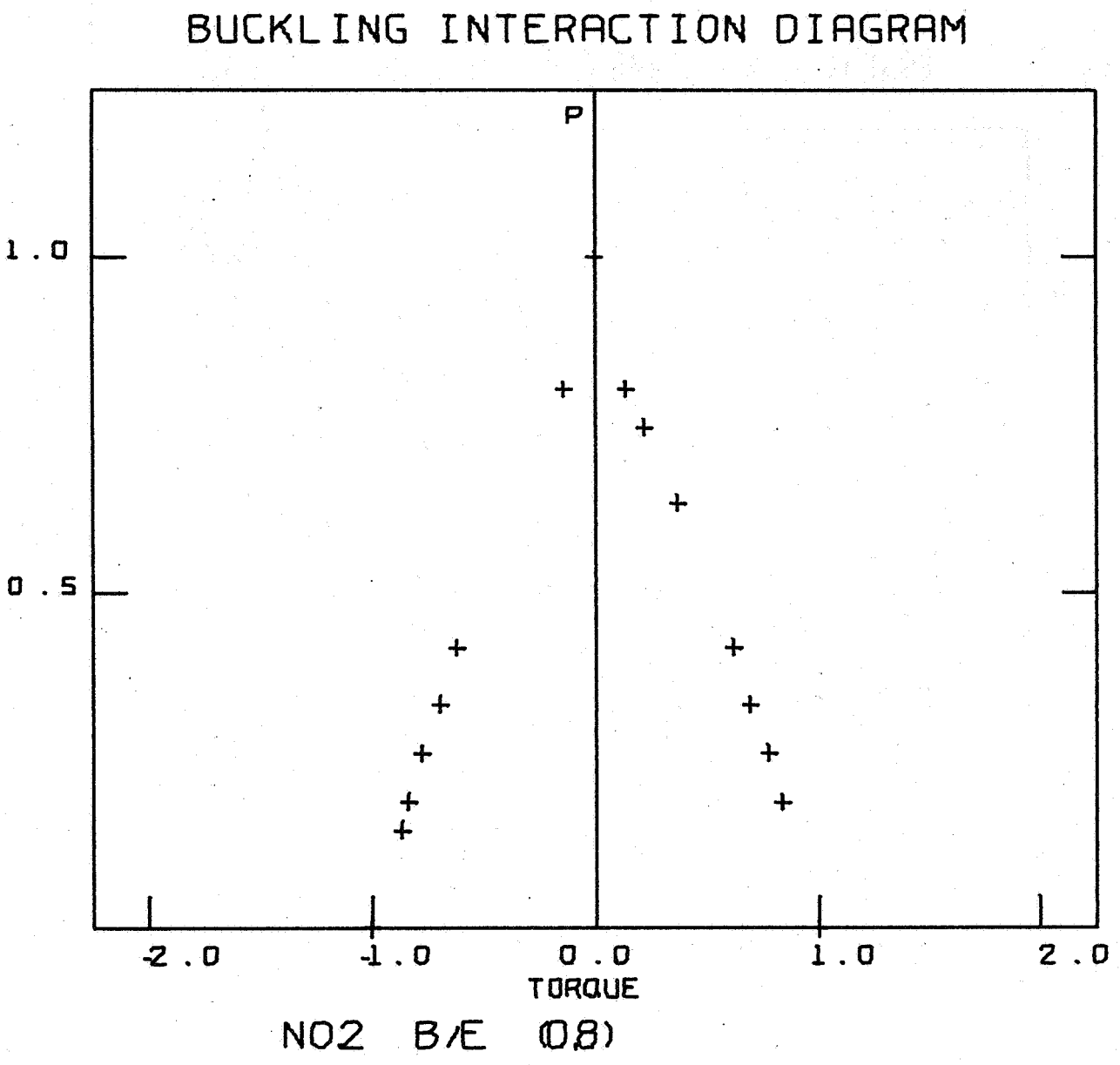

MAX TORQUE/COMPRESSION VALUES

T (+)		T (-)		P	
13679.6	LB-IN	-13879.6	LB-IN	27208.2	LB
1545.5	N-M	-1545.5	N-M	121028.4	N

Fig. 11. Point Interaction Diagram - Spec. #2 [0_8] B/E

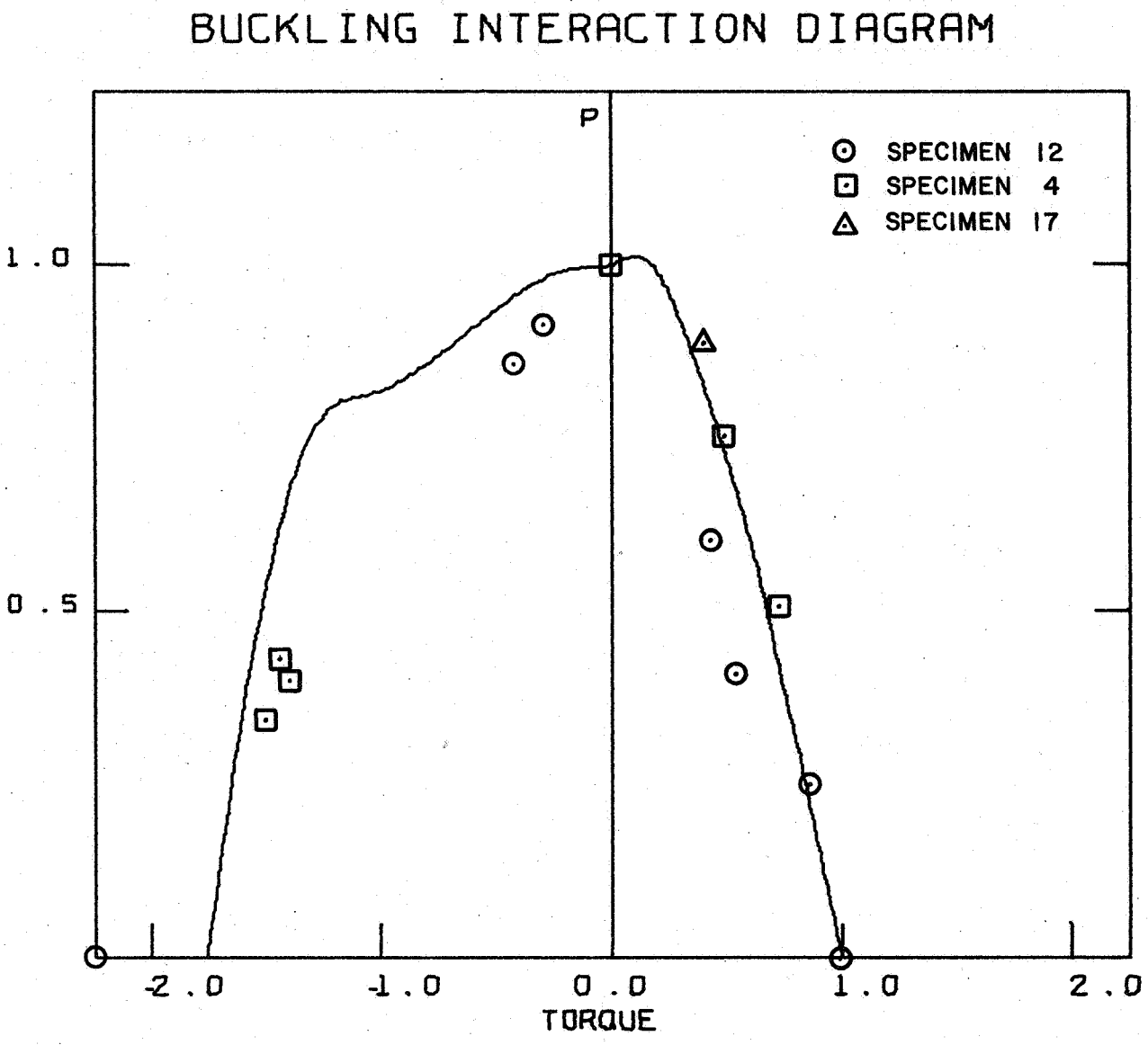

MAX TORQUE/COMPRESSION VALUES

T (+)		T (-)		P	
7273.9	LB-IN	-12775.5	LB-IN	8903.8	LB
821.8	N-M	-1443.4	N-M	39606.3	N

Fig. 12. Line Interaction Diagram - Spec. #3 [-82.5/30/20/-82.5] B/E

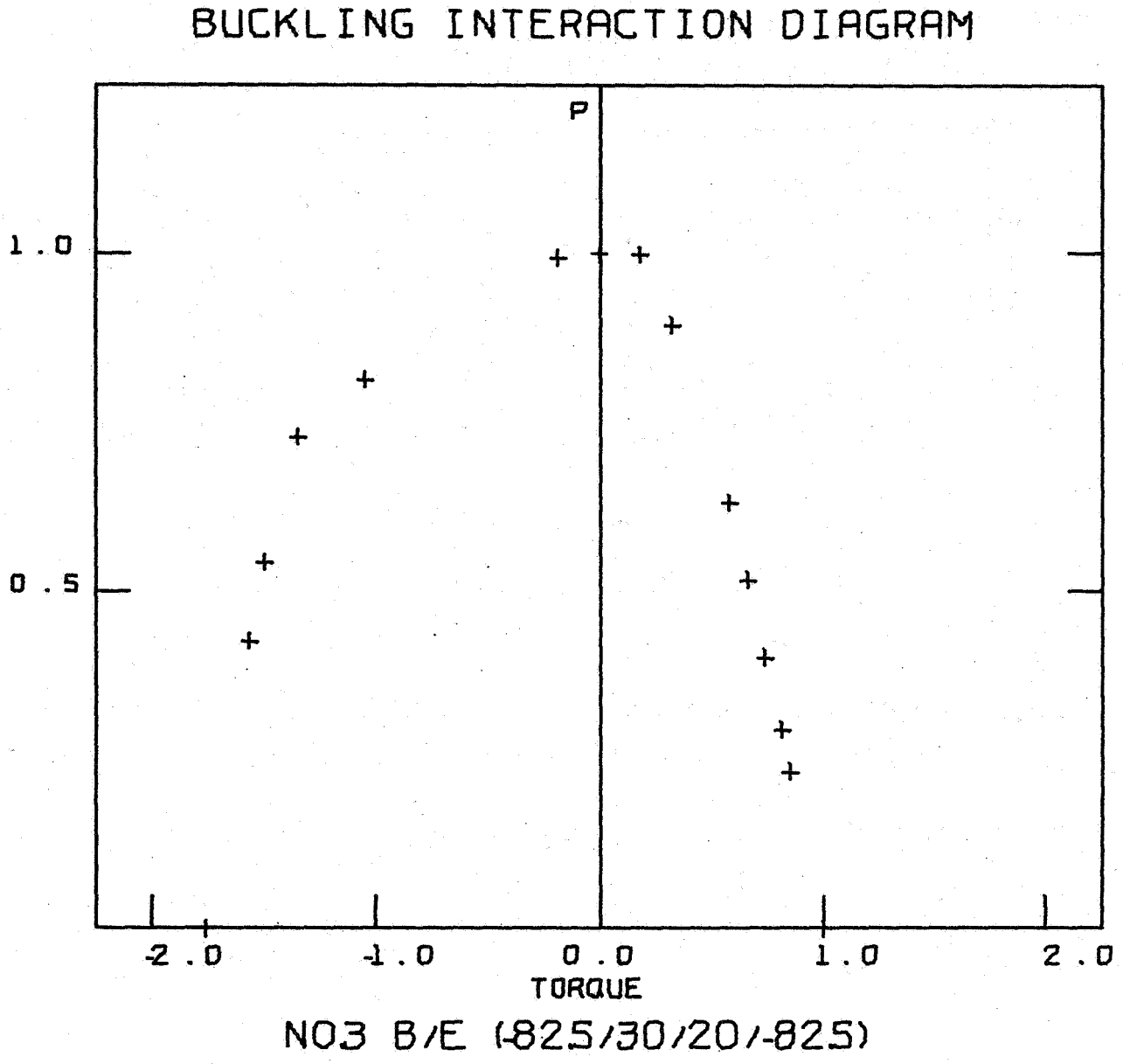

MAX TORQUE/COMPRESSION VALUES

T (+)		T (-)		P	
7273.9	LB-IN	-12775.5	LB-IN	8903.8	LB
821.8	N-M	-1443.4	N-M	39606.3	N

Fig. 13. Point Interaction Diagram - Spec #3 [-82.5/30/20/-82.5] B/E

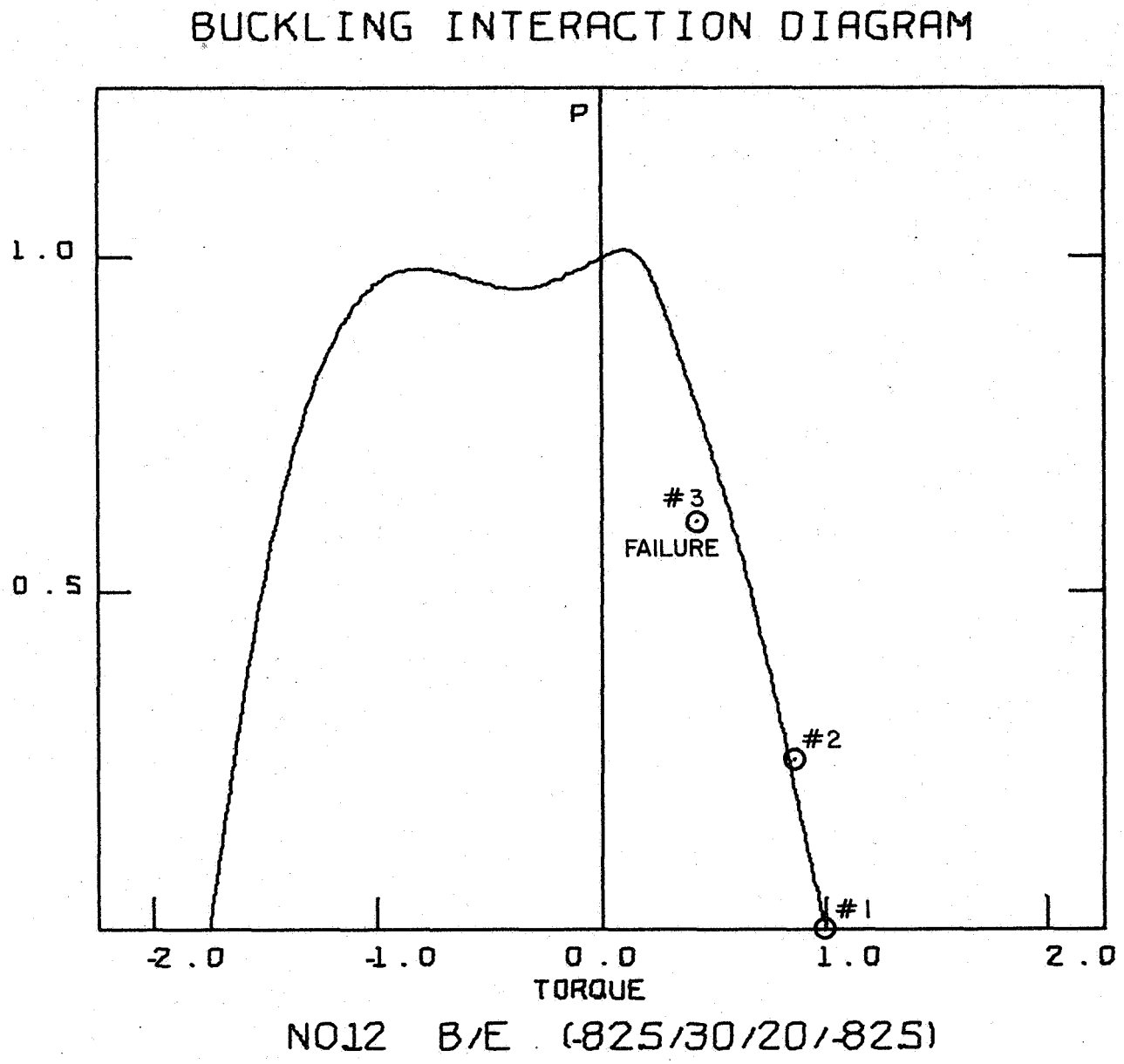

Fig. 14. Line Interaction Diagram - Spec. #12 [-82.5/30/20/-82.5] B/E

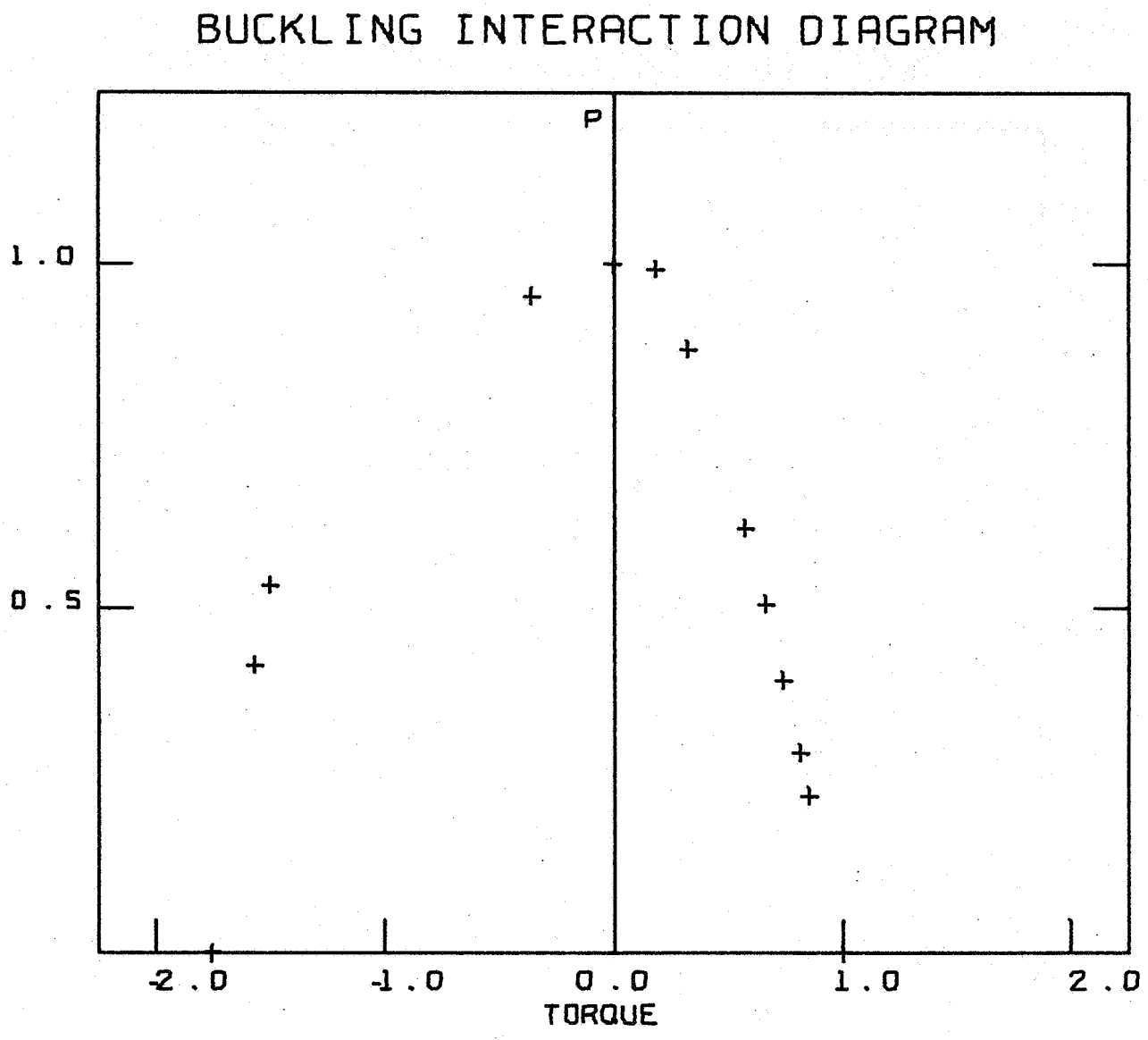

MAX TORQUE/COMPRESSION VALUES

T (+)		T (-)		P	
7499.1	LB-IN	-13121.8	LB-IN	9368.8	LB
847.2	N-M	-1482.5	N-M	41674.8	N

Fig. 15. Point Interaction Diagram - Spec #12 [-82.5/30/20/-82.5] B/E

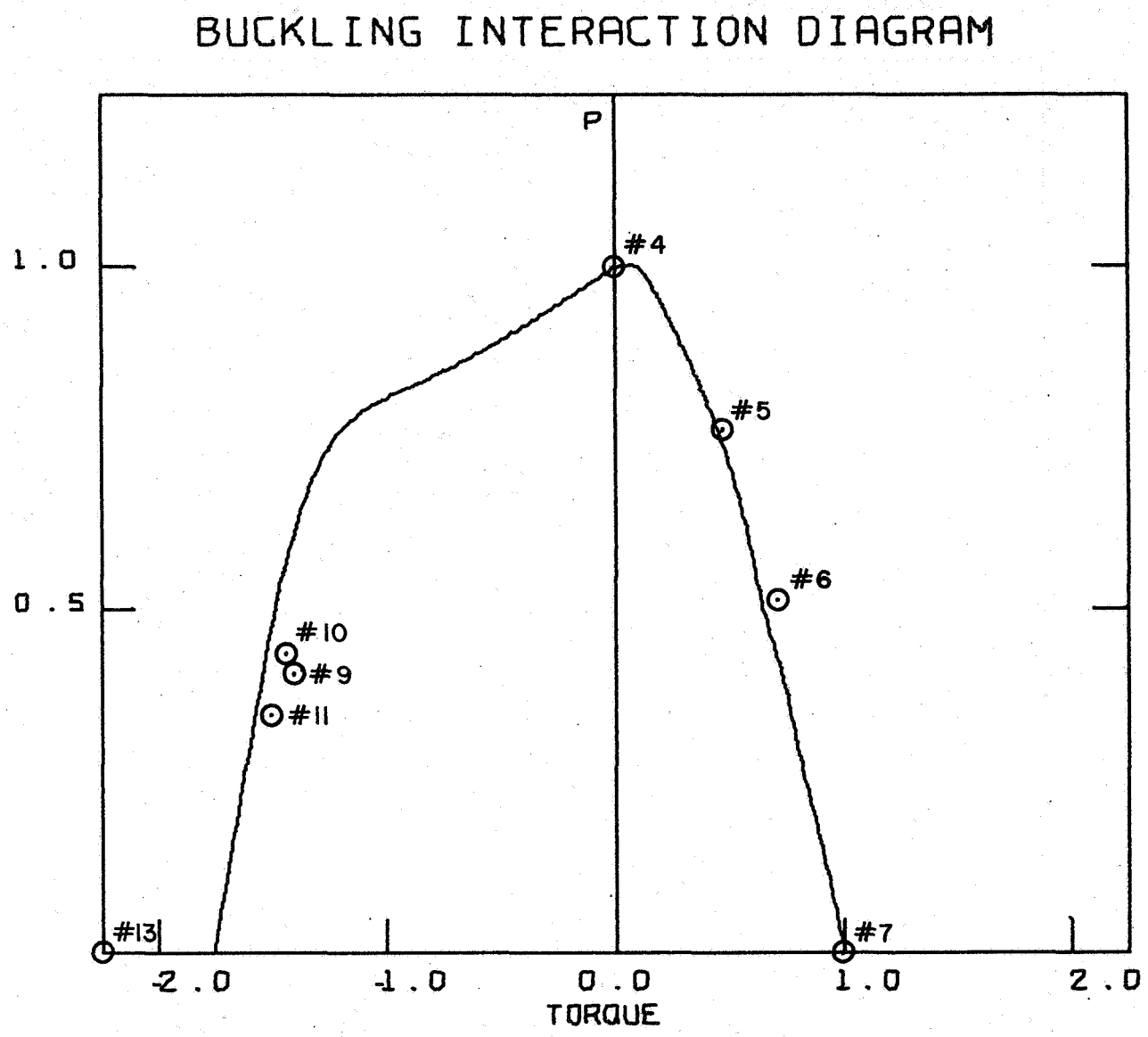

Fig. 16. Line Interaction Diagram - Spec. #4 [-82.5/30/20/-82.5] B/E

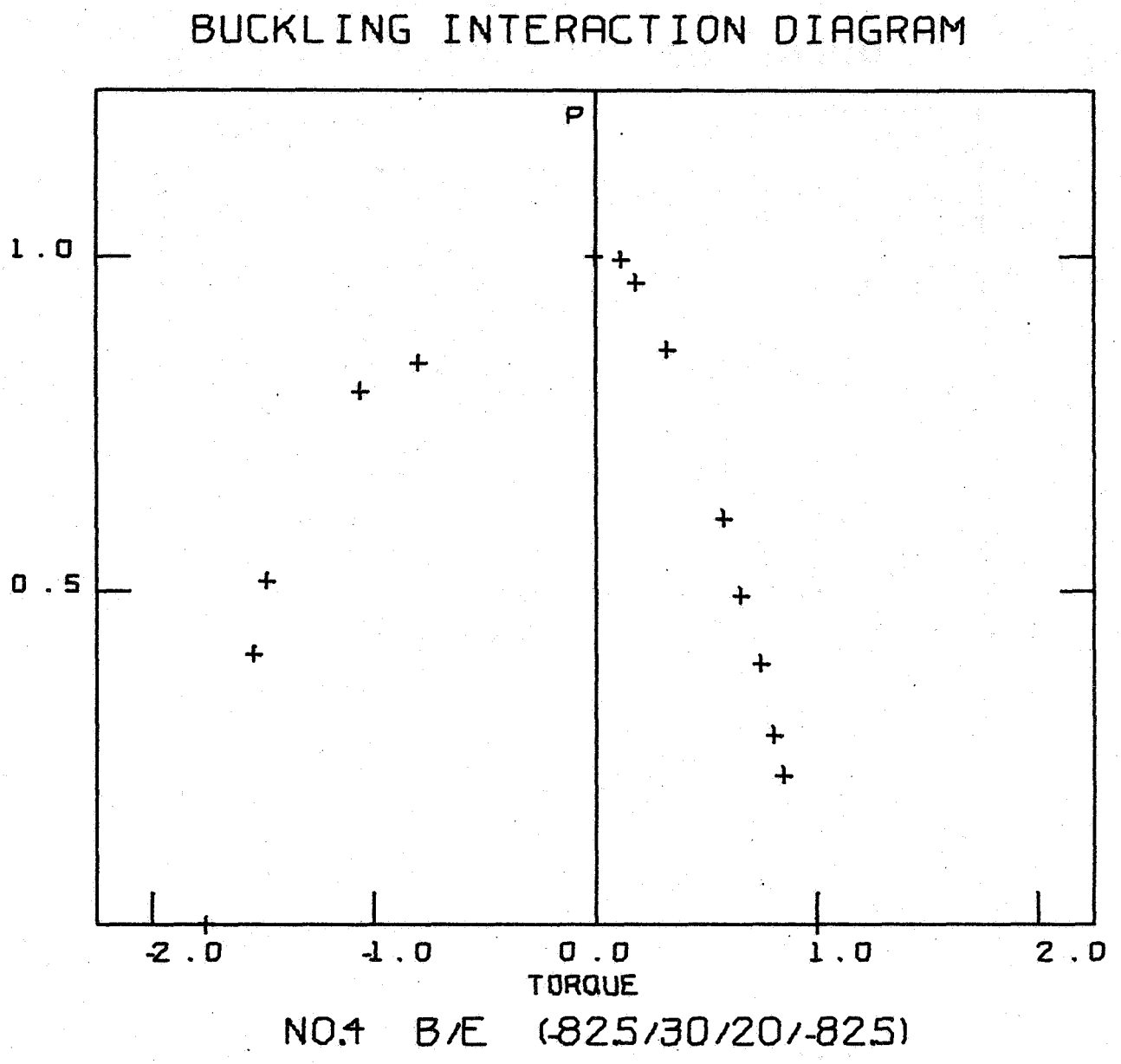

MAX TORQUE/COMPRESSION VALUES

T (+)		T (-)		P	
7746.1	LB-IN	-13632.2	LB-IN	9819.6	LB
875.1	N-M	-1540.2	N-M	43679.8	N

Fig. 17. Point Interaction Diagram - Spec #4 [-82.5/30/20/-82.5] B/E

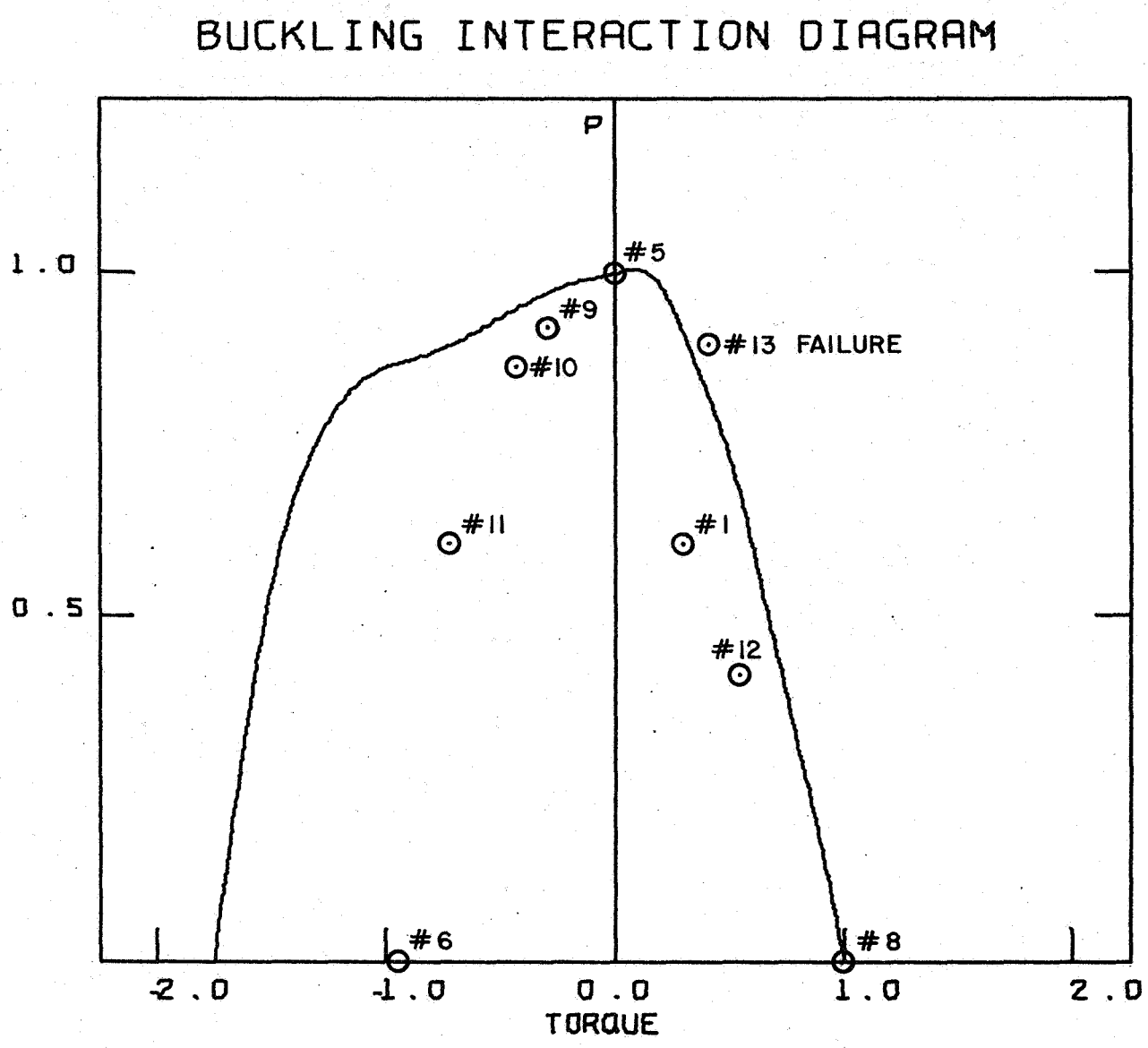

Fig. 18. Line Interaction Diagram - Spec. #17 [-82.5/30/20/-82.5] B/E

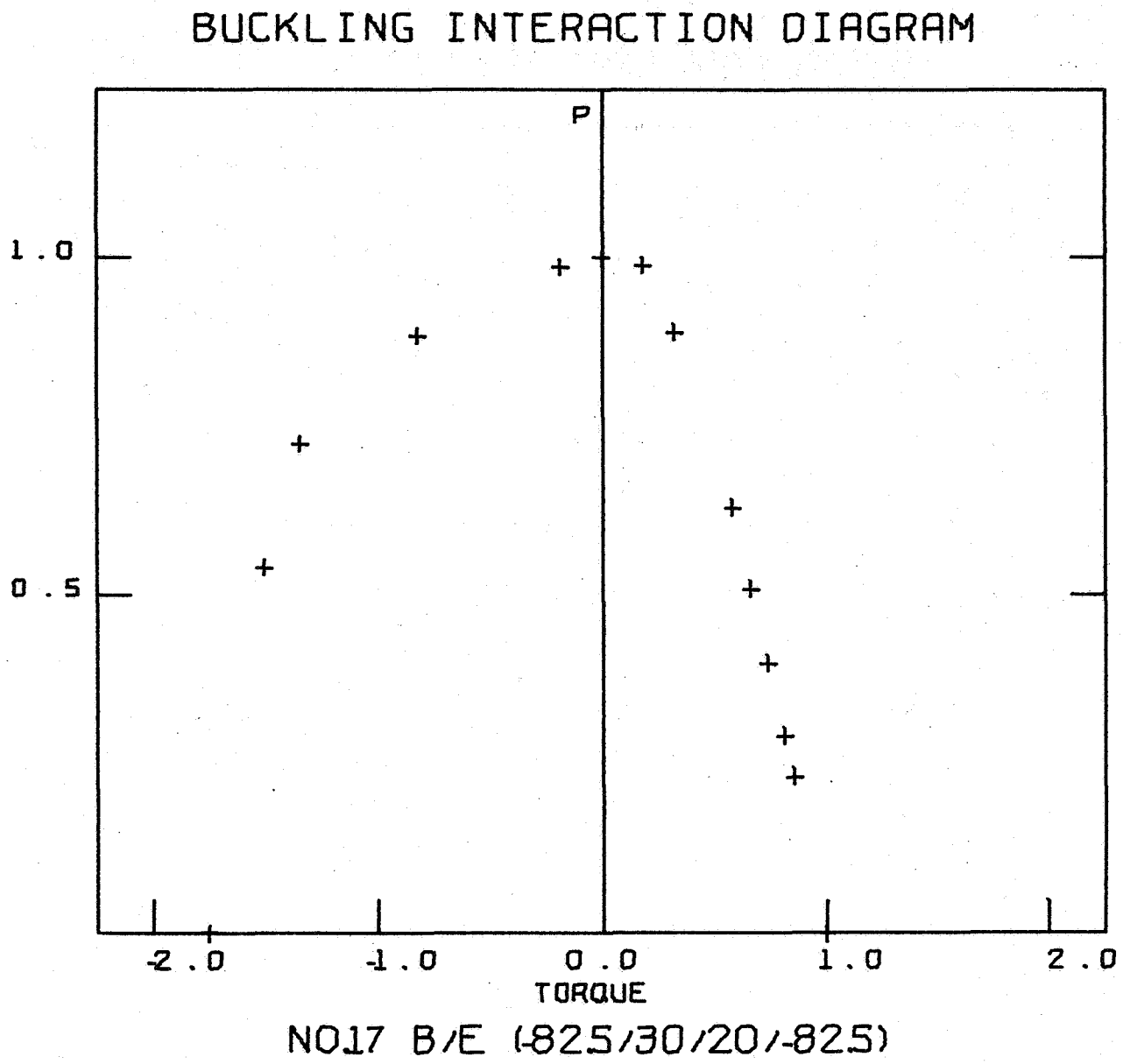

Fig. 19. Point Interaction Diagram - Spec #17 [-82.5/30/20/-82.5] B/E

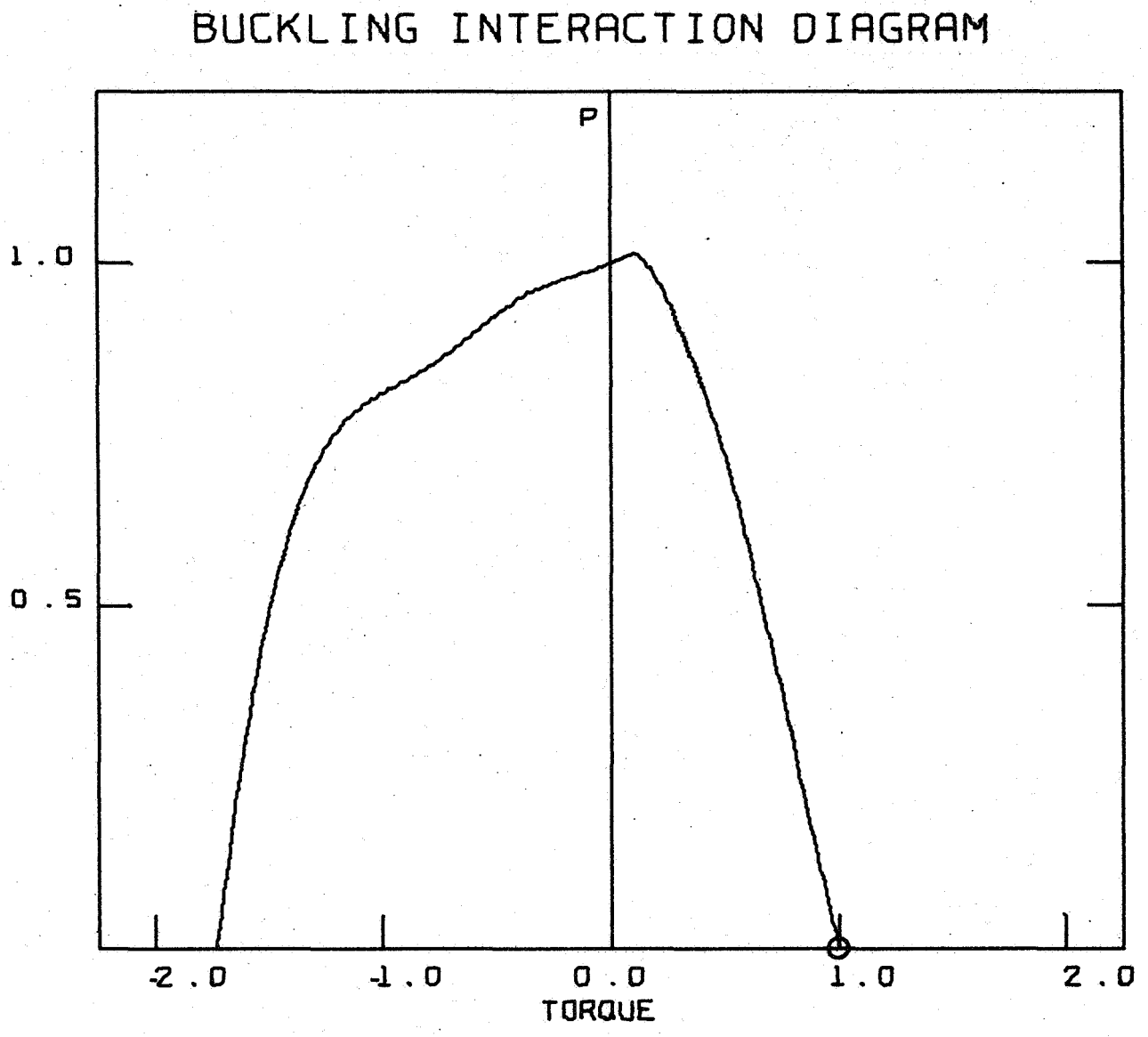

Fig. 20. Line Interaction Diagram - Spec. #5 [-82.5/30/20/-82.5] B/E

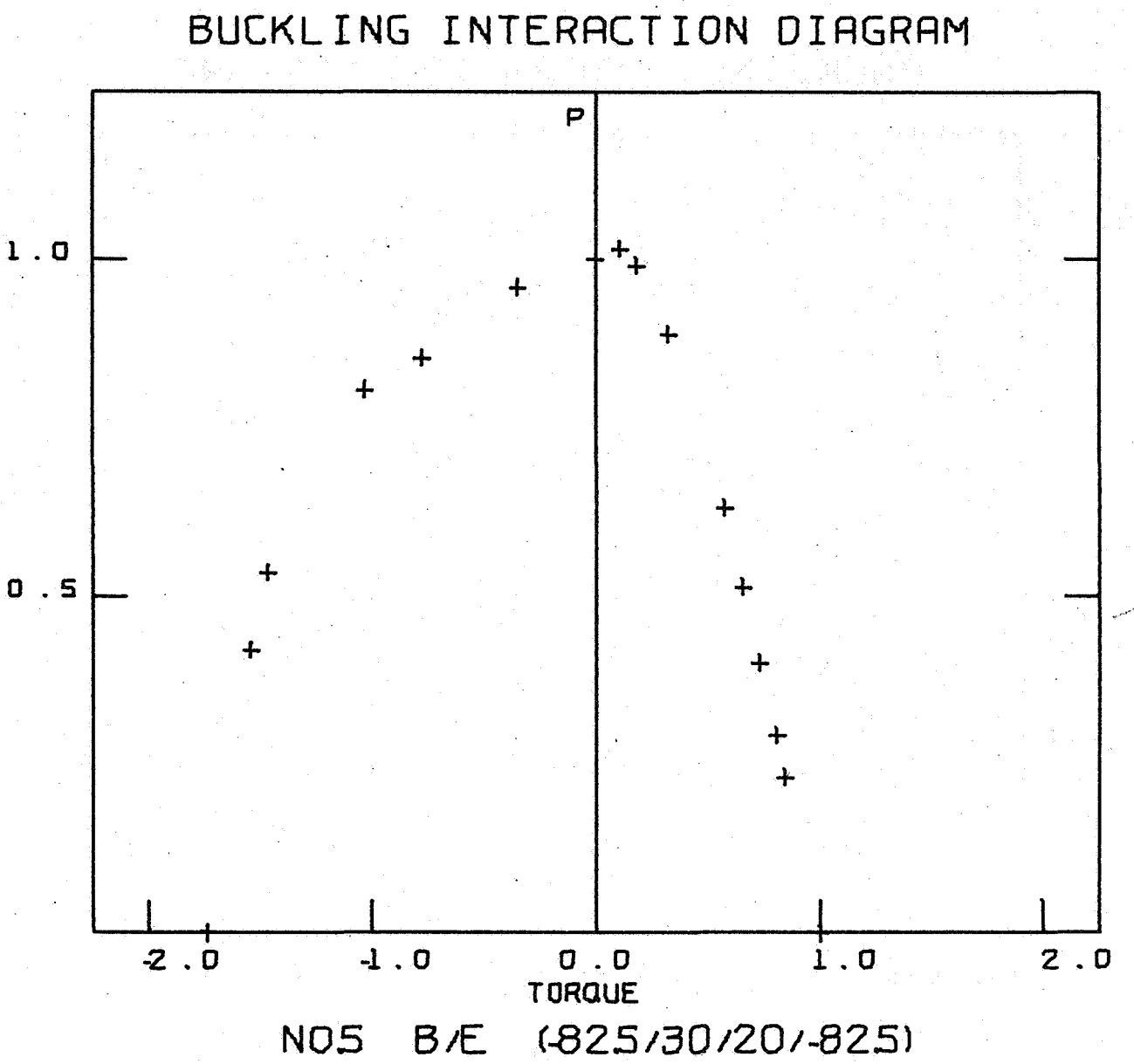

MAX TORQUE/COMPRESSION VALUES

T (+)		T (-)		P	
7579.0	LB-IN	-13133.0	LB-IN	9208.5	LB
856.3	N-M	-1483.8	N-M	40961.5	N

Fig. 21. Point Interaction Diagram - Spec #5 [-82.5/30/20/-82.5] B/E

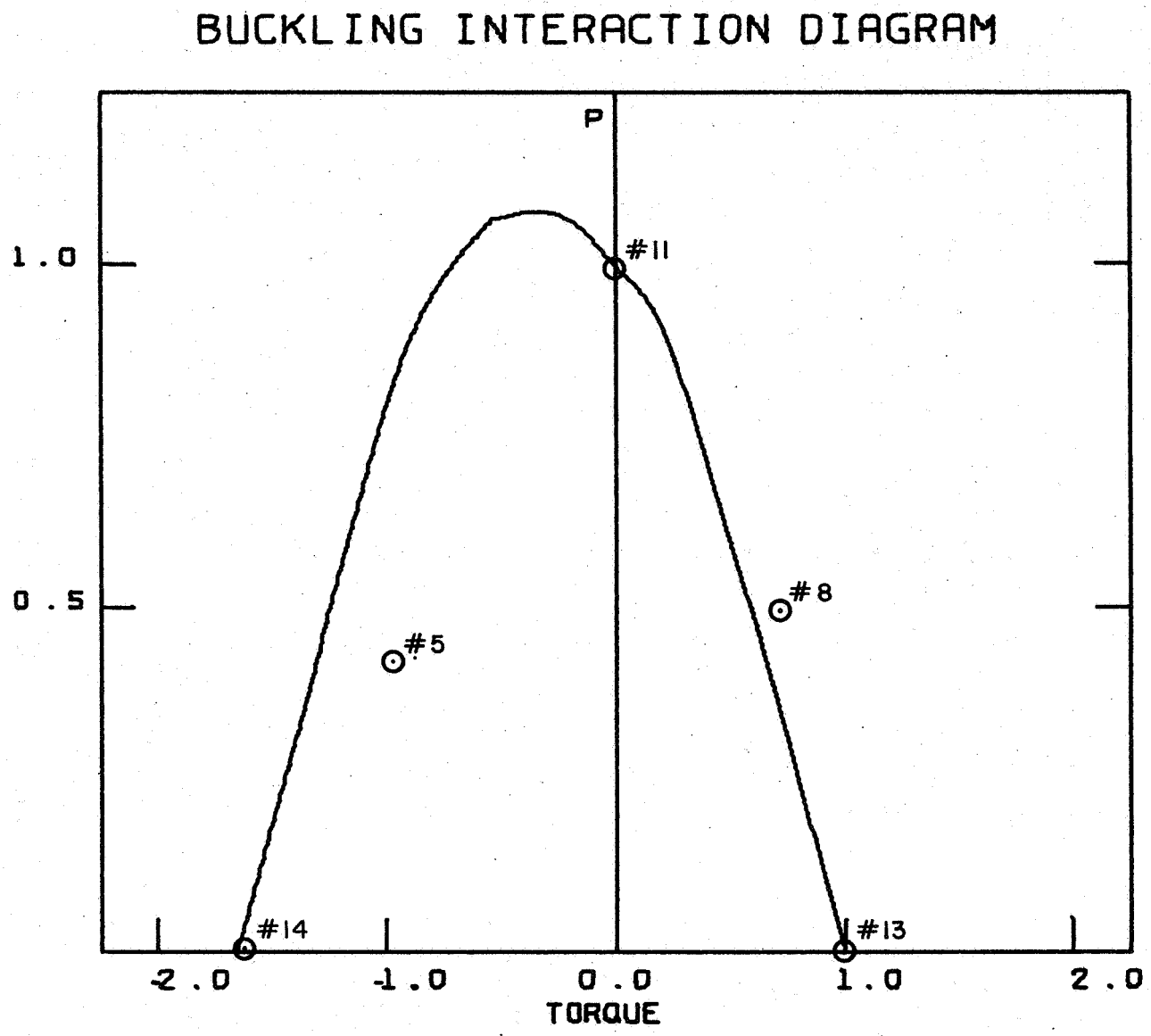

Fig. 22. Line Interaction Diagram - Spec. #6 $[-45_2/45_2]_S$ B/E

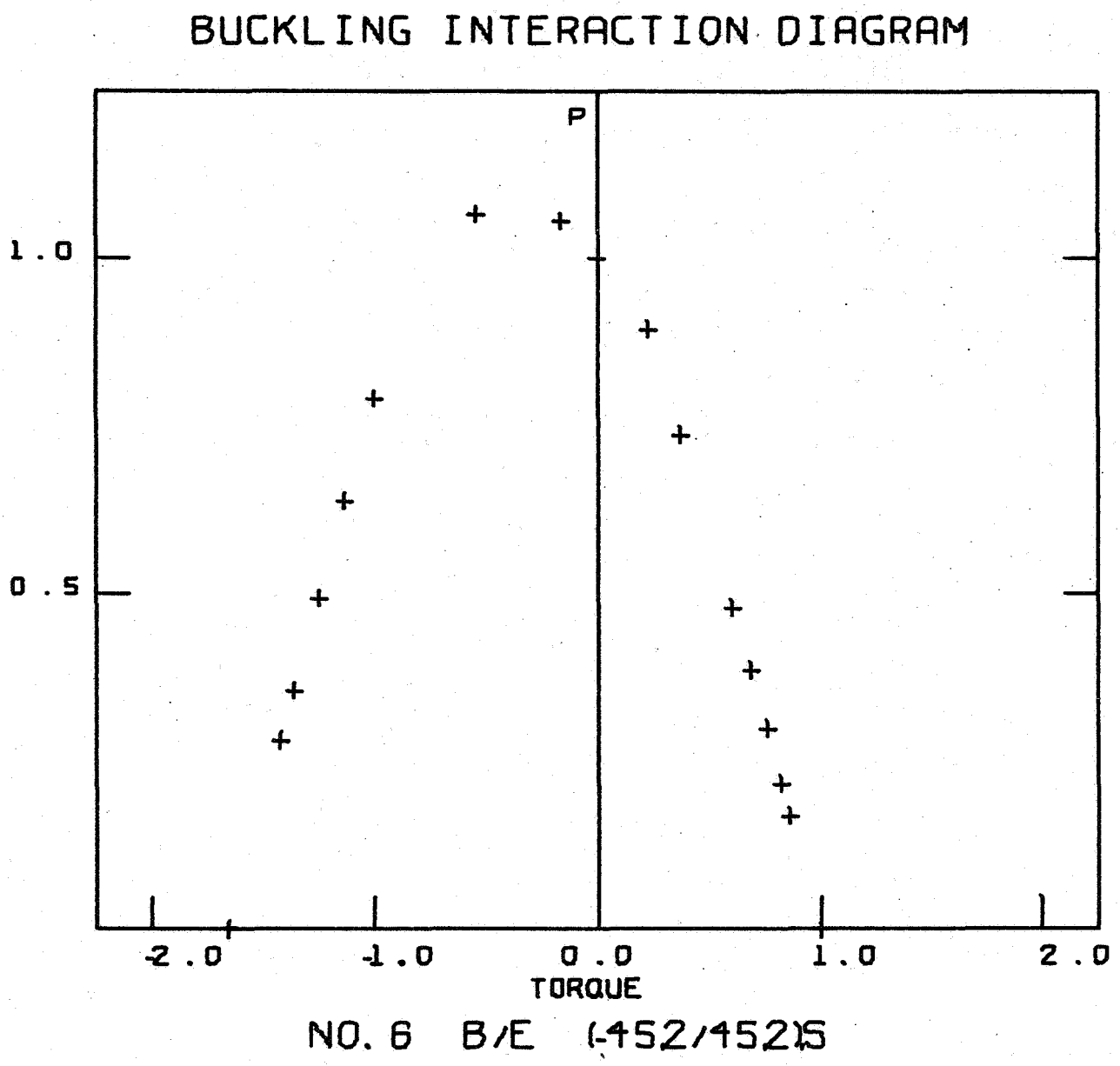

Fig. 23. Point Interaction Diagram - Spec. #6 $[-45_2/45_2]_s$ B/E

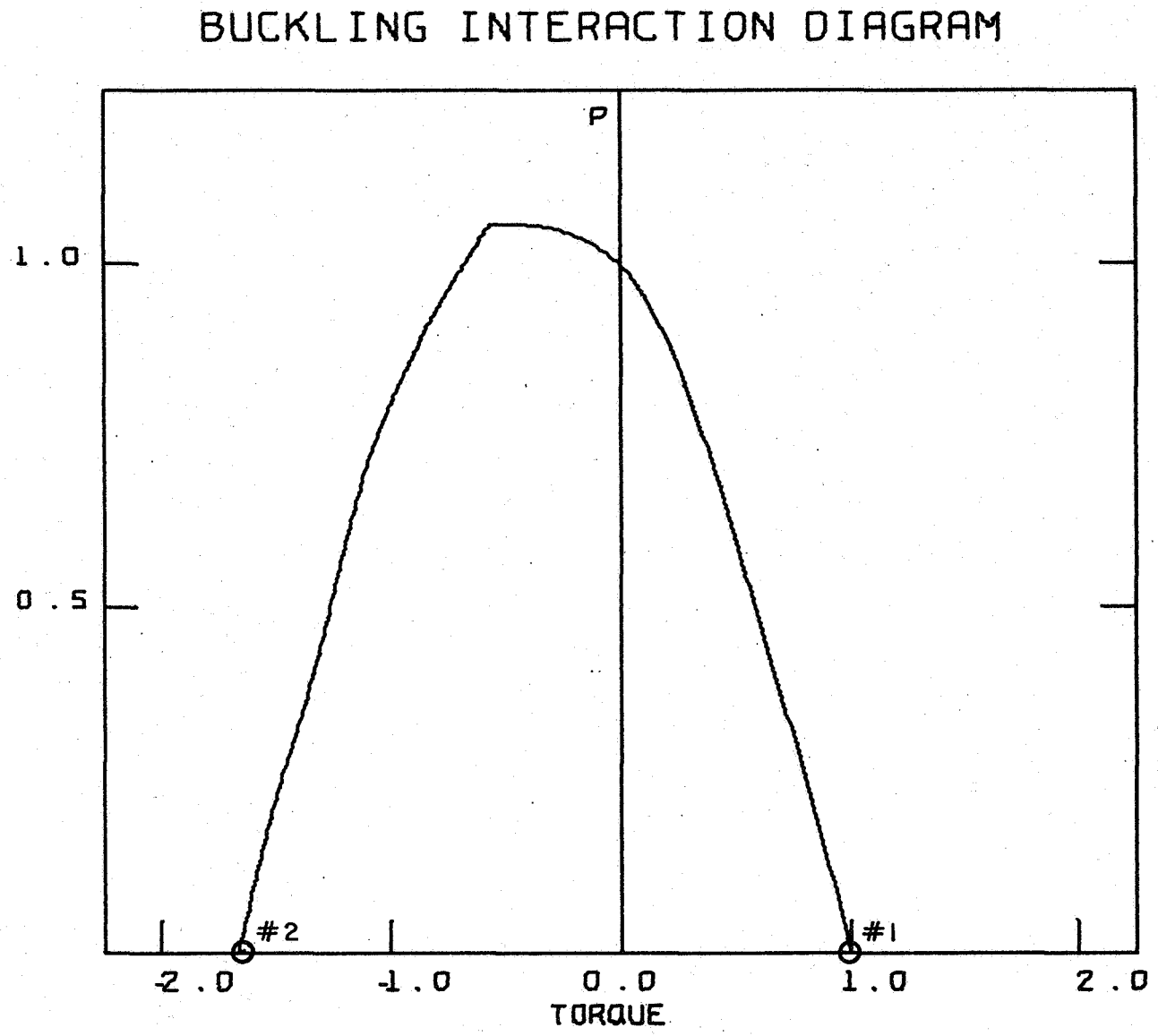

MAX TORQUE/COMPRESSION VALUES

T (+)		T (-)		P	
16619.7	LB-IN	-27746.3	LB-IN	29631.2	LB
1877.7	N-M	-3134.9	N-M	131806.2	N

Fig. 24. Line Interaction Diagram - Spec. #19 [-82.5/30/20/-82.5] B/E

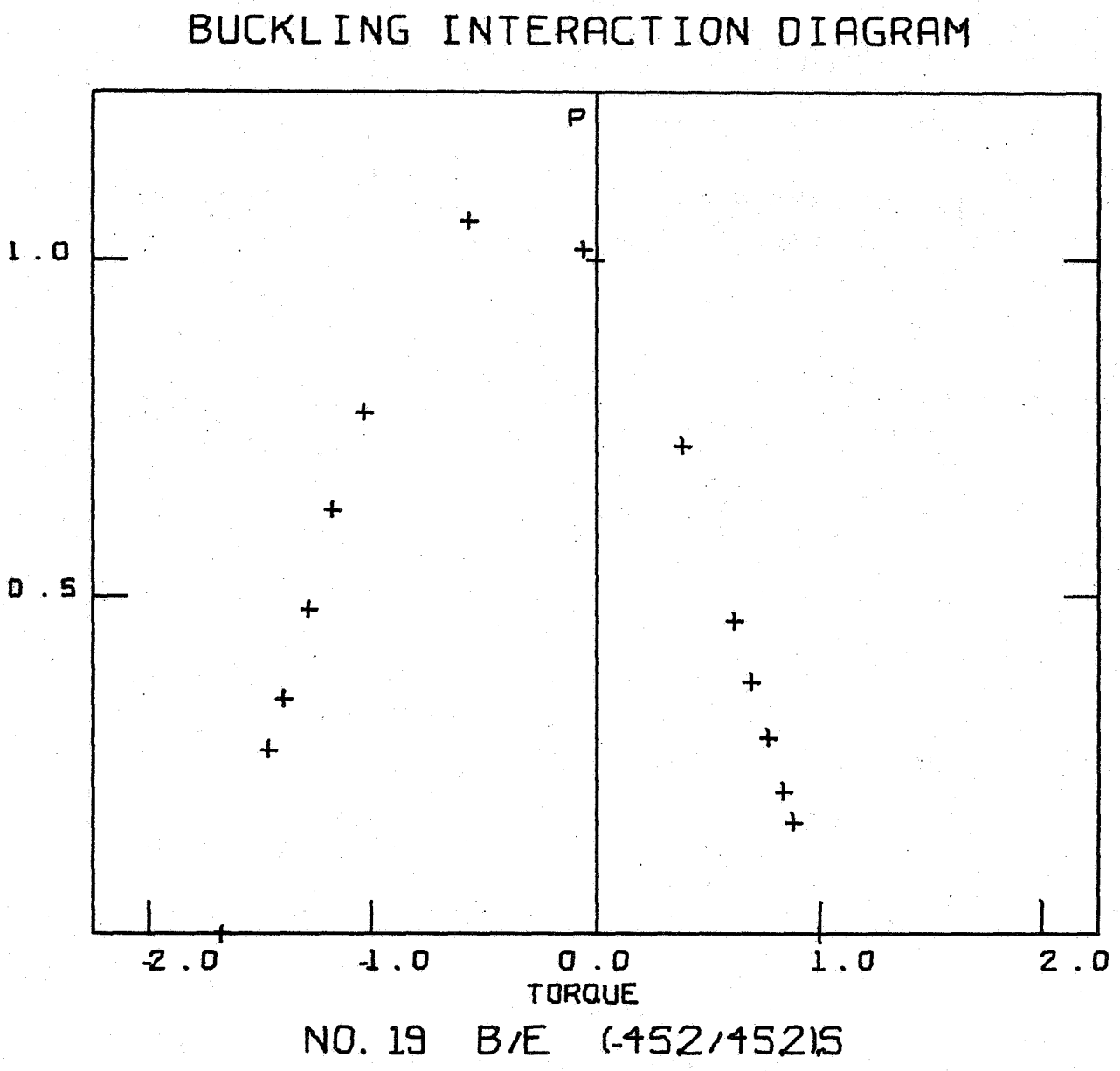

MAX TORQUE/COMPRESSION VALUES

T (+)		T (-)		P	
16619.7	LB-IN	-27746.3	LB-IN	29631.2	LB
1877.7	N-M	-3134.9	N-M	131806.2	N

Fig. 25. Point Interaction Diagram - Spec #19 $[-45_2/45_2]_s$ B/E

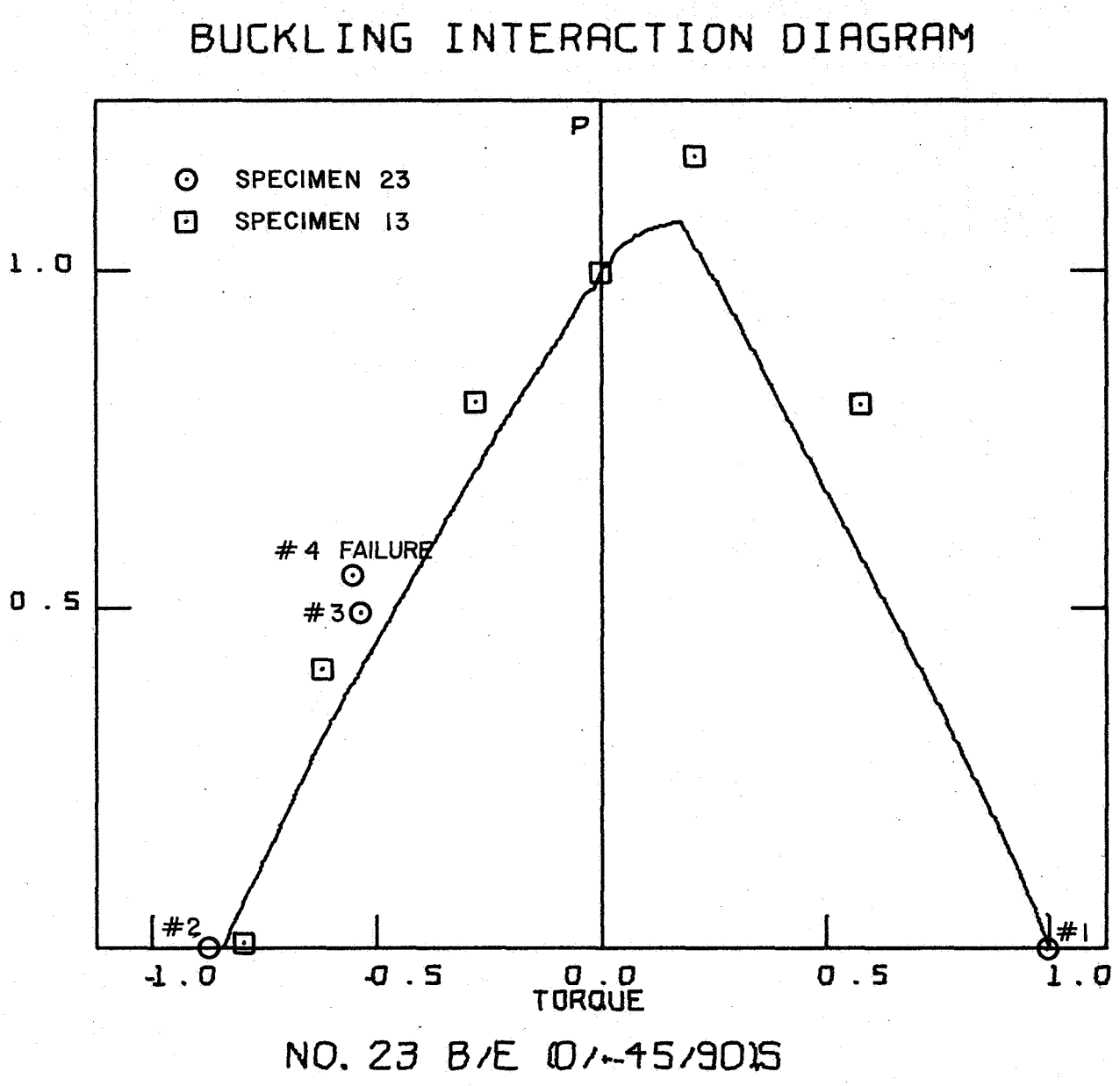

Fig. 26. Line Interaction Diagram - Spec. #23 $[0/\pm45/90]_S$ B/E

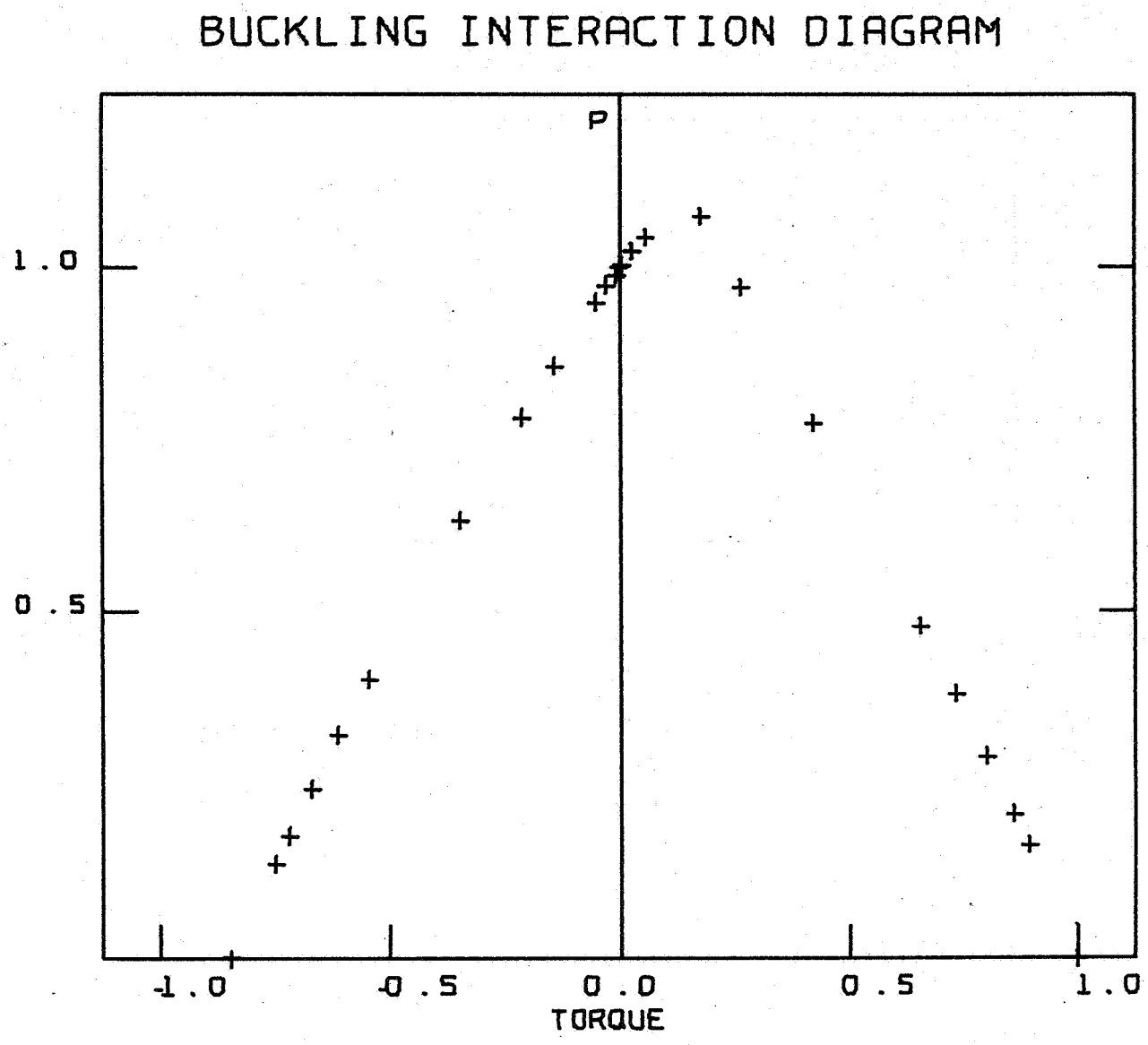

Fig. 27. Point Interaction Diagram - Spec #23 $[0/\pm45/90]_S$ B/E

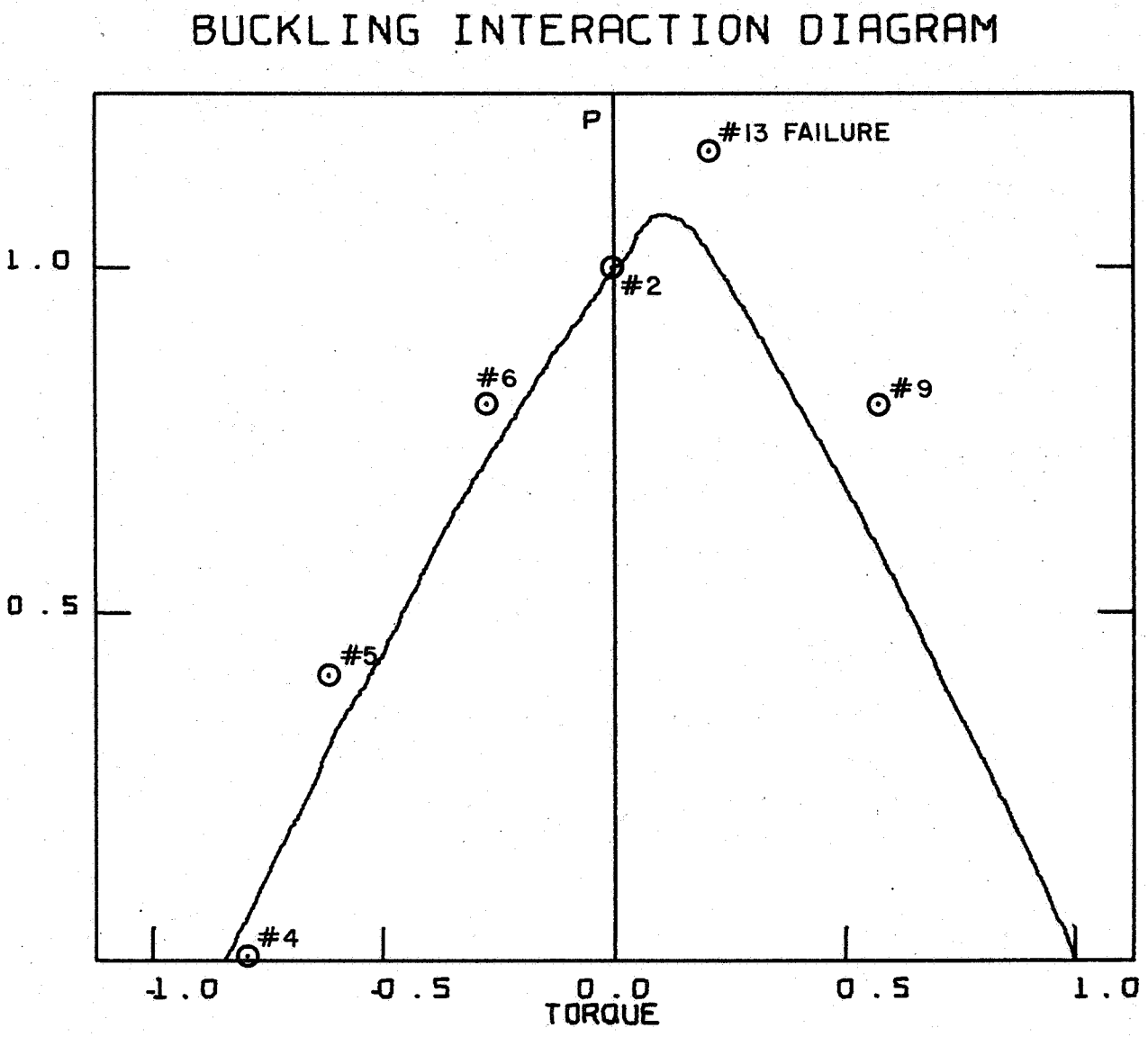

MAX TORQUE/COMPRESSION VALUES

T (+)		T (-)		P	
25230.5	LB-IN	-21285.1	LB-IN	46509.3	LB
2850.6	N-M	-2404.8	N-M	206884.0	N

Fig. 28. Line Interaction Diagram - Spec. #13 $[0/\pm45/90]_s$ B/E

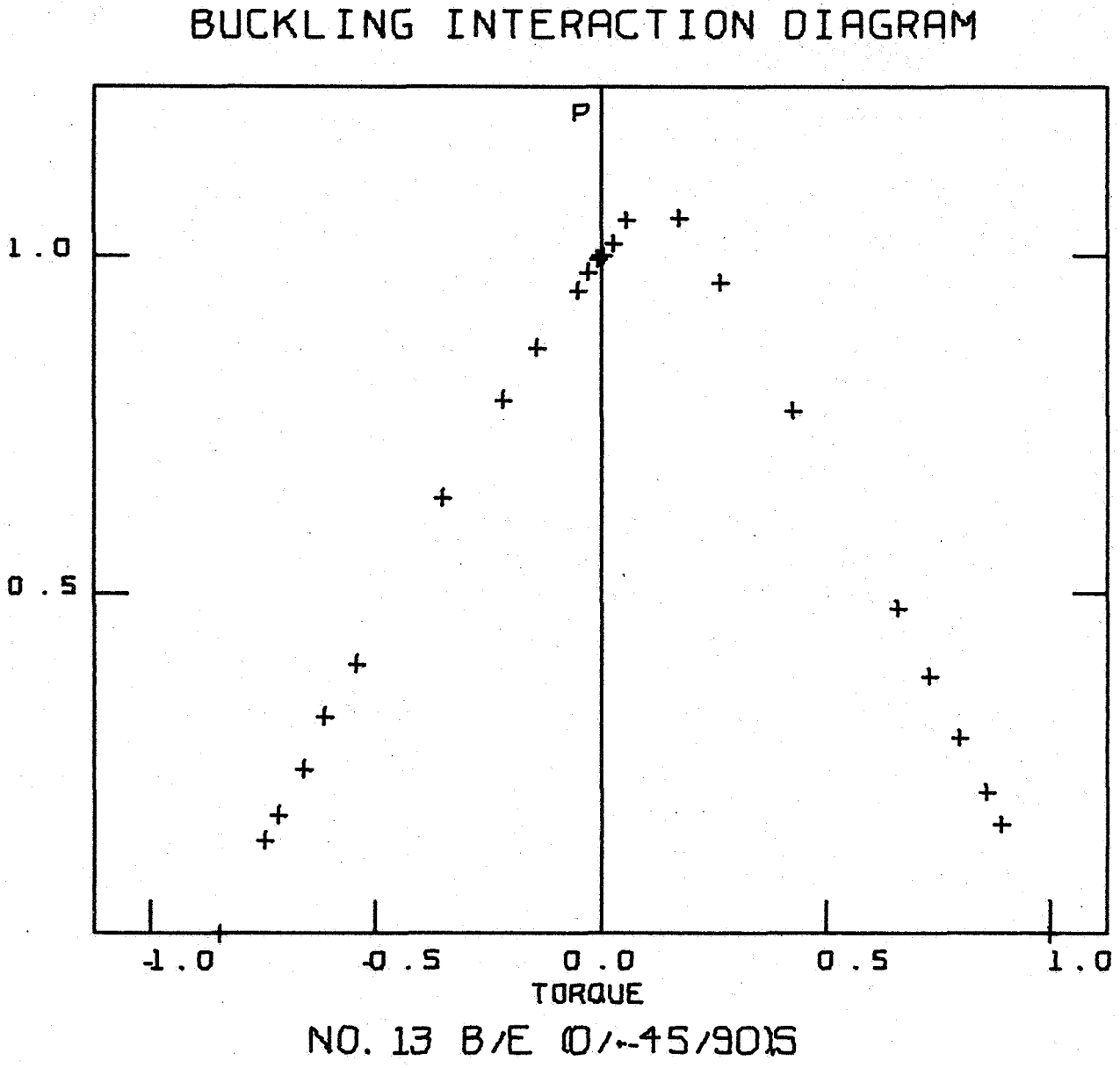

MAX TORQUE/COMPRESSION VALUES

T (+)		T (-)		P	
25230.5	LB-IN	-21285.1	LB-IN	46509.3	LB
2850.6	N-M	-2404.8	N-M	206884.0	N

Fig. 29. Point Interaction Diagram - Spec #13 $[0/\pm45/90]_S$ B/E

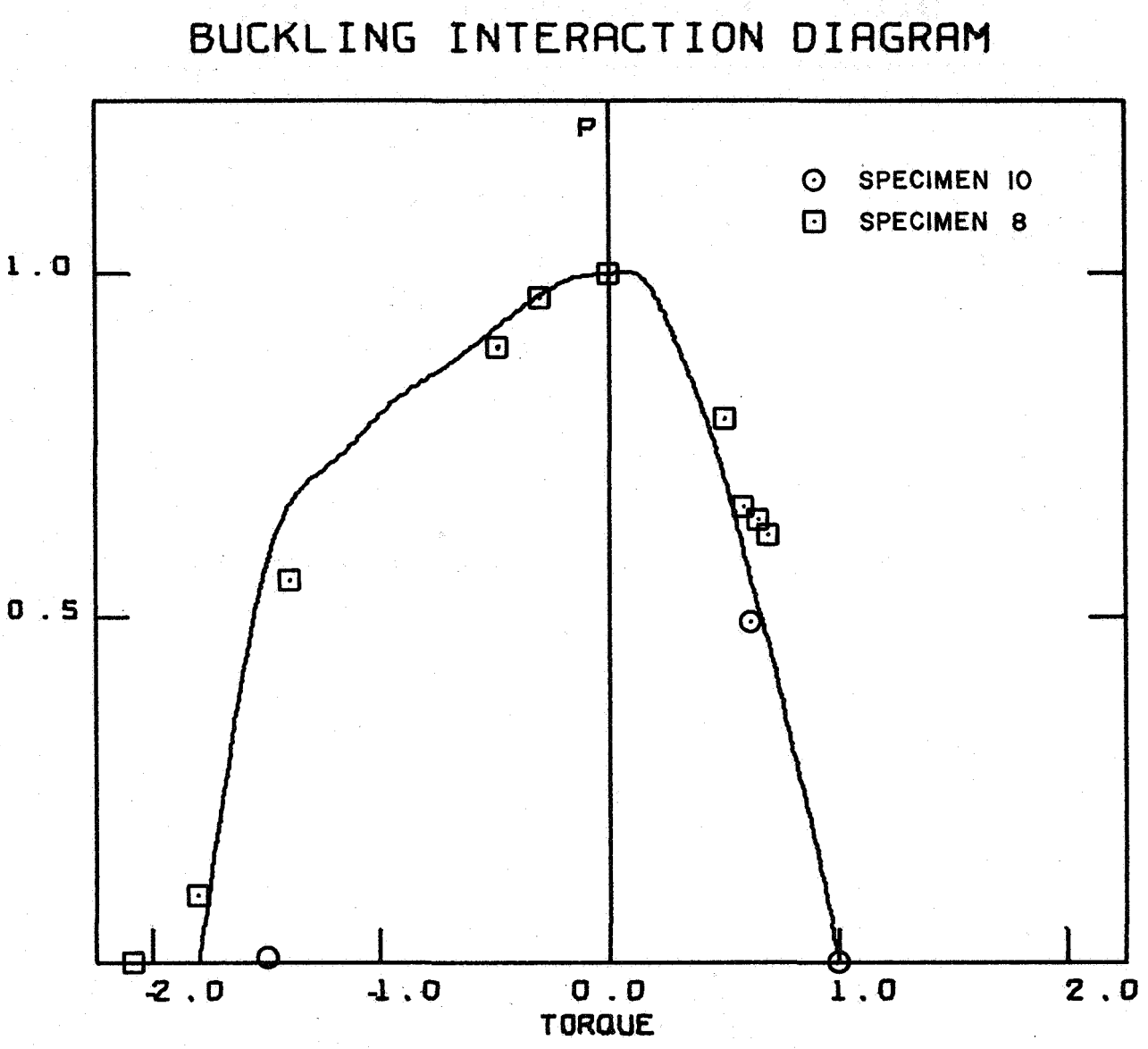

MAX TORQUE/COMPRESSION VALU

T (+)		T (-)		P	
6072.6	LB-IN	-10905.9	LB-IN	6832.2	LB
686.1	N-M	-1232.2	N-M	30391.4	N

Fig. 30. Line Interaction Diagram - Spec. #7 [-82.5/30/20/-82.5] Gr/E

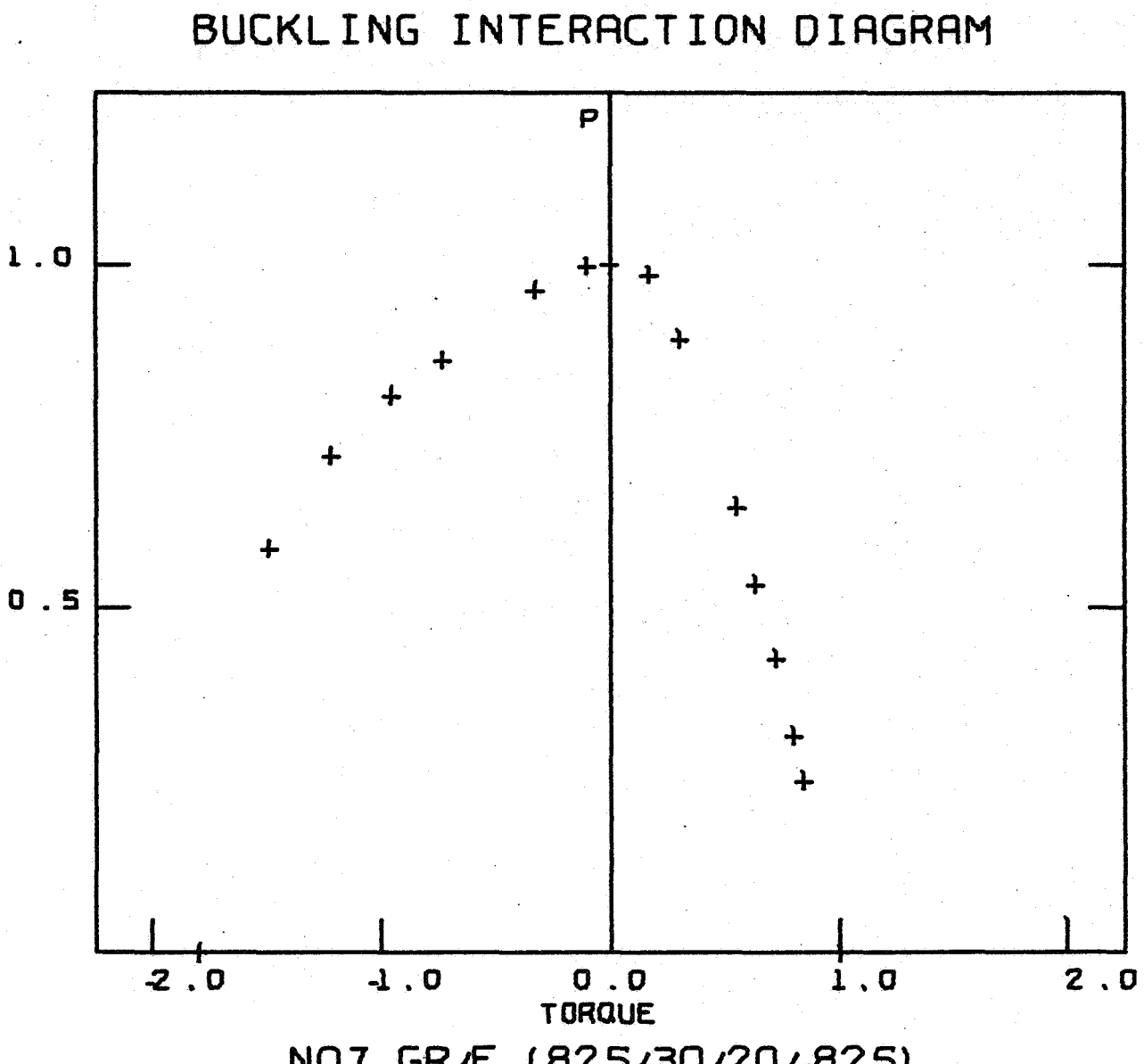

Fig. 31. Point Interaction Diagram - Spec. #7 [-82.5/30/20/-82.5] Gr/E

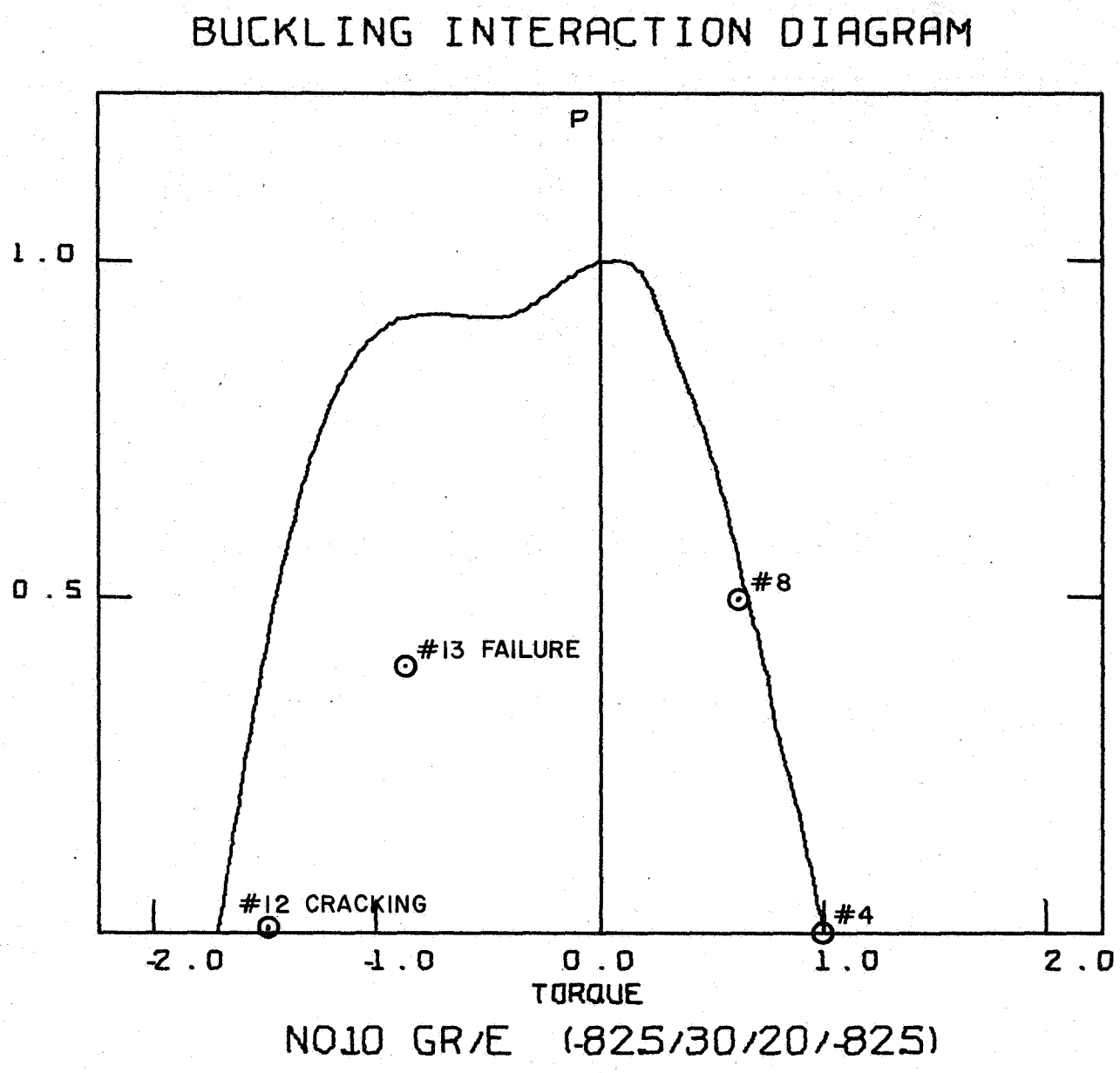

Fig. 32. Line Interaction Diagram - Spec. #10 [-82.5/30/20/-82.5] Gr/E

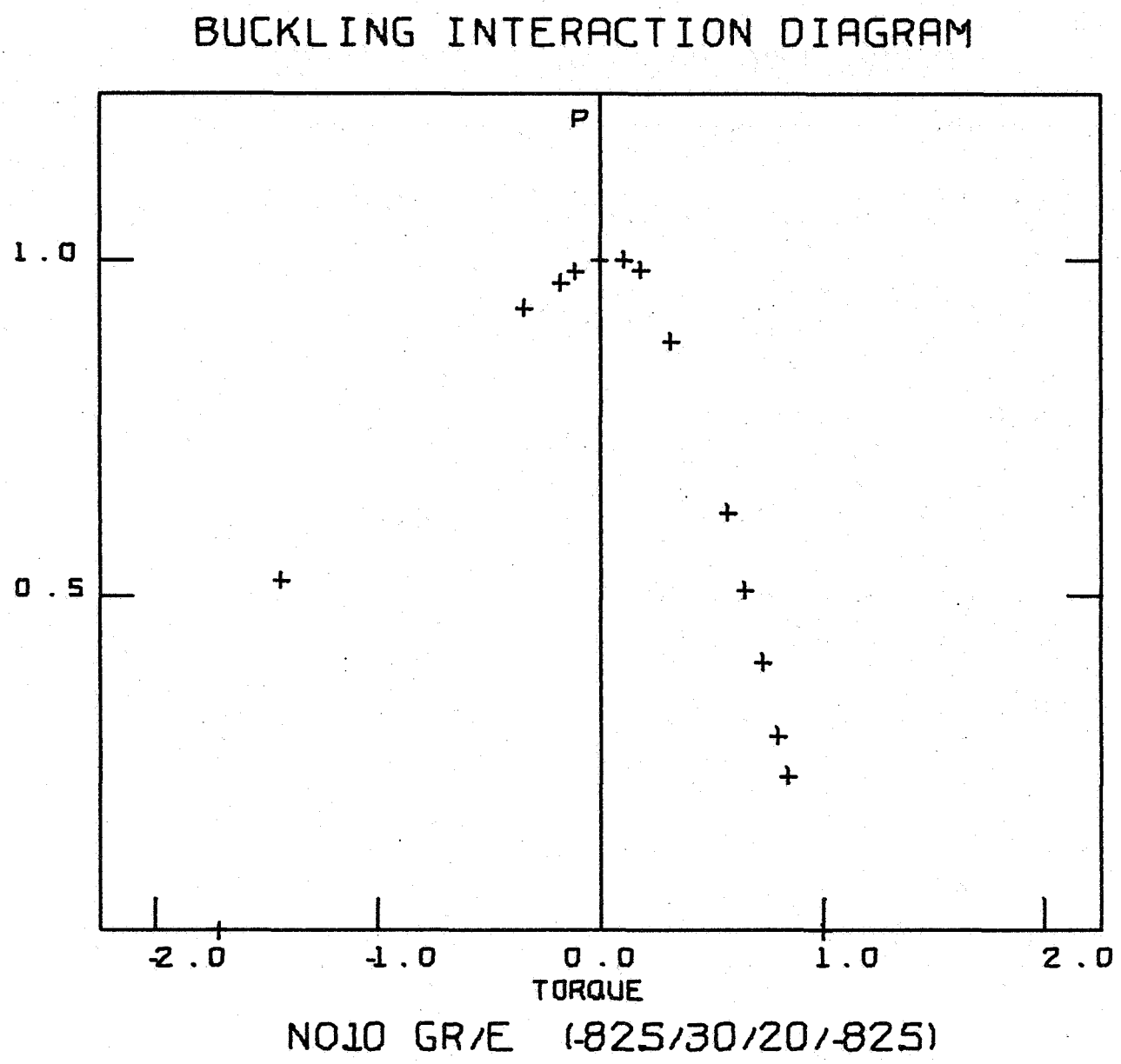

Fig. 33. Point Interaction Diagram - Spec #10 [-82.5/30/20/-82.5] Gr/E

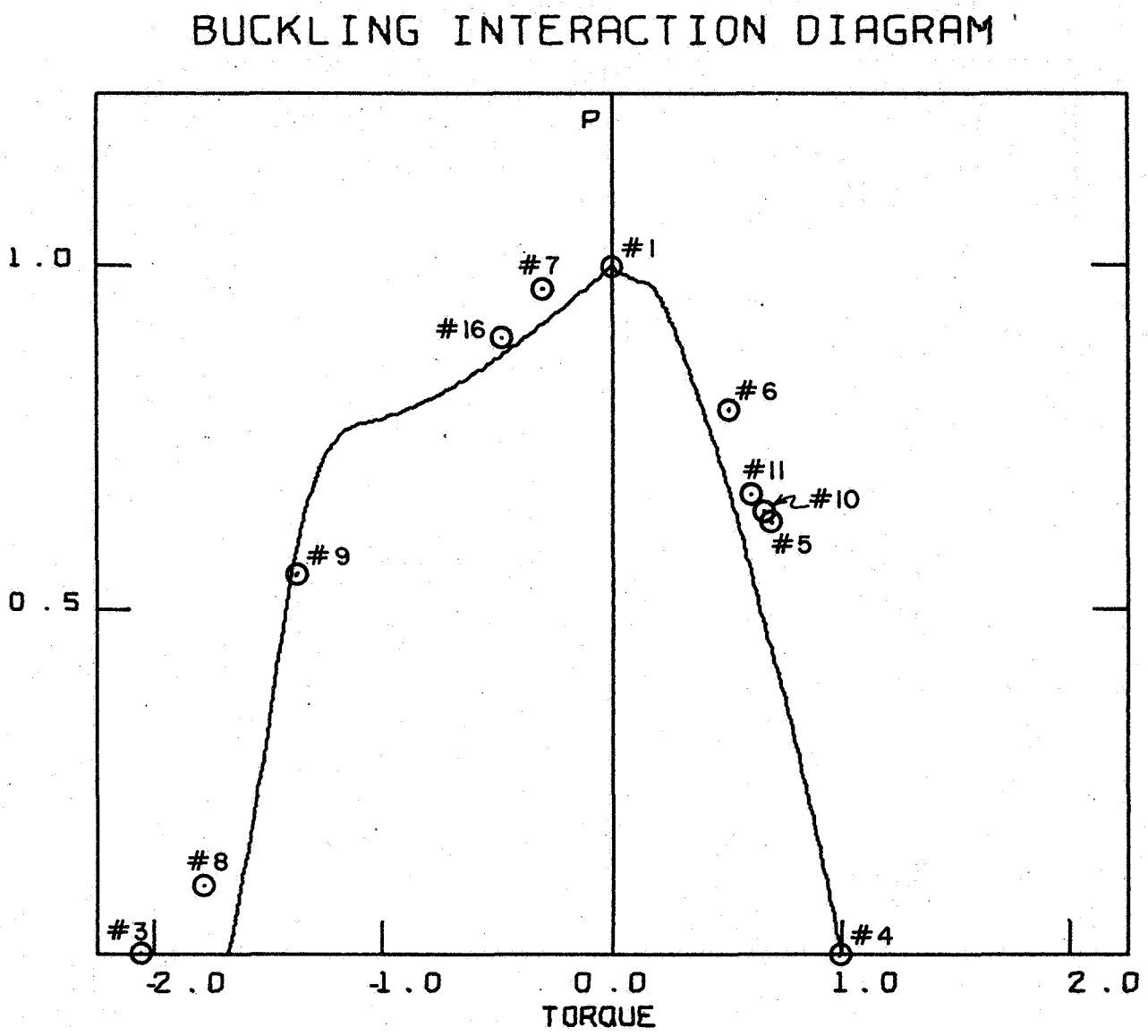

NO8 GR/E (-825/30/20/-825)

MAX TORQUE/COMPRESSION VALUES

T (+)		T (-)		P	
6096.0	LB-IN	-10184.8	LB-IN	7780.1	LB
688.7	N-M	-1150.7	N-M	34607.8	N

Fig. 34. Line Interaction Diagram - Spec. #8 [-82.5/30/20/-82.5] Gr/E

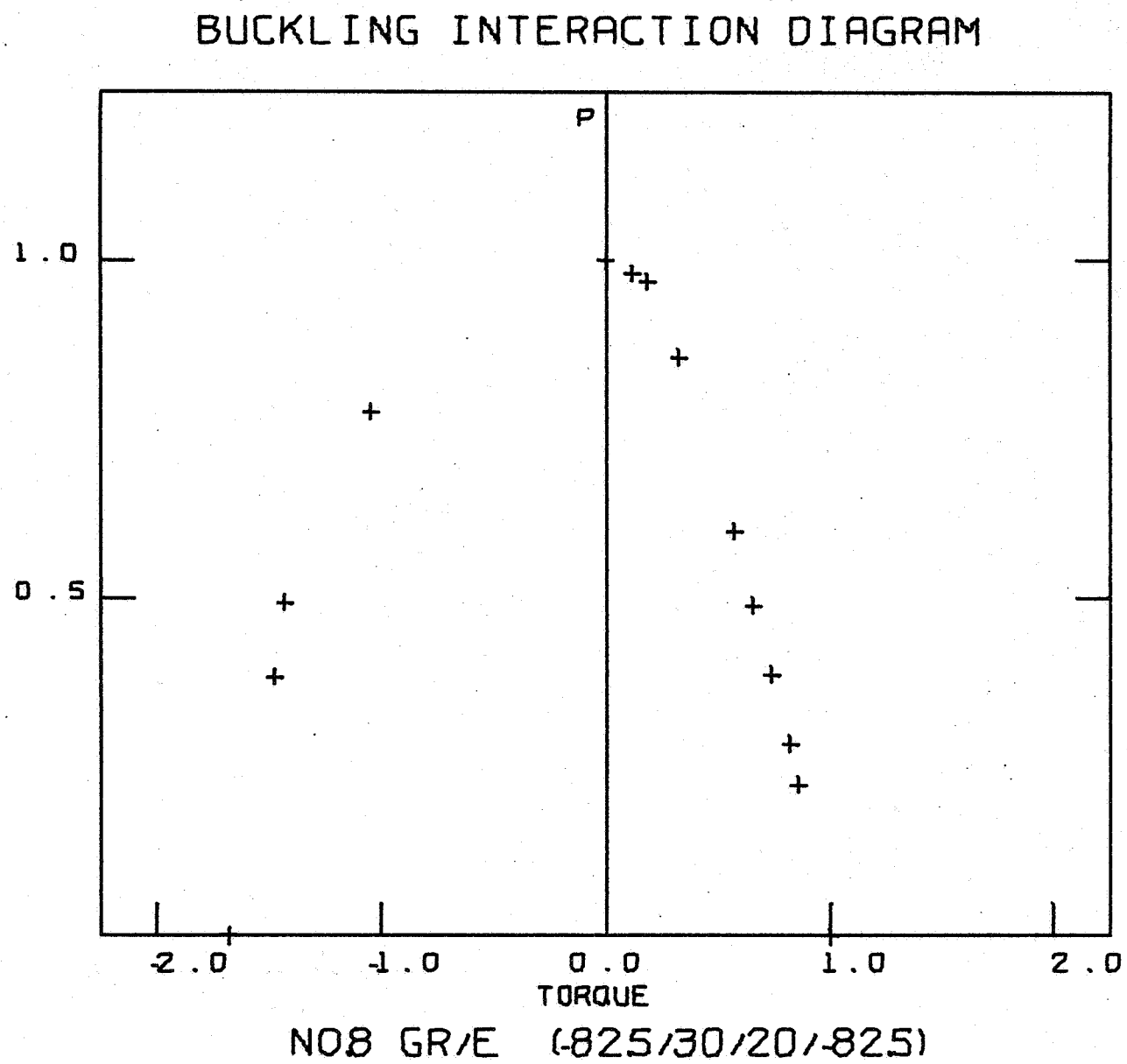

MAX TORQUE/COMPRESSION VALUES

T (+)		T (-)		P	
6096.0	LB-IN	-10184.8	LB-IN	7780.1	LB
688.7	N-M	-1150.7	N-M	34607.8	N

Fig. 35. Point Interaction Diagram - Spec. #8 [-82.5/30/20/-82.5] Gr/E

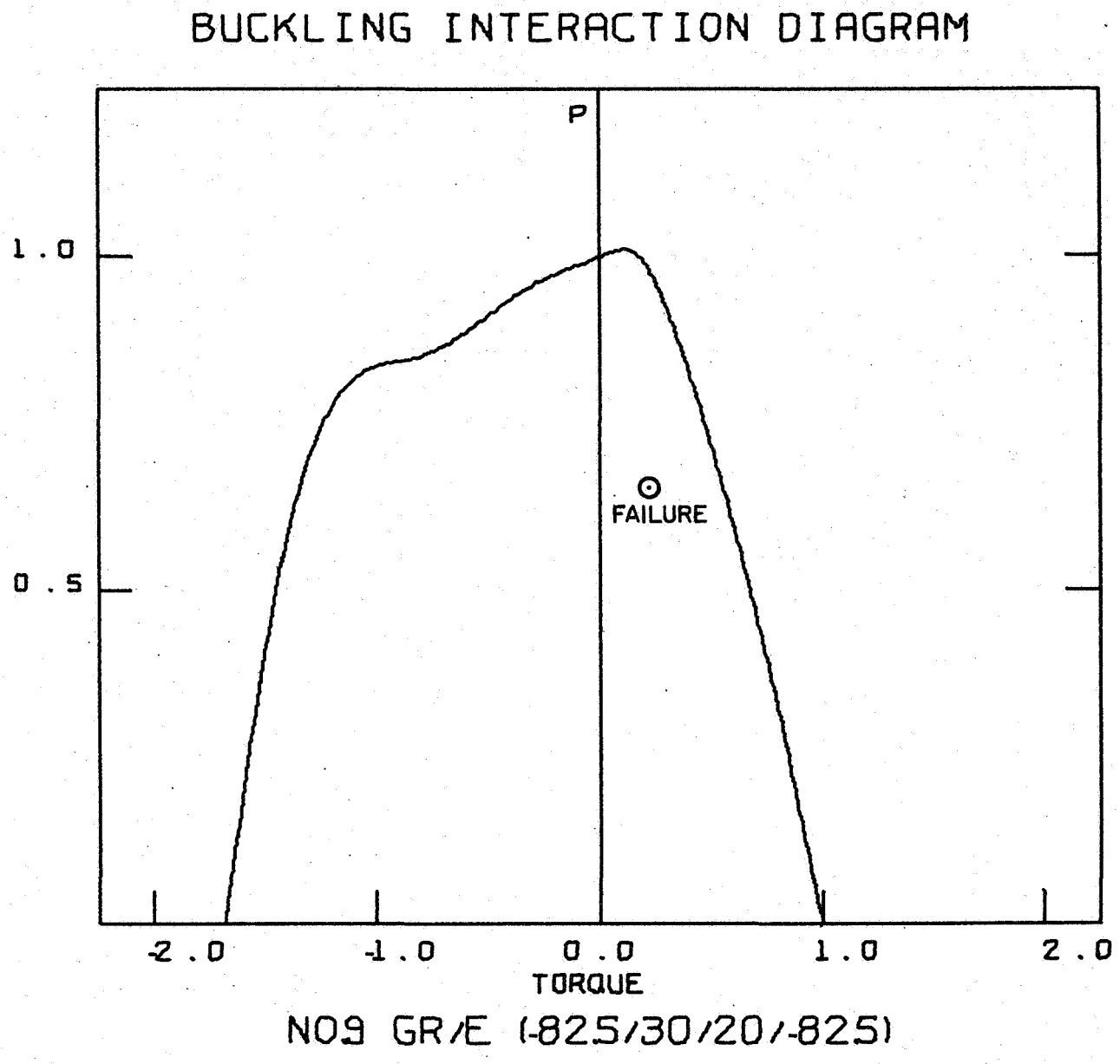

Fig. 36. Line Interaction Diagram - Spec. #9 [-82.5/30/20/-82.5] Gr/E

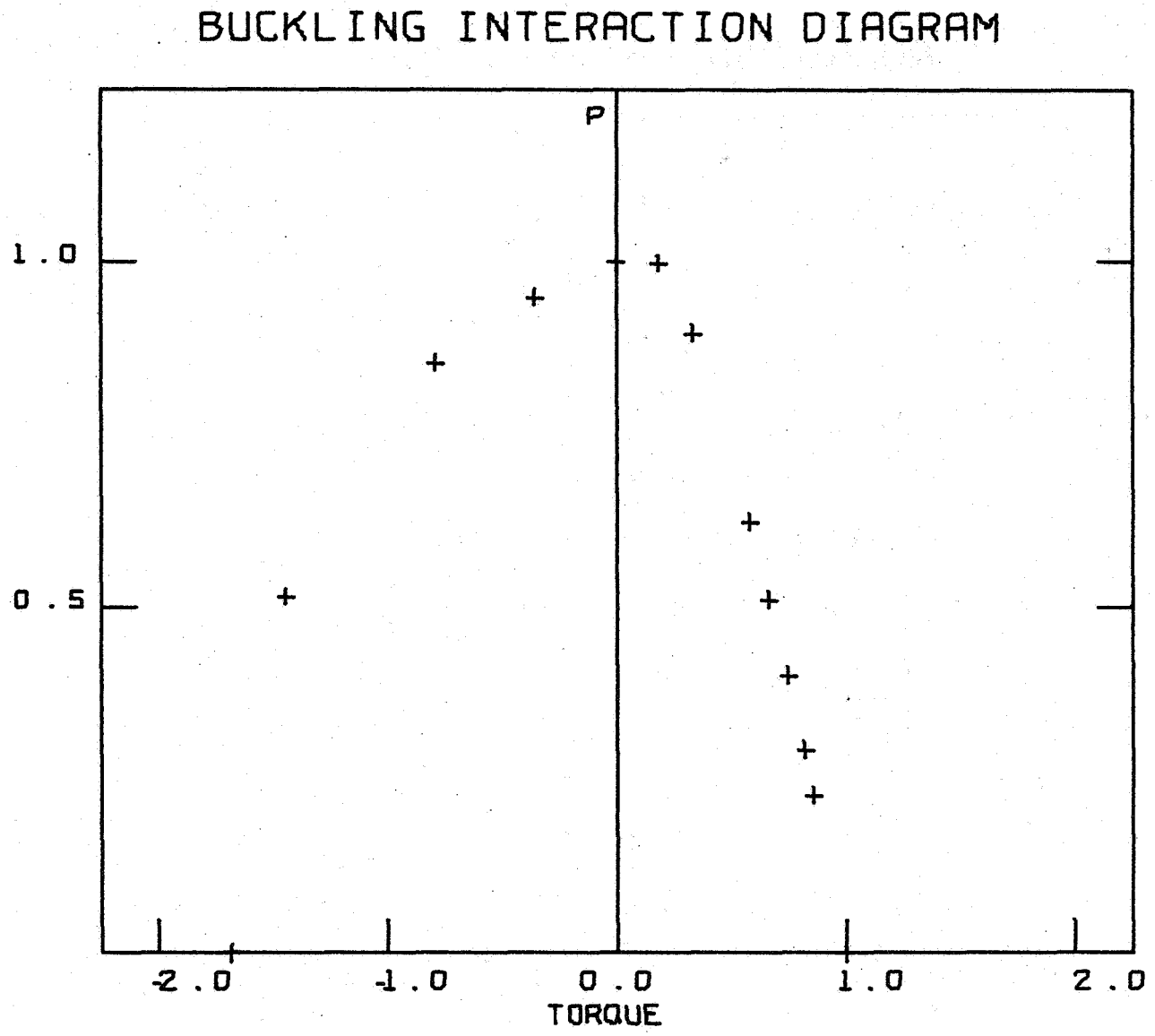

MAX TORQUE/COMPRESSION VALUES

T (+)		T (-)		P	
5430.6	LB-IN	-9152.2	LB-IN	6722.5	LB
613.5	N-M	-1034.0	N-M	29903.4	N

Fig. 37. Point Interaction Diagram - Spec. #9 [-82.5/30/20/-82.5] Gr/E

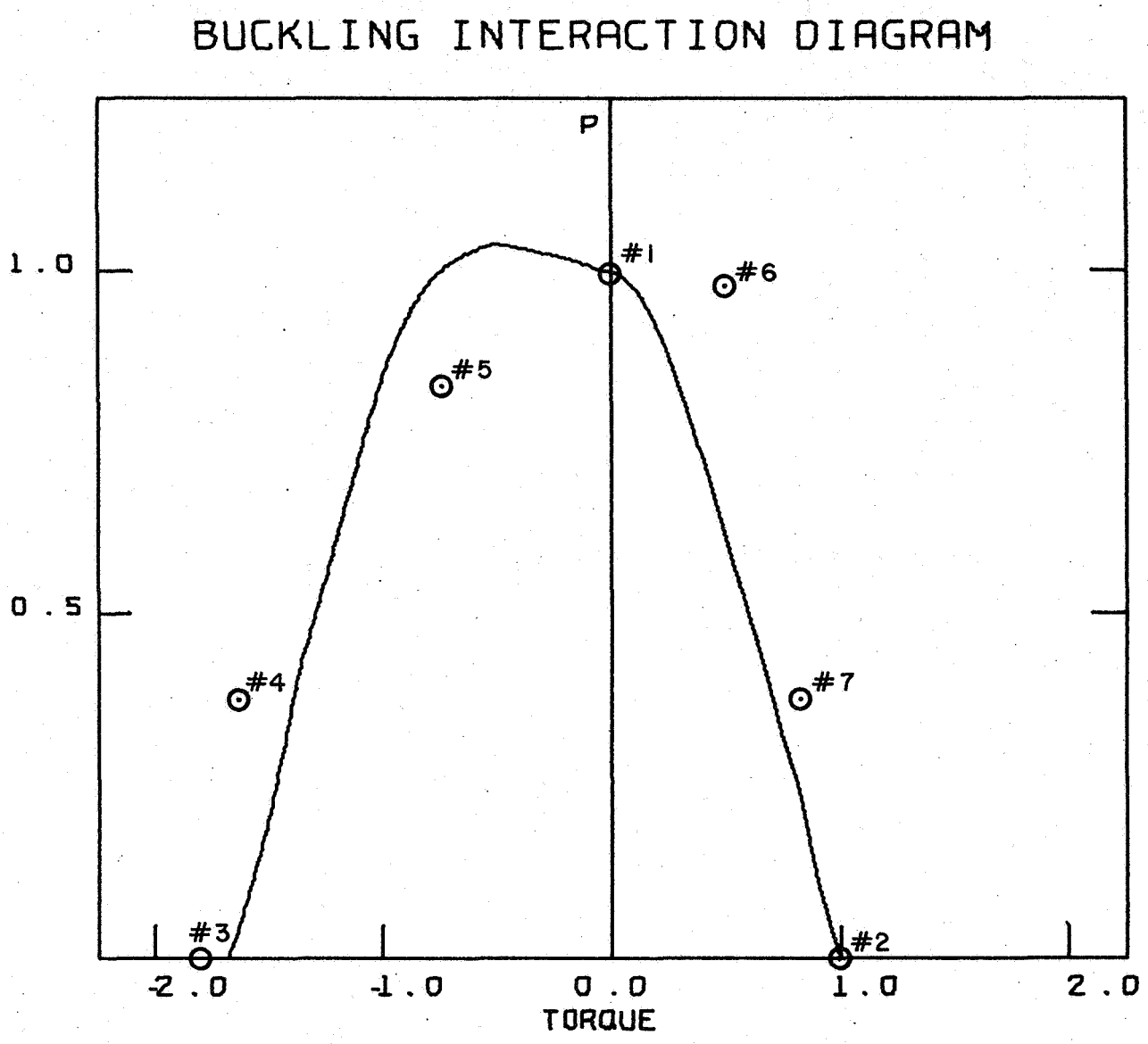

MAX TORQUE/COMPRESSION VALUES

T (+)		T (-)		P	
5732.0	LB-IN	-9603.5	LB-IN	9344.7	LB
647.6	N-M	-1085.0	N-M	41567.3	N

Fig. 38. Line Interaction Diagram - Spec. #11 $[\overline{+}45]_S$ Gr/E

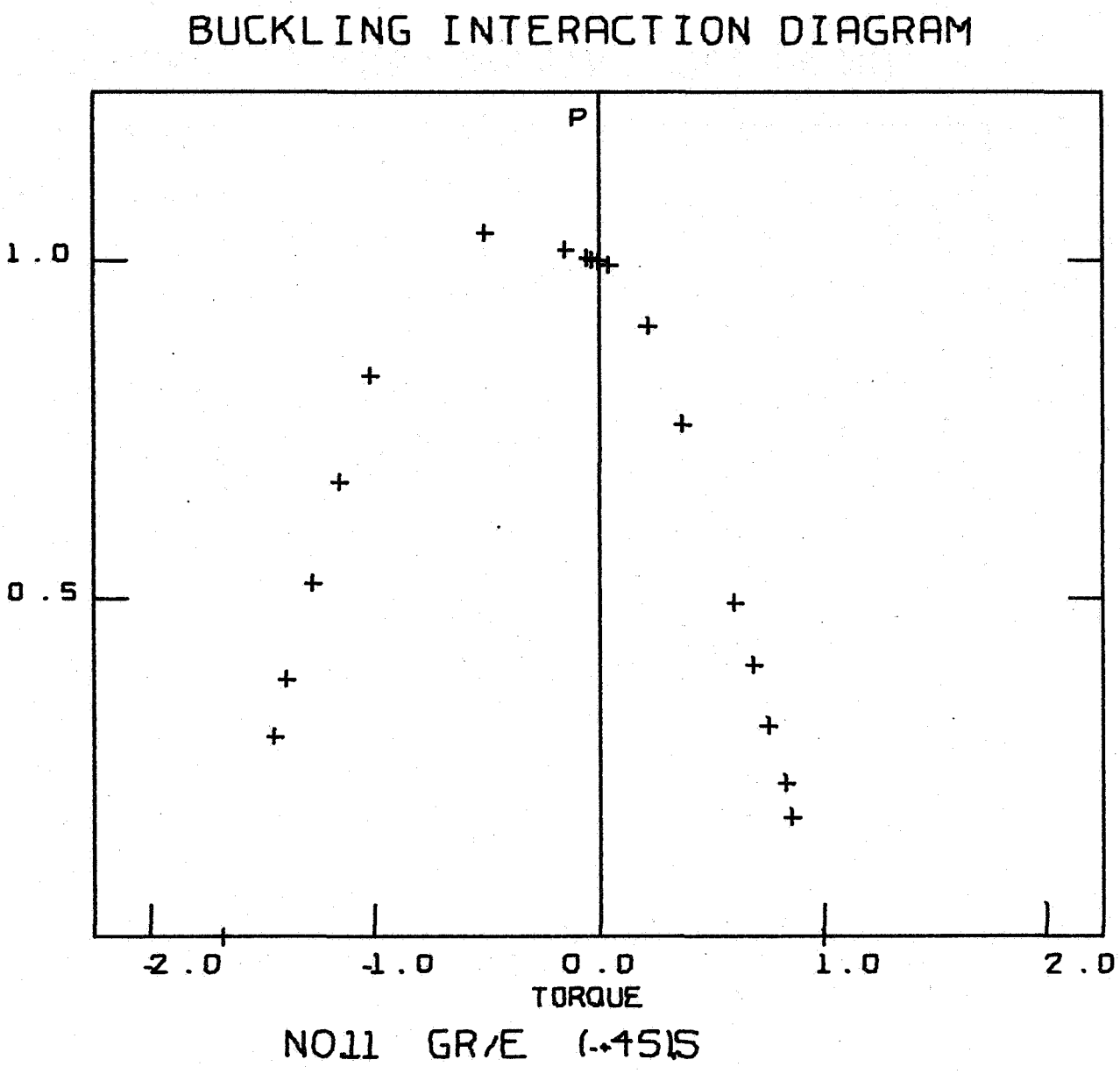

Fig. 39. Point Interaction Diagram - Spec. #11 $[\pm 45]_S$ Gr/E

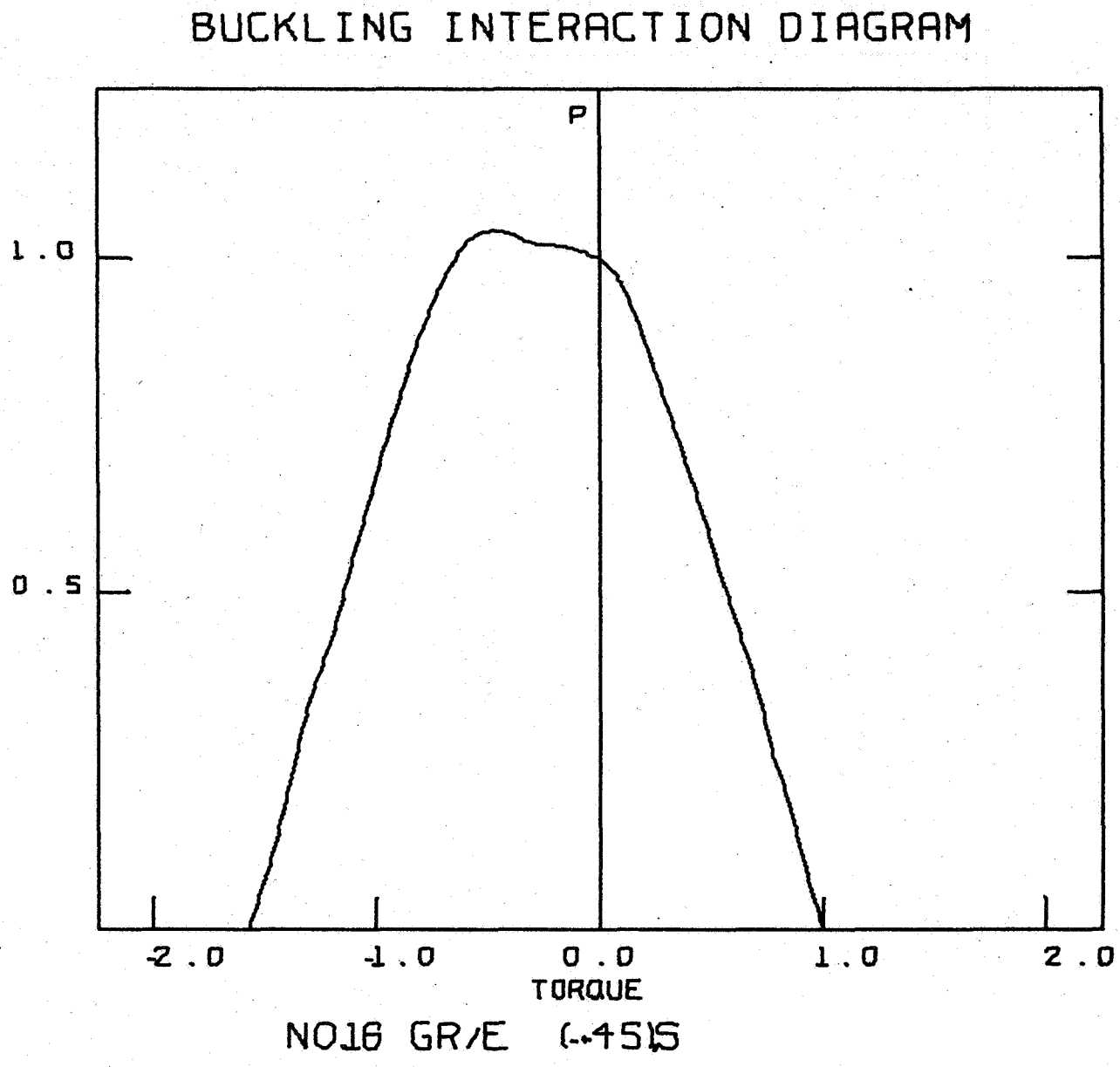

MAX TORQUE/COMPRESSION VALUES

T (+)		T (-)		P	
4528.6	LB-IN	-7118.1	LB-IN	8919.0	LB
511.8	N-M	-804.2	N-M	39673.8	N

Fig. 40. Line Interaction Diagram - Spec. #16 $[\mp 45]_s$ Gr/E

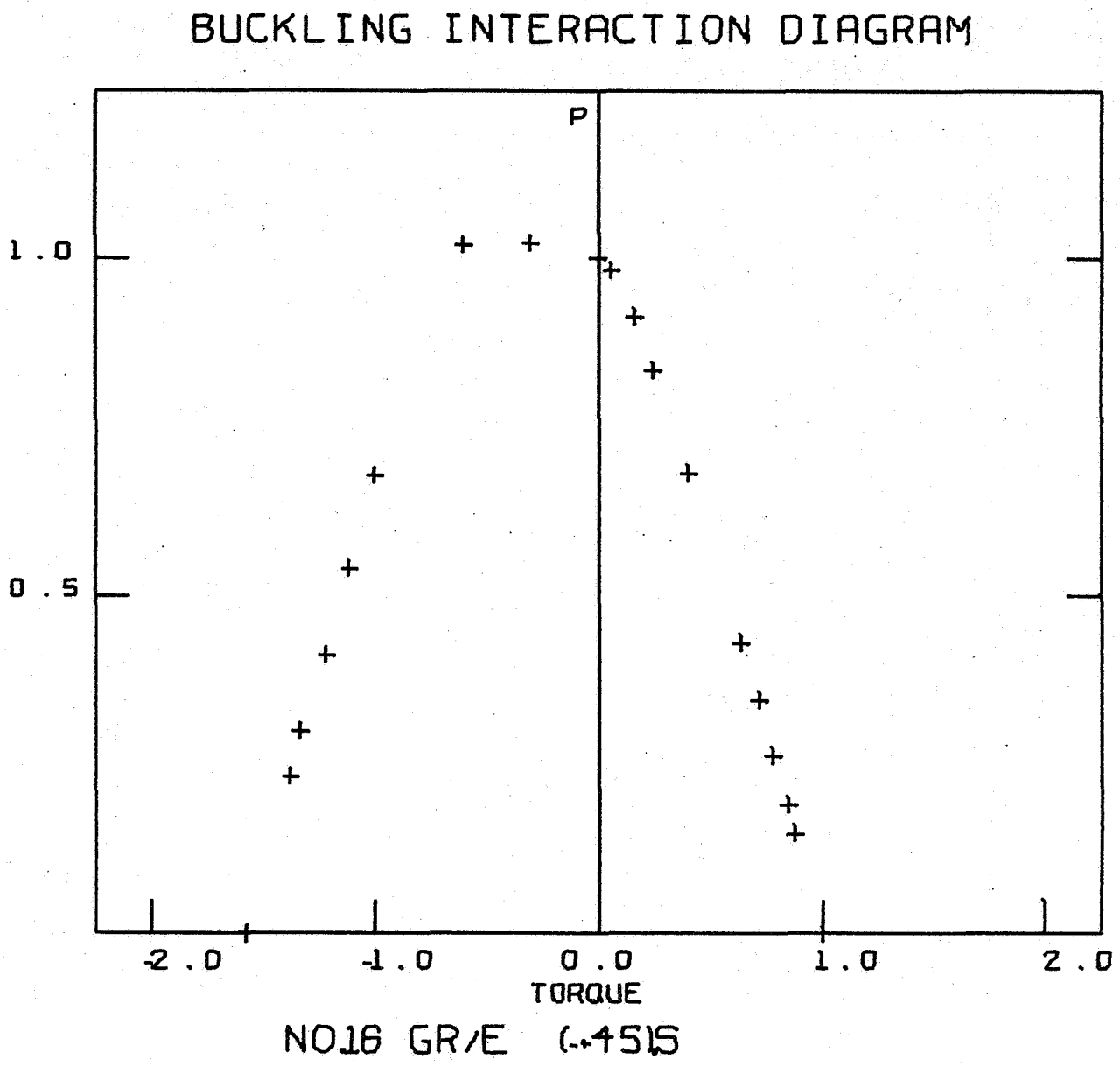

MAX TORQUE/COMPRESSION VALUES

T (+)		T (-)		P	
4528.6	LB-IN	-7118.1	LB-IN	8919.0	LB
511.6	N-M	-804.2	N-M	39673.8	N

Fig. 41. Point Interaction Diagram - Spec. #16 $[\mp 45]_S$ Gr/E

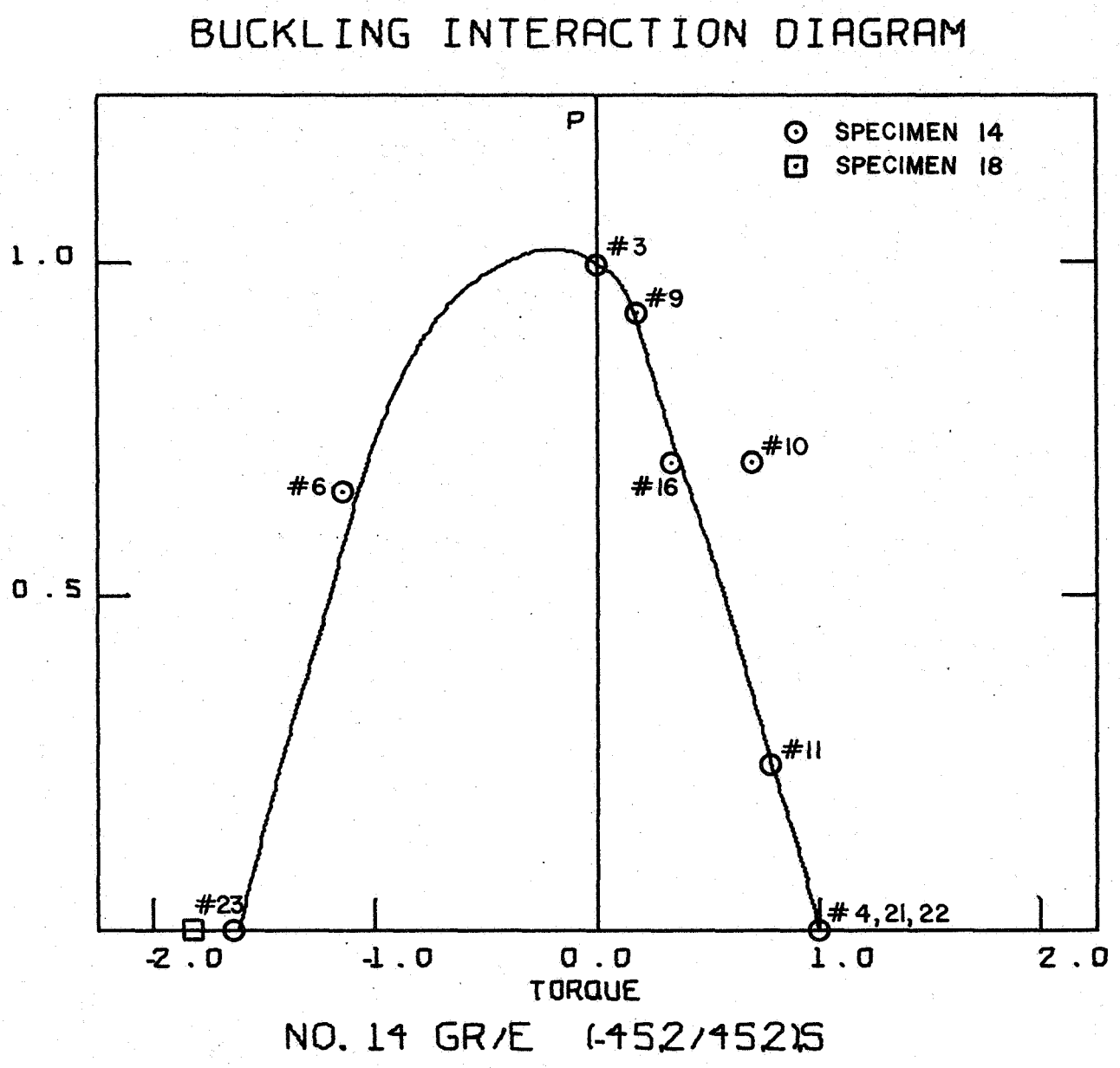

MAX TORQUE/COMPRESSION VALUES

T (+)		T (-)		P	
20440.9	LB-IN	-33005.5	LB-IN	35045.1	LB
2309.5	N-M	-3729.1	N-M	155868.6	N

Fig. 42. Line Interaction Diagram - Spec. #14 $[-45_2/45_2]_s$ Gr/E

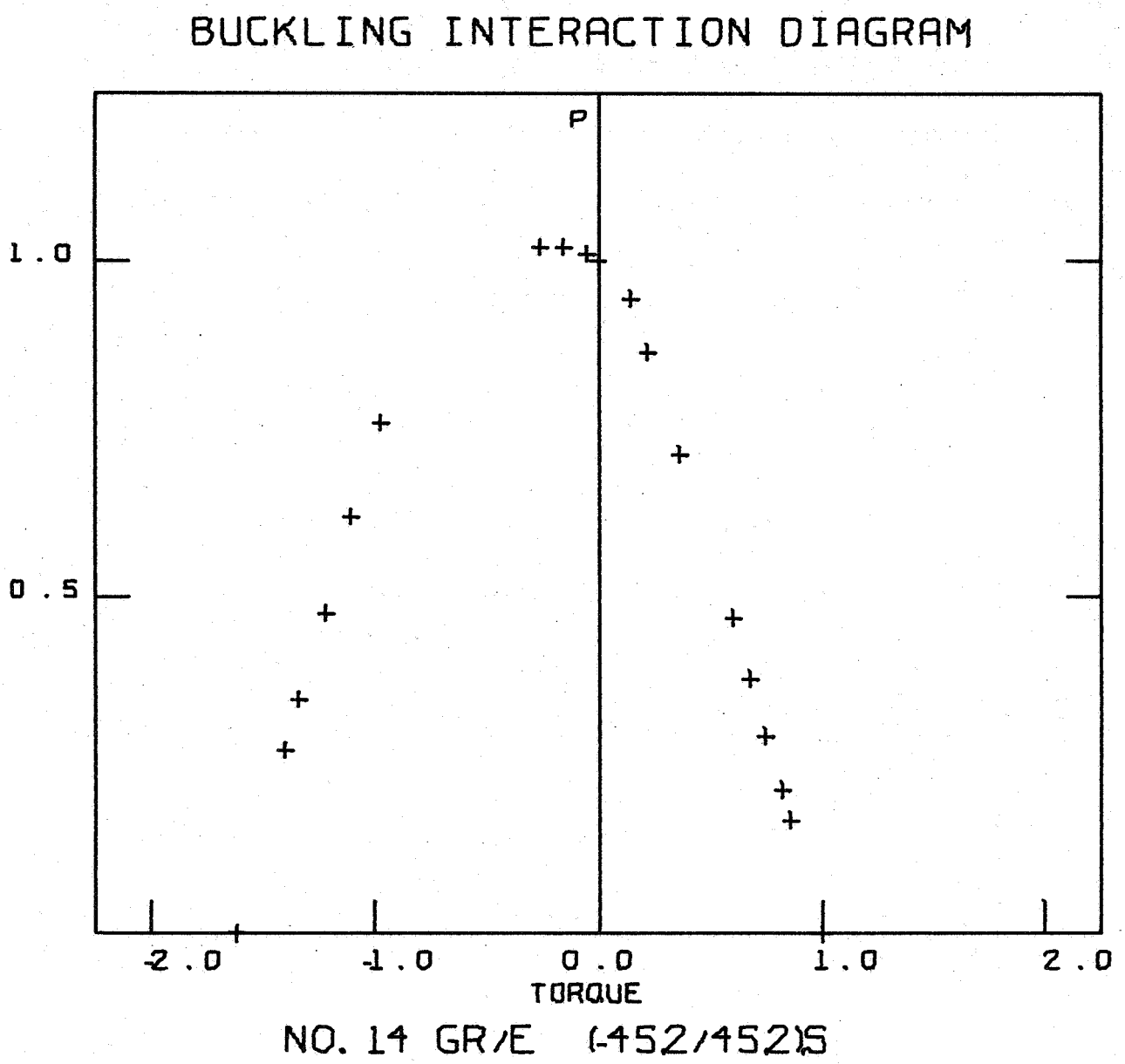

MAX TORQUE/COMPRESSION VALUES

T (+)		T (-)		P	
20440.9	LB-IN	-33005.5	LB-IN	35045.1	LB
2308.5	N-M	-3729.1	N-M	155888.6	N

Fig. 43. Point Interaction Diagram - Spec. #14 $[-45_2/45_2]_S$ Gr/E

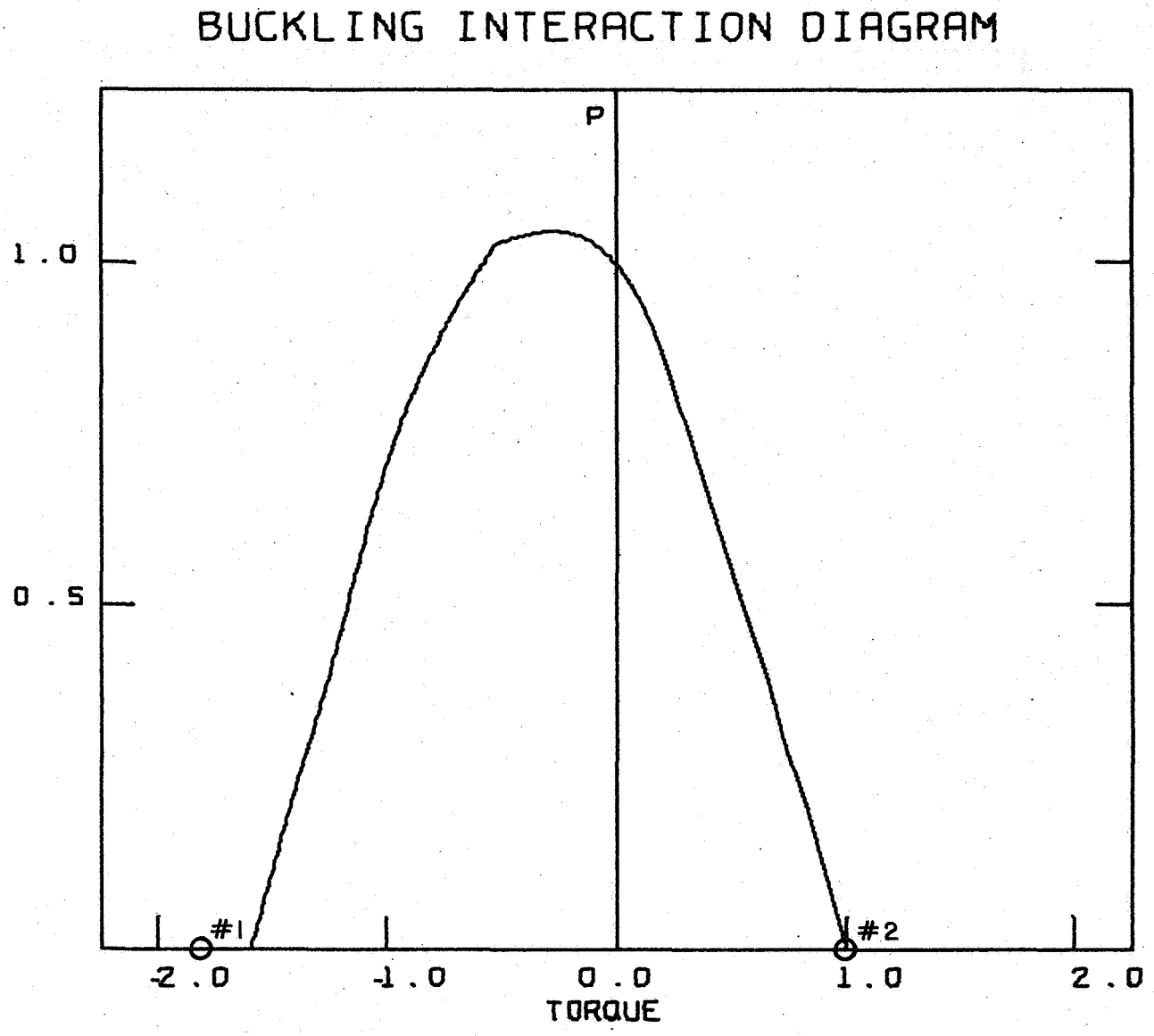

MAX TORQUE/COMPRESSION VALUES

T (+)		T (-)		P	
23709.1	LB-IN	-37762.9	LB-IN	40383.0	LB
2678.7	N-M	-4266.6	N-M	179677.0	N

Fig. 44. Line Interaction Diagram - Spec. #18 $[-45_2/45_2]_s$ Gr/E

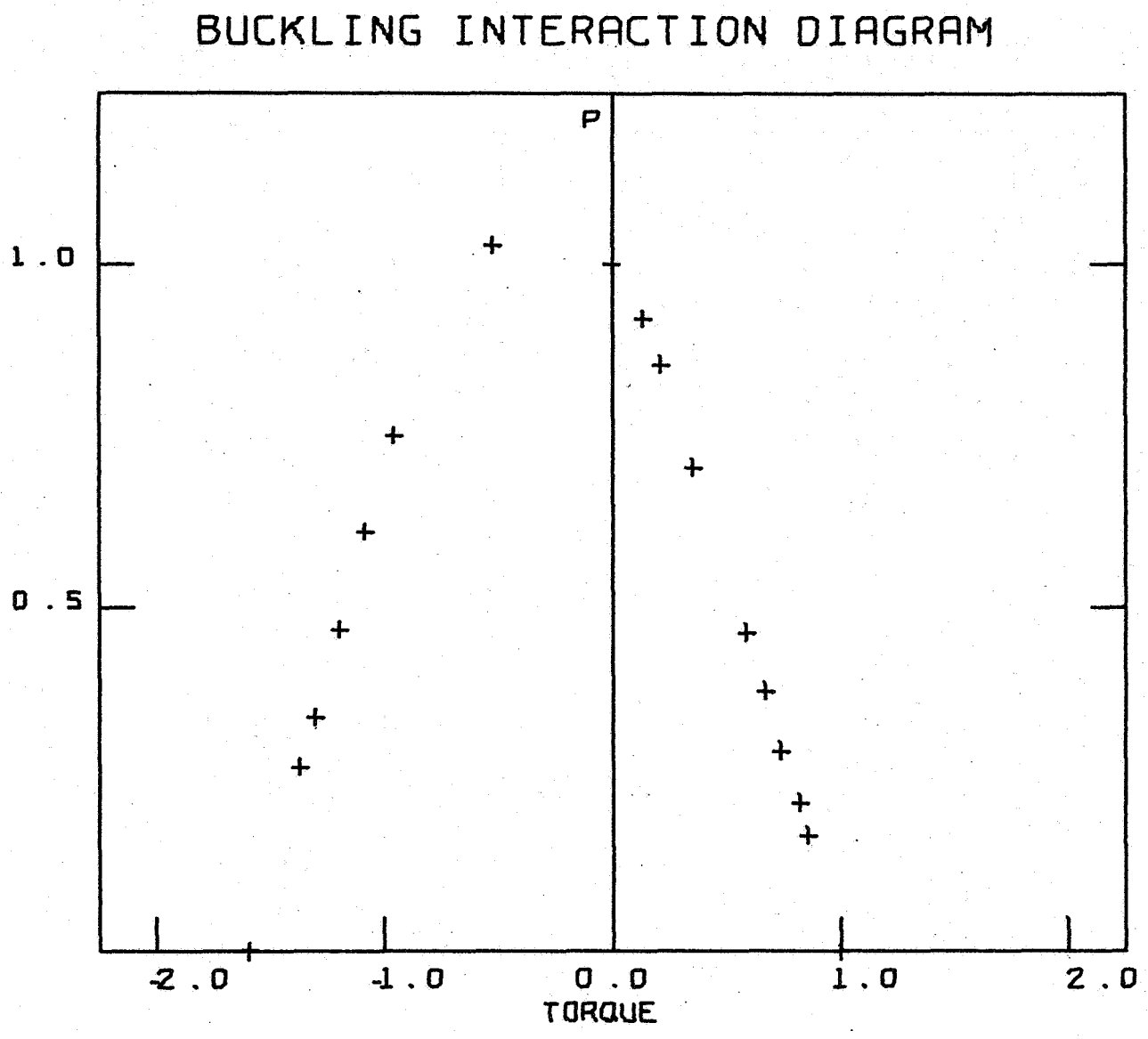

Fig. 45. Point Interaction Diagram - Spec. #18 $[-45_2/45_2]_s$ Gr/E

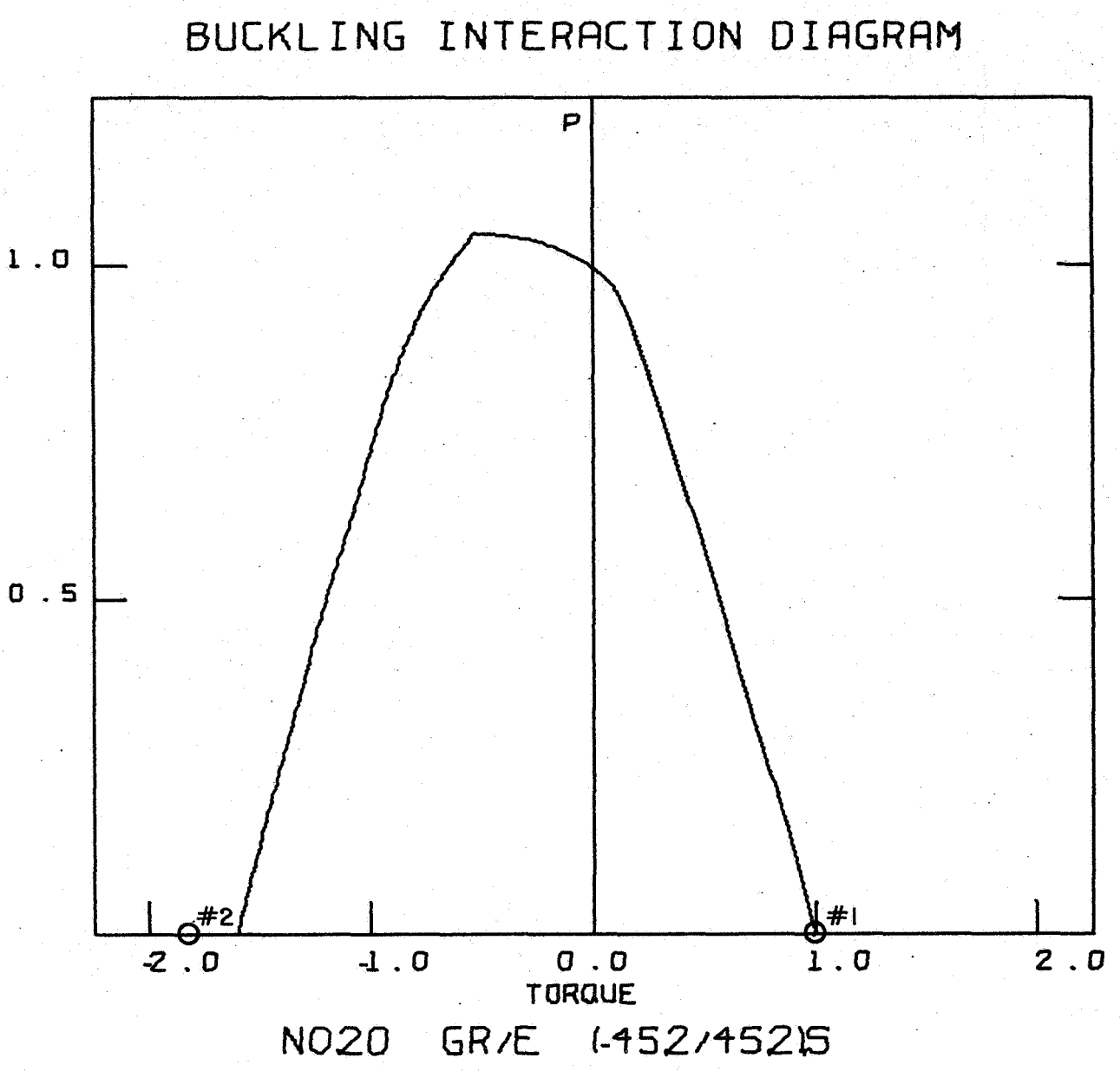

Fig. 46. Line Interaction Diagram - Spec. #20 $[-45_2/45_2]_s$ Gr/E

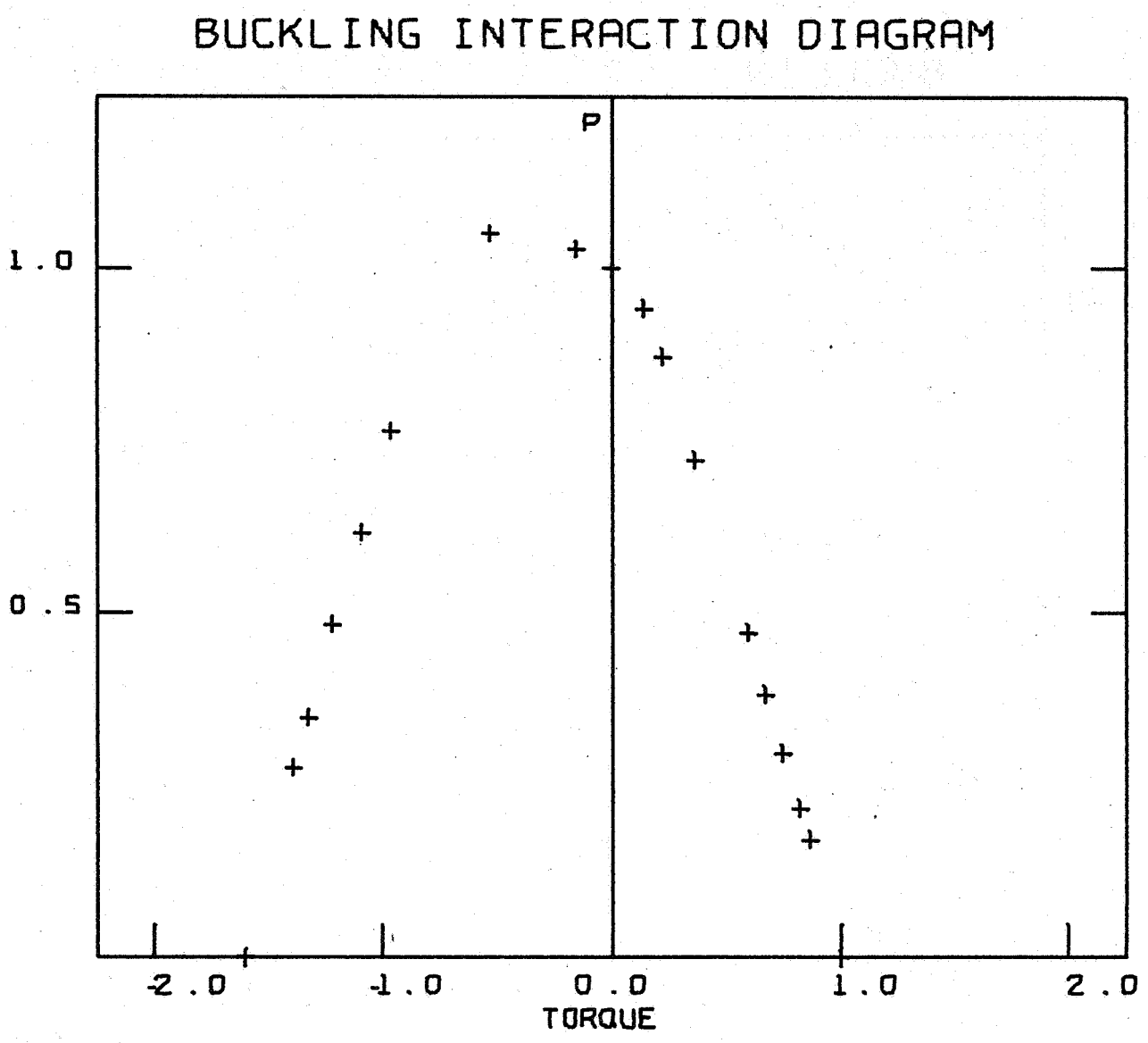

MAX TORQUE/COMPRESSION VALUES

T (+)		T (-)		P	
21946.5	LB-IN	-35160.5	LB-IN	37184.9	LB
2479.6	N-M	-3972.6	N-M	165406.7	N

Fig. 47. Point Interaction Diagram - Spec. #20 $[-45_2/45_2]_S$ Gr/E

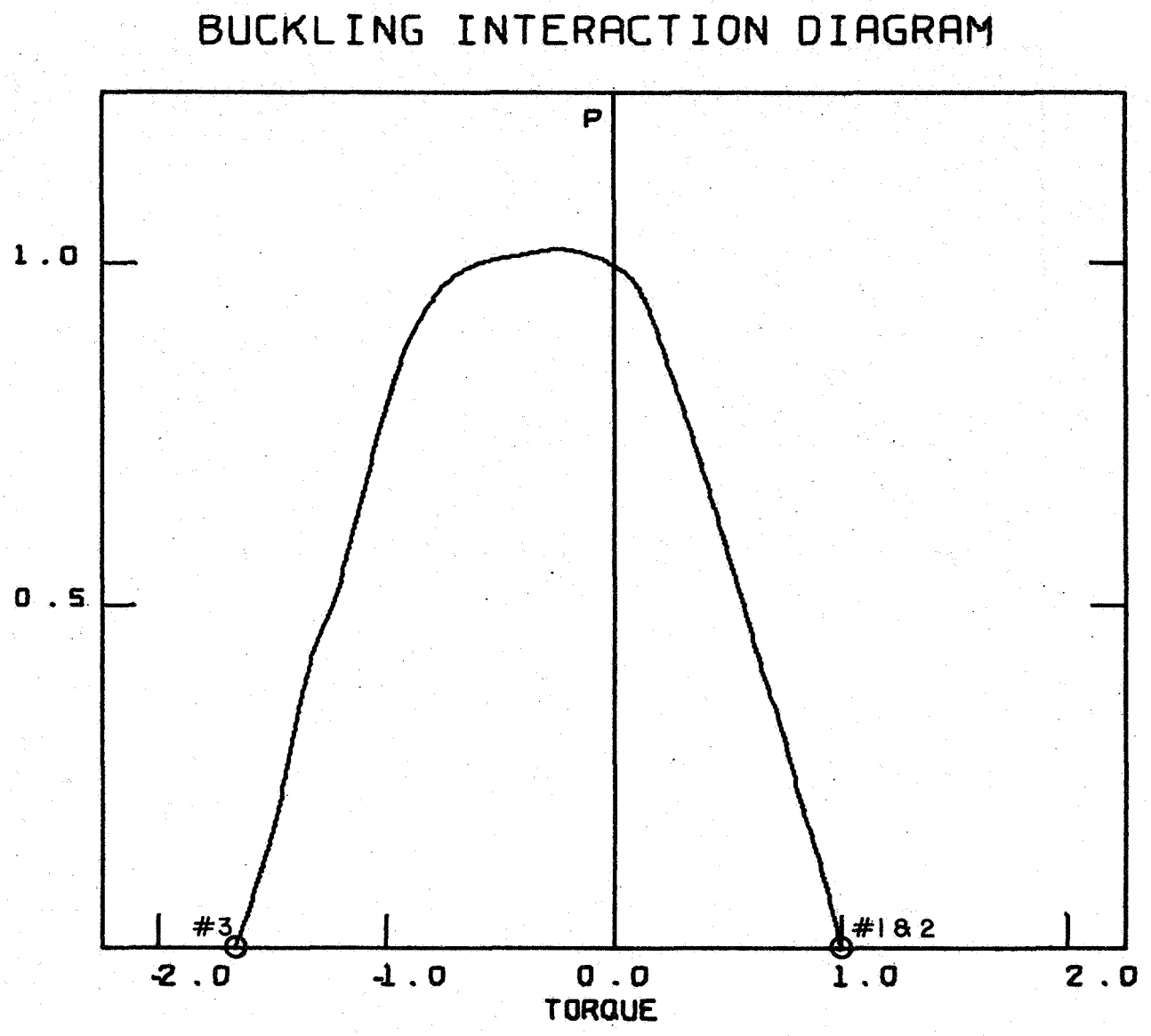

Fig. 48. Line Interaction Diagram - Spec. #21 $[-45_2/45_2]_s$ Gr/E

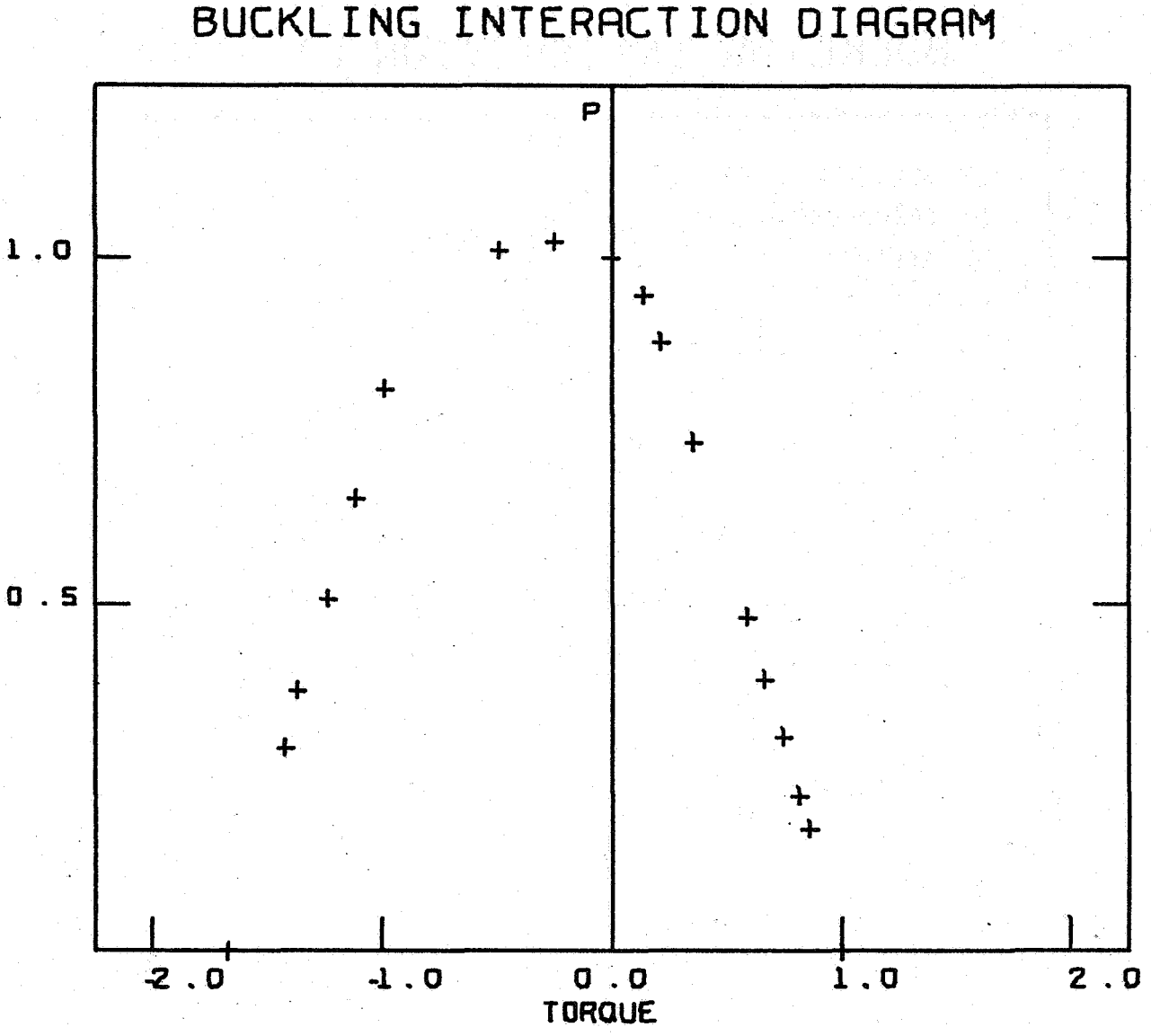

Fig. 49. Point Interaction Diagram - Spec. #21 $[-45_2/45_2]_s$ Gr/E

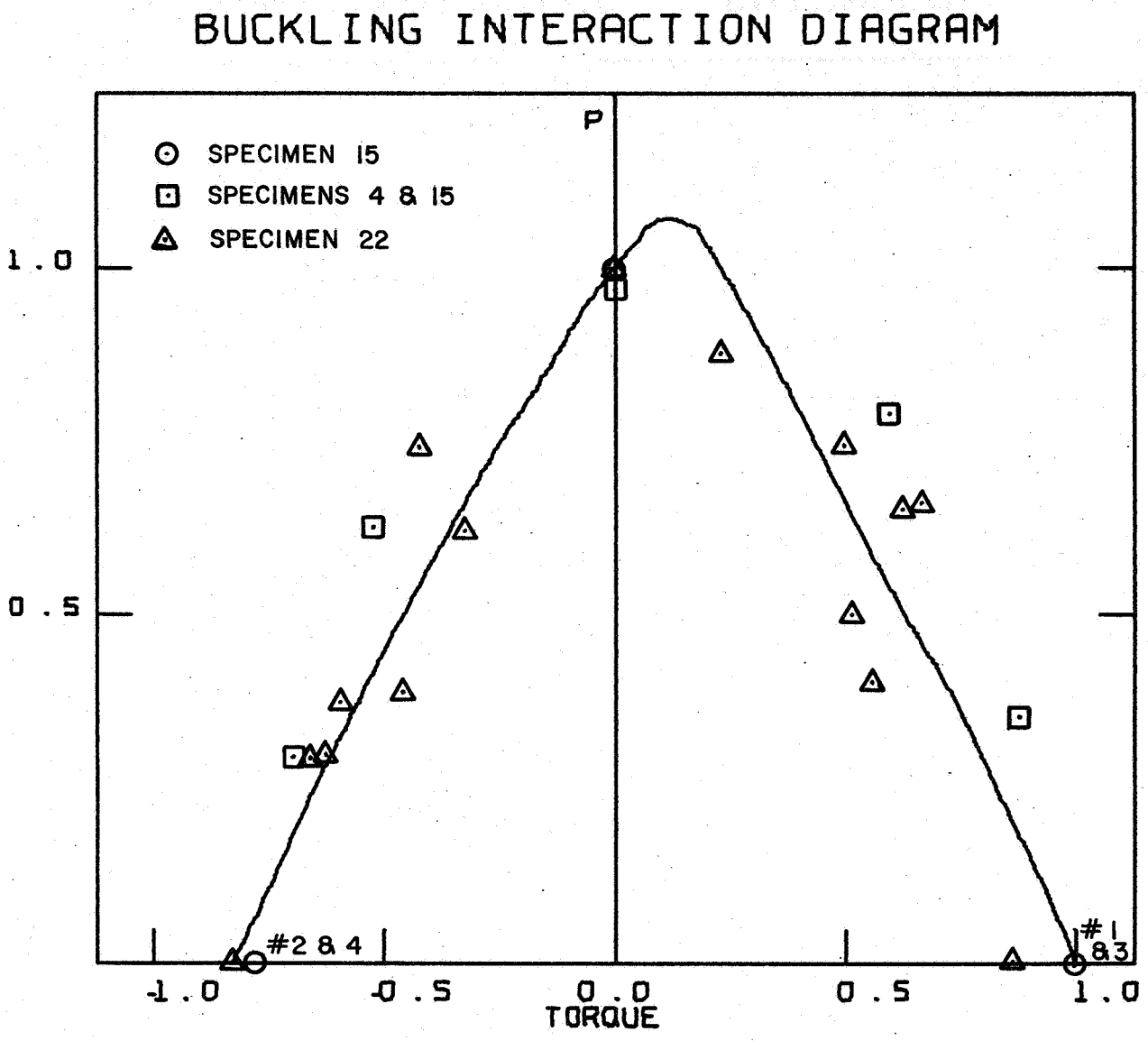

MAX TORQUE/COMPRESSION VALUES

T (+)		T (-)		P	
17659.2	LB-IN	-14673.5	LB-IN	32203.1	LB
1995.2	N-M	-1657.8	N-M	143246.8	N

Fig. 50. Line Interaction Diagram - Spec. #15 $[0/\pm45/90]_S$ Gr/E

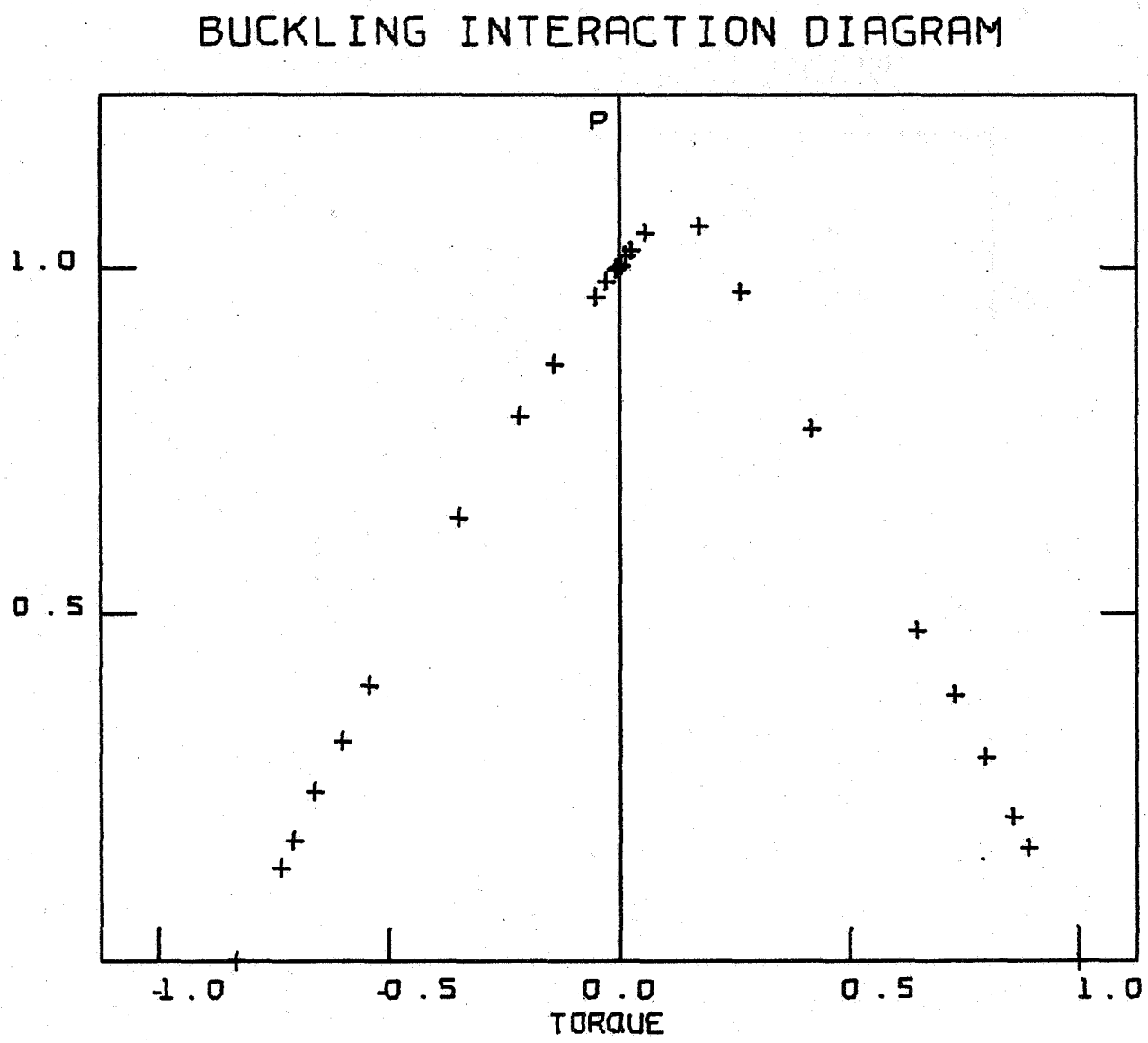

MAX TORQUE/COMPRESSION VALUES

T (+)		T (-)		P	
17659.2	LB-IN	-14673.5	LB-IN	32203.1	LB
1995.2	N-M	-1657.8	N-M	143246.8	N

Fig. 51. Point Interaction Diagram - Spec. #15 $[0/\pm45/90]_S$ Gr/E

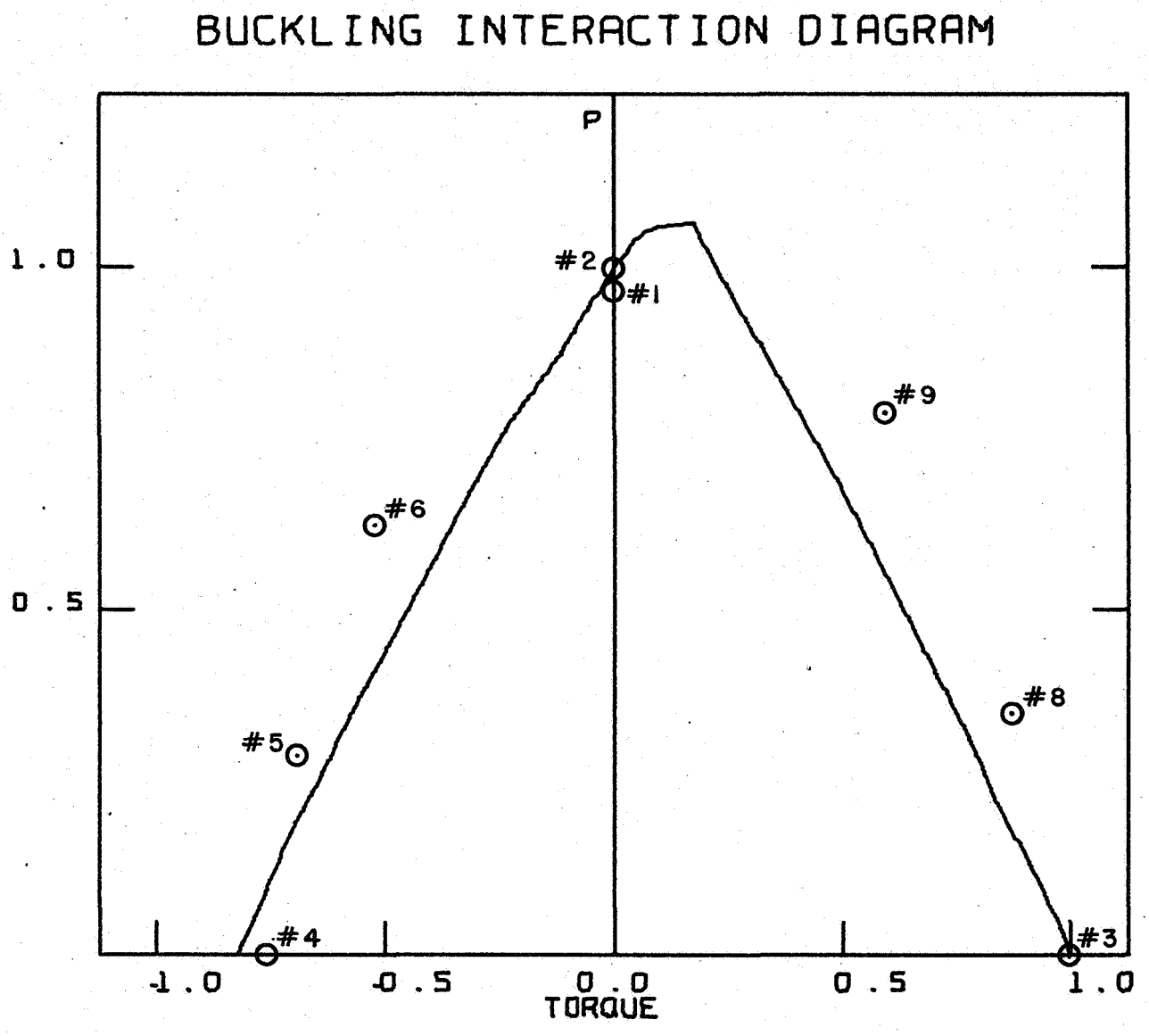

Fig. 52. Line Interaction Diagram - Spec. #AB $[0/\pm45/90]_s$ Gr/E

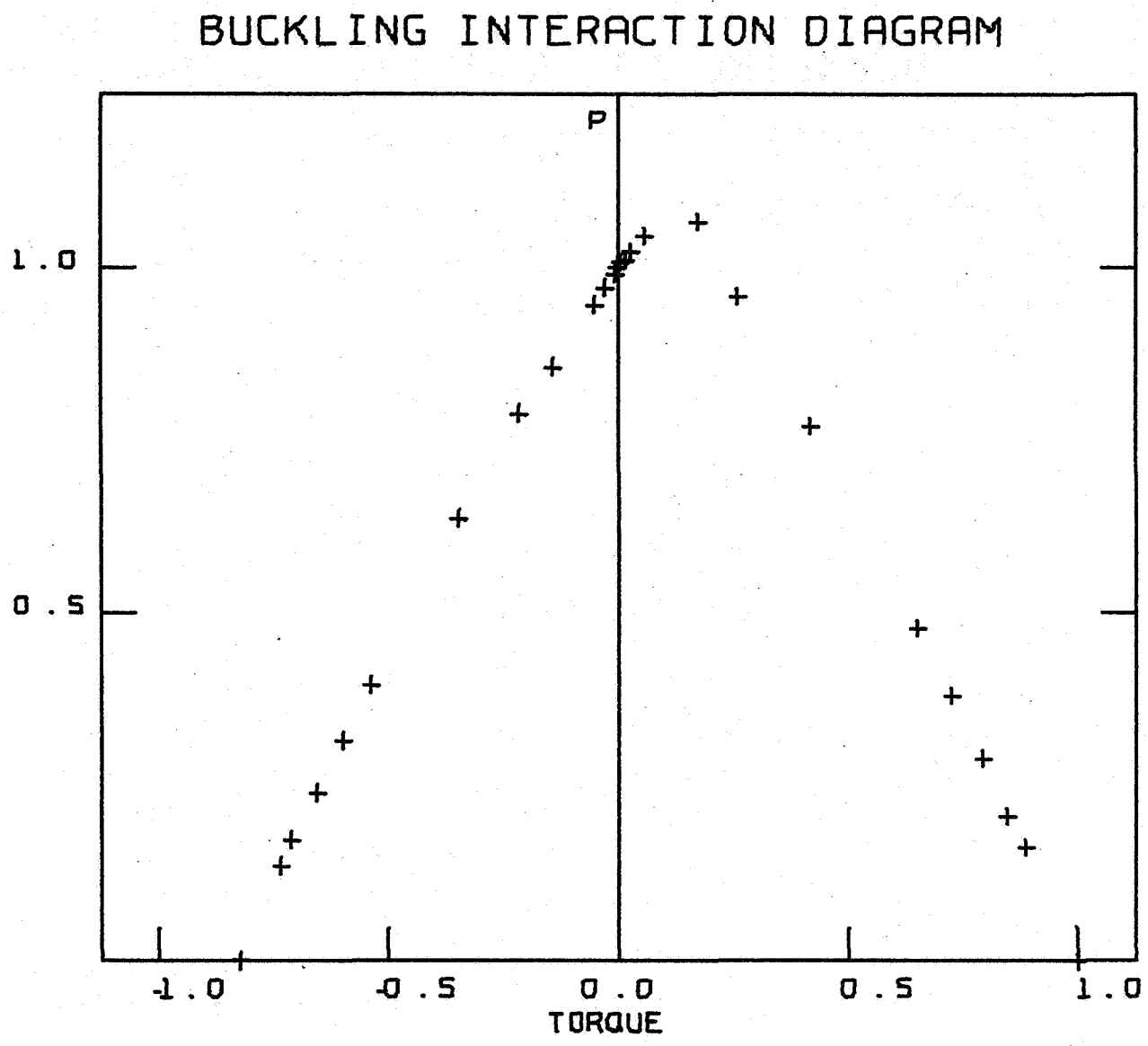

MAX TORQUE/COMPRESSIOI

T (+)		T (-)		P	
18255.8	LB-IN	-15032.4	LB-IN	33332.3	LB
2062.6	N-M	-1698.4	N-M	148269.7	N

Fig. 53. Point Interaction Diagram - Spec. #AB $[0/\pm45/90]_s$ Gr/E

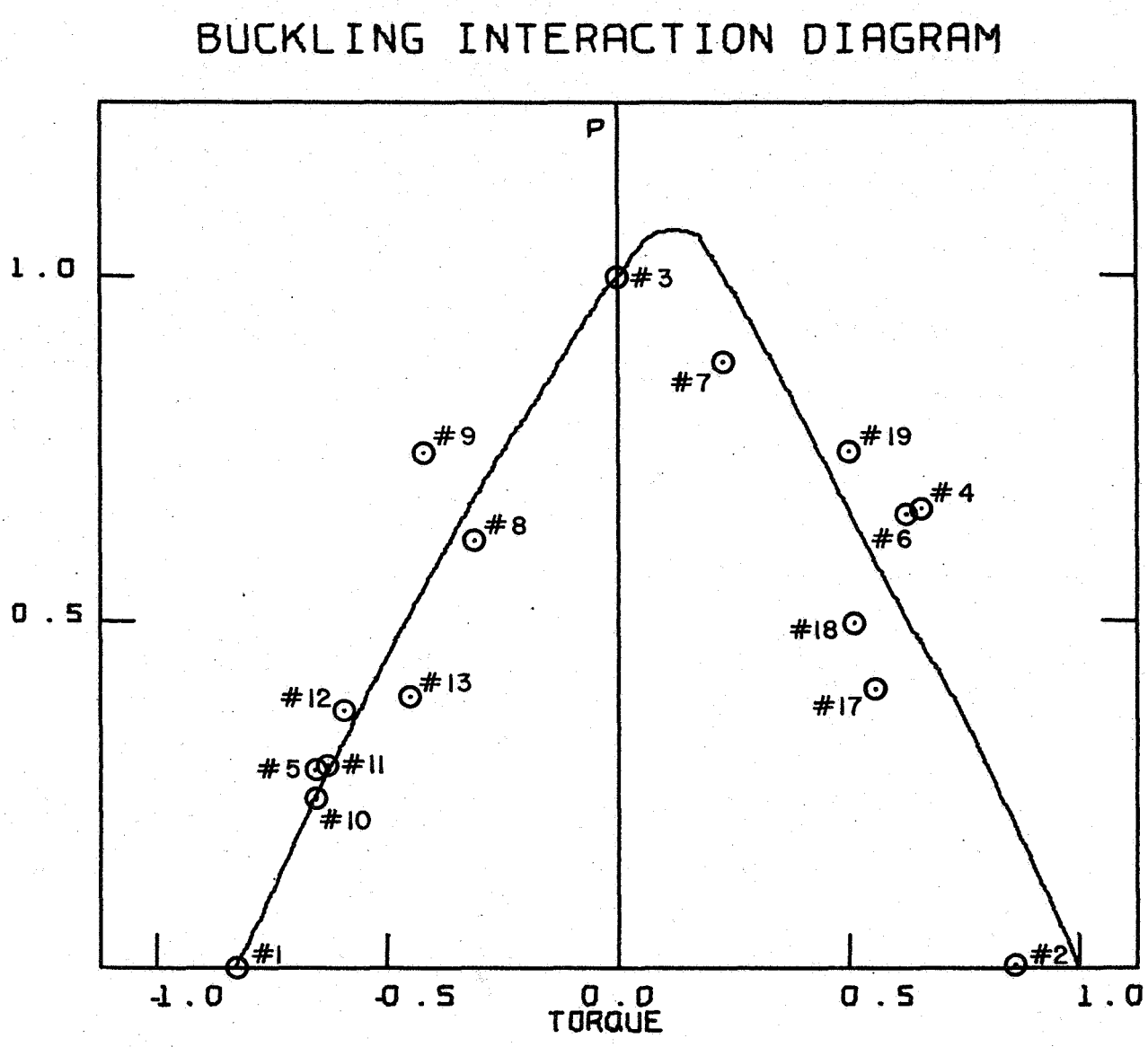

NO22 GR/E [0/±45/90]S

MAX TORQUE/COMPRESSION VALUES

T (+)		T (-)		P	
17611.8	LB-IN	-14634.1	LB-IN	32159.9	LB
1989.8	N-M	-1653.4	N-M	143054.6	N

Fig. 54. Line Interaction Diagram - Spec. #22 $[0/\pm45/90]_s$ Gr/E

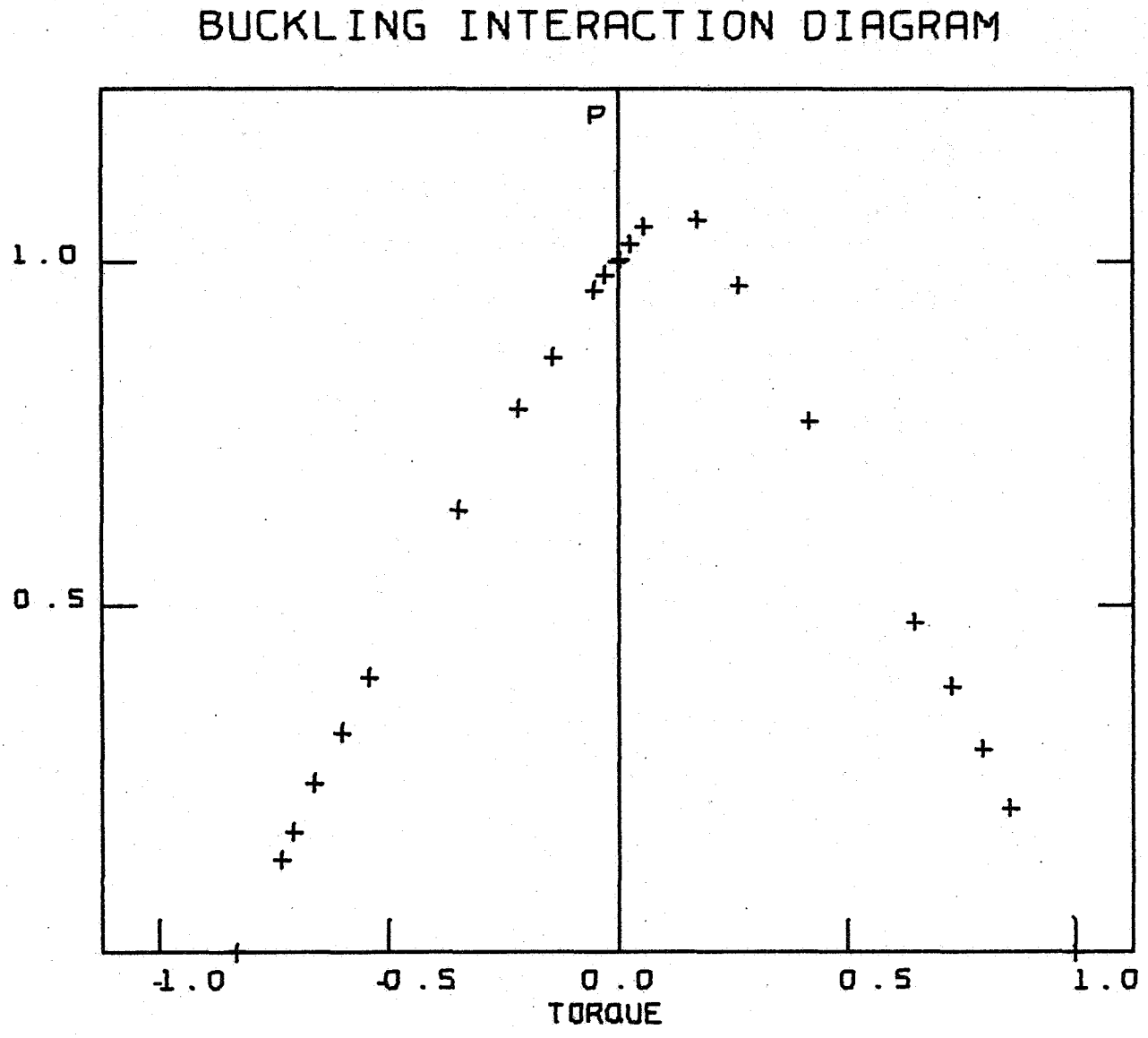

MAX TORQUE/COMPRESSION VALUES

T (+)		T (-)		P	
17611.8	LB-IN	-14634.1	LB-IN	32159.9	LB
1989.8	N-M	-1653.4	N-M	143054.6	N

Fig. 55. Point Interaction Diagram - Spec. #22 $[0/\pm45/90]_S$ Gr/E

TABLE 9

EXPERIMENTAL MAXIMUM LOADS FOR COMBINED LOADING

Test No.	Maximum Loads P(KIPS)	Maximum Loads T(K IN)	Load Ratios P/P*	Load Ratios T/T*
Spec No. 1	$[\mp 45]_s$	B/E	p*=4.0** Kip	T*=4.0 k-in
01-01	-	4.0	-	1.0
01-02	2.78	1.75	0.7	0.44
01-03	4.05	-5.3	1.01	-1.33
Spec No. 2	[0]	B/E	P*=12.5 Kip	T*=8.9**Kip-in
02-01	2.29	-	-	-
02-02	-	-2.31	-	-
02-03	-	-8.9	-	-1.0
02-04	12.5	-	1.0	-
Spec No. 3 - Not Tested				
Spec No. 4	[-82.5/30/20/-82.5]	B/E	P*=5.8 Kip	T*=6.3 Kip-in
04-01	-	-4.8	-	-
04-02	-	-10.1	-	-
04-03	-	-13.5	-	-2.14
04-04	5.8	-	1.0	-
04-05	4.4	2.95	0.76	0.47
04-06	2.95	4.45	0.51	0.71
04-07	-	6.3	-	1.0
04-08	3.1	-7.0	0.53	-1.11
04-09	2.4	-8.85	0.41	-1.40
04-10	2.55	-9.0	0.44	-1.43
04-11	2.0	-9.4	0.34	-1.49
04-12	-	-13.8	-	-2.19
04-13	-	-14.3	-	-2.27
Spec No. 5	[-82.5/30/20/-82.5]	B/E	P*=6.0** Kip	T*=7.0 K-in
05-01	-	7.0	-	1.0
Spec No. 6	$[-45/45]_s$	B/E	P*=13.85 Kip	T*=20.85 K-in
06-01	6.3	-	-	-
06-02	6.55	-	-	-
06-03	-	17.76	-	-
06-04	-	-20.8	-	-
06-05	5.75	-20.2	0.42	-0.97
06-06	6.1	-2.6	0.44	-0.12
06-07	8.35	3.4	0.60	0.16
06-08	6.83	14.95	0.49	0.72
06-09	5.5	-	-	-
06-10	6.5	-	-	-
06-11	13.85	-	1.0	-
06-12	7.5	-	-	-
06-13(155-9)+		20.85	-	1.0
06-14(155-10)+		-34.80	-	-1.67

** estimated

\+ LaRC test and run numbers

TABLE 9 EXPERIMENTAL MAXIMUM LOADS FOR COMBINED LOADING
(continued)

Test No.	Maximum Loads P(KIPS)	T(K IN)	Load Ratios P/P*	T/T*
Spec No. 7 - Not Tested				
Spec No. 8	[-82.5/30/20/-82.5]	Gr/E	P*=4.52 Kip	T*=5.6 K-in
08-01	4.52	-	1.0	-
08-02	-	-10.9	-	-1.95
08-03	-	-11.5	-	-2.05
08-04	-	5.6	-	1.0
08-05	2.85	3.85	0.63	0.69
08-06	3.57	2.75	0.79	0.49
08-07	4.37	-1.8	0.97	-0.32
08-08	0.47	-10.0	0.10	-1.79
08-09	2.5	-7.75	0.55	-1.38
08-10	2.9	3.72	0.64	0.66
08-11	3.05	3.42	0.67	0.61
08-12	2.8	-1.68	0.62	-0.30
08-13	3.25	-1.76	0.72	-0.31
08-14	3.35	-2.48	0.74	-0.44
08-15	0.18	-2.75	-	-
08-16	4.05	-2.68	0.90	-0.48
Spec No. 9	[-82.5/30/20/-82.5]	Gr/E	P**=4.5 Kip	T**=5.4 K-in
09-01	-	-	-	-
09-02	2.97	1.75	0.66	0.22
Spec No. 10	[-82.5/30/20/-82.5]	Gr/E	P**=4.5 Kip	T*=5.1 K-in
10-01	0.0	-5.0	-	-
10-02	0.0	-6.2	-	-
10-03	0.0	-7.2	-	-
10-04	0.0	5.1	-	1.0
10-05	2.31	-0.91	0.51	-0.18
10-06	2.3	-0.51	0.51	-0.10
10-07	2.0	2.57	0.44	0.50
10-08	2.24	3.16	0.50	0.62
10-09	1.46	-0.29	0.32	0.04
10-10	3.09	-0.4	0.69	-
10-11	3.61	-1.18	0.80	-0.11
10-12	0.18	-7.49	0.04	-1.47
10-13	1.76	-4.5	0.39	-0.88
Spec No. 11	$[\mp 45]_s$	Gr/E	p*=4.1 Kip	T*=5.22 K-in
11-01	4.1	-	1.0	-
11-02	-	5.22	-	1.0
11-03	-	-9.45	-	-1.81
11-04	1.5	-8.6	0.37	-1.65
11-05	3.4	-3.9	0.83	-0.75
11-06	4.0	2.6	0.98	0.50
11-07	1.56	4.25	0.38	0.81

** estimated

TABLE 9 EXPERIMENTAL MAXIMUM LOADS FOR COMBINED LOADING
(continued)

Test No.	Maximum Loads P(KIPS)	Maximum Loads T(K IN)	Load Ratios P/P*	Load Ratios T/T*
Spec No. 12	[-82.5/30/20/-82.5]		B/E P*=6.0 Kip	T*=5.0 K-in
12-01	-	5.0	-	1.0
12-02	1.55	4.1	0.26	0.82
12-03	3.6	2.1	0.60	0.42
Spec No. 13	$[0/\pm45/90]_s$		B/E P*=30.75 Kip	T*=25.0** K-in
13-01	25.0	-	-	-
13-02	30.75	-	1.0	-
13-03	-	17.2	-	-
13-04	-	-19.8	-	-0.79
13-05	13.13	-15.8	0.43	-0.61
13-06	25.0	-7.0	0.81	-0.28
13-07	25.0	4.86	0.81	0.19
13-08	25.0	4.7	0.81	0.19
13-09	24.6	14.6	0.80	0.58
13-10	15.0	6.1	0.49	0.24
13-11	25.0	10.0	0.81	0.40
13-12	22.5	8.8	0.73	0.35
13-13	36.25	10.6	1.18	0.42
Spec No. 14	$[-45_2/45_2]_s$		Gr/E P*=12.2 Kip	T*=17.6 K-in
14-01	6.2	-	-	-
14-02	11.2	-	-	-
14-03	12.2	-	1.0	-
14-04	-	17.6	-	1.0
14-05	-	-20.0	-	-1.14
14-06	8.0	-19.9	0.66	-1.13
14-07	7.8	-2.6	0.64	-0.15
14-08	7.1	-2.4	0.58	-0.14
14-09	11.4	3.3	0.93	0.19
14-10	8.5	12.0	0.70	0.68
14-11	3.0	12.9	0.25	0.73
14-12	6.25	-4.9	-	-0.28
14-13	4.0	5.2	0.33	0.30
14-14	4.9	-5.8	0.40	-0.33
14-15	6.88	-7.5	0.56	-0.43
14-16	8.5	5.6	0.70	0.32
14-17	8.13	-5.76	0.67	-0.33
14-18	5.15	-9.02	0.42	-0.51
14-19	5.43	-9.78	0.45	-0.56
14-20	7.10	-12.46	0.58	-0.71
14-21(155-1)+	0.0	17.5	-	0.99
14-22(155-2)+	0.0	17.5	-	0.99
14-23(155-3)+	0.0	-32.1	-	-1.82

** estimated
+ LaRC test and run numbers

TABLE 9 EXPERIMENTAL MAXIMUM LOADS FOR COMBINED LOADING
(continued)

Test No.	Maximum Loads P(KIPS)	T(K IN)	Load Ratios P/P*	T/T*
Spec No. 15	$[0/\pm45/90]_s$ Gr/E		P*=22.5 Kip	T*=20.4 K-in
15-01(50-1)+	-	20.4	-	1.0
15-02(50-2)+	-	-16.0	-	-0.78
15-03(50-3)+	-	20.4	-	1.0
15-04(50-4)+	-	-16.3	-	-0.80
Spec No. 16 - Not Tested				
Spec No. 17	[-82.5/30/20/-82.5] B/E		P*=6.1 Kip	T*=7.9 K-in
17-01	3.75	2.25	0.61	0.28
17-02	2.5	-	-	-
17-03	-	3.7	-	-
17-04	3.05	-	-	-
17-05	6.1	-	1.0	-
17-06	-	-7.5	-	-0.95
17-07	-	6.5	-	0.82
17-08	-	7.9	-	1.0
17-09	5.61	-2.40	0.92	-0.3
17-10	5.26	-3.5	0.86	-0.44
17-11	3.67	-5.9	0.60	-0.75
17-12	2.57	4.0	0.42	0.51
17-13	5.5	3.2	0.90	0.41
Spec No. 18	$[-45_2/45_2]_s$ Gr/E		P**=40.4 Kip	T*=19.4 K-in
18-01(155-4)+	0.0	-35.35	-	-1.82
18-02(155-5)+	0.0	19.40	-	1.0
Spec No. 19	$[-45_2/45_2]_s$ B/E		P*=13.0** Kip	T*=16.8 K-in
19-01(50-8)+	-	16.8	-	1.0
19-02(50-9)+	-	-27.7	-	-1.65
Spec No. 20	$[-45_2/45_2]_s$ Gr/E		P*=12.0** Kip	T*=18.0 K-in
20-01(50-5)+	-	18.0	-	1.0
20-02(50-7)+	-	-33.3	-	-1.85
Spec No. 21	$[-45_2/45_2]_s$ Gr/E		P**=37.3 Kip	T*=19.85 K-in
21-01(155-6)+	0.0	19.85	-	1.0
21-02(155-7)+	0.0	19.65	-	0.99
21-03(155-8)+	0.0	-33.2	-	-1.67

** estimated
+ LaRC test and run numbers

TABLE 9 EXPERIMENTAL MAXIMUM LOADS FOR COMBINED LOADING
(continued)

Test No.	Maximum Loads P(KIPS)	Maximum Loads T(K IN)	Load Ratios P/P*	Load Ratios T/T*
Spec No. 22	$[0/\pm45/90]_s$	Gr/E	P*=22.5 Kip	T*=21.0** K-in
22-01	-	-17.0	-	-0.81
22-02	-	17.9	-	0.85
22-03	22.5	-	1.0	-
22-04	14.9	13.8	0.66	0.66
22-05	6.55	-13.7	0.29	-0.65
22-06	14.6	13.4	0.65	0.64
22-07	18.75	4.8	0.83	0.23
22-08	14.1	-7.15	0.63	-0.34
22-09	16.95	-8.9	0.75	-0.42
22-10	5.75	-13.8	0.26	-0.77
22-11	6.7	-13.3	0.30	-0.63
22-12	8.38	-12.4	0.37	-0.59
22-13	8.88	-9.4	0.39	-0.45
22-14	7.13	-6.1	0.32	-0.29
22-15	8.28	-4.56	0.37	-0.22
22-16	8.43	-4.6	0.37	-0.22
22-17	9.15	11.46	0.41	0.55
22-18	11.43	10.35	0.51	0.49
22-19	16.6	10.8	0.74	0.51
22-20	17.18	-	0.76	-
Spec No. 23	$[0/\pm45/90]_s$	B/E	P*=30.0** Kip	T*=23.8** K-in
23-01(630-1)+	-	23.8	-	1.0
23-02(630-2)+	-	-20.8	-	-0.87
23-03	14.76	-13.56	0.49	-0.57
23-04	17.15	-13.72	0.57	-0.58
Specs A & B	$[0/\pm45/90]_s$	Gr/E	P*=19.25 Kip	T*=20.2 K-in
AB-01(623-1)+	18.65	-	0.97	-
AB-02(623-2)+	19.25	-	1.0	-
AB-03(624-1)+	-	20.2	-	1.0
AB-04(624-2)+	-	-15.3	-	-0.76
AB-05(625-1)+	5.3	-14.1	0.28	-0.70
AB-06(625-2)+	12.5	-10.6	0.65	-0.52
AB-07(625-3)+	6.5	-10.1	0.34	0.50
AB-08(625-4)+	6.5	17.8	0.34	0.88
AB-09(625-5)+	15.4	12.0	0.80	0.59

* estimated
\+ LaRC test and run numbers

REFERENCES

1. Wu, C. H., "Buckling of Anisotropic Circular Cylindrical Shells," Ph.D. Thesis, Case Western Reserve University, June, 1971.

2. Marlowe, D. E., Sushinsky, G. F., and Dexter, H. B., "Elastic Torsional Buckling of Thin-Walled Composite Cylinders," Composite Materials Testing and Design (Third Conference) ASTM STP 546, Am. Soc. for Testing and Materials, 1974, pp. 84-108.

3. Wilkins, D. J., and Love, T. S., "Combined Compression-Torsion Buckling Tests of Laminated Composite Cylindrical Shells," AIAA Paper No. 74-379, AIAA/ASME/SAE 15th Structures, Structural Dynamics and Materials Conference, Las Vegas, Nev., April, 1974.

4. Tennyson, R. C., "Buckling of Laminated Composite Cylinders: A Review," Composites, January, 1975.

5. Flügge, W. Stresses in Shells, Springer-Verlag, Berlin, 1962.

6. Wilson, G. W., III and Herakovich, C. T., "Application of a Dedicated Microprocessor for Automatic Data Acquisition of Load Strain and Acoustic Emission Data," Experimental Mechanics, Vol. 16, No. 3, March 1976.

7. Jones, R. M., Mechanics of Composite Materials, McGraw-Hill, New York, 1975.

APPENDIX A

Buckling Loads as Predicted by Wu Program

BUCKLING LOADS AS PREDICTED BY WU PROGRAM

Tube No: 1 Laminate: $[-45/45]_s$ Material: B/E

Length (in): L = 19.875 Avg. Radius (in): R = 2.987 Thickness (in): t = 0.022

Max Torque: T* = 4607.0 in-lbs Max Axial Load/cir.: P* = 486.99 lbs/in Max Axial Load: $2\pi RP^*$ = 9139.77 lbs

Given Load Ratios		Predicted Buckling Loads		Buckling Ratios	
P	T	P(lbs/in)	T(in-lbs)	P/P*	T/T*
0.0	1.0	0.0	4607.0	0.0	1.0
0.0	-1.0	0.0	-7613.2	0.0	-1.6525
1.0	0.0	486.99	0.0	1.0	0.0
1.0	1.0	72.122	4043.2	0.1481	0.8776
1.0	-1.0	120.76	-6770.0	0.2480	-1.4695
1.0	0.75	92.511	3889.6	0.1900	0.8443
1.0	-0.75	153.79	-6466.0	0.3153	-1.4035
1.0	-0.5	213.56	-5986.2	0.4385	-1.2994
1.0	0.5	129.76	3637.1	0.2665	0.7895
1.0	0.35	168.20	3300.2	0.3454	0.7163
1.0	-0.35	282.26	-5538.2	0.5796	-1.2021
1.0	-0.25	350.67	-4914.6	0.7201	-1.0668
1.0	0.25	209.50	2936.1	0.4302	0.6373
1.0	0.1	335.55	1881.1	0.6890	0.4083
1.0	-0.1	498.51	-2794.6	1.0237	-0.6066
1.0	-0.05	488.88	-1370.3	1.0039	-0.2974
1.0	0.05	416.59	1167.7	0.8554	0.2535
1.0	0.03	458.50	771.10	0.9415	0.1674
1.0	-0.03	485.78	-816.98	0.9975	-0.1773
1.0	-0.01	484.99	-271.88	0.9959	-0.0590
1.0	0.01	493.32	276.55	1.0130	0.0600
1.0	0.005	476.61	133.59	0.9787	0.0290
1.0	-0.005	493.08	-138.21	1.0125	-0.0300
1.0	-0.003	487.75	-82.030	1.0016	-0.0178
1.0	0.003	477.54	80.312	0.9806	0.0174
1.0	0.001	483.47	27.103	0.9928	0.0059
1.0	-0.001	483.47	-27.103	0.9928	0.0059

BUCKLING LOADS AS PREDICTED BY WU PROGRAM

Tube No: 2 | Laminate: [0] | Material: B/E

Length (in): L = 20.0 | Avg. Radius (in): R = 2.9765 | Thickness (in): t = 0.0368

Max Torque: T* = 11209.0 | Max Axial Load/cir.: P* = 1215.4 | Max Axial Load: $2\pi RP^*$ = 22730.29

Given Load Ratios		Predicted Buckling Loads		Buckling Ratios	
P	T	P(lbs/in)	T(in-lbs)	P/P*	T/T*
0.0	1.0	0.0	11209.0	0.0	1.0
0.0	-1.0	0.0	-11209.0	0.0	-1.0
1.0	0.0	1215.4	0.0	1.0	0.0
1.0	1.0	179.62	9998.6	0.1478	0.8920
1.0	0.75	229.07	9563.5	0.1885	0.8532
1.0	-0.75	229.07	-9563.5	0.1885	-0.8532
1.0	-0.5	320.05	-8908.0	0.2633	-0.7947
1.0	0.5	320.05	8908.0	0.2633	0.7947
1.0	0.35	420.31	8189.0	0.3458	0.7306
1.0	-0.35	420.31	-8189.0	0.3458	-0.7306
1.0	-0.25	523.25	-7281.8	0.4305	-0.6496
1.0	0.25	523.25	7281.8	0.4305	0.6496
1.0	0.1	805.89	4486.1	0.6631	0.4002
1.0	-0.1	805.89	-4486.1	0.6631	-0.4002
1.0	-0.05	995.30	-2770.2	0.8189	-0.2471
1.0	0.05	968.66	2696.1	0.7970	0.2405
1.0	0.03	1026.7	1714.6	0.8447	0.1530
1.0	-0.03	1123.7	-1876.6	0.9246	-0.1674
1.0	-0.01	1109.1	-617.41	0.9125	-0.0551
1.0	0.01	1101.0	612.87	0.9059	0.0547
1.0	0.005	1120.6	311.89	0.9220	0.0278
1.0	-0.005	1078.9	-300.29	0.8877	-0.0268
1.0	-0.003	647.97	-108.21	0.5331	-0.0097
1.0	0.003	1121.0	187.21	0.9223	0.0167
1.0	0.001	769.50	42.835	0.6331	0.0038
1.0	-0.001	1198.0	-66.690	0.9857	-0.0059
1.0	-1.0	138.03	-7683.4	0.1136	-0.6855

BUCKLING LOADS AS PREDICTED BY WU PROGRAM

Tube No: 12 Laminate: [-82.5/30/20/-82.5] Material: B/E

Length (in): L = 20.063 Avg. Radius (in): R = 2.984 Thickness (in): t = 0.021

Max Torque: T* = 7330.8 Max Axial Load/cir.: P* = 454.08 Max Axial Load: $2\pi RP^*$ = 8513.56

Given Load Ratios		Predicted Buckling Loads		Buckling Ratios	
P	T	P(lbs/in)	T(in-lbs)	P/P*	T/T*
0.0	1.0	0.0	7330.8	0.0	1.0
0.0	-1.0	0.0	-13845.0	0.0	-1.8886
1.0	0.0	454.08	0.0	1.0	0.0
1.0	1.0	111.57	6242.2	0.2457	0.8520
1.0	-1.0	218.18	-12207.0	0.4805	-1.6652
1.0	0.75	140.26	5885.4	0.3089	0.8028
1.0	-0.75	279.61	-11733.0	0.6158	-1.6005
1.0	0.5	191.78	5364.7	0.4223	0.7318
1.0	-0.5	332.73	-9307.5	0.7328	-1.2696
1.0	0.35	241.71	4733.0	0.5323	0.6456
1.0	-0.35	377.54	-7392.8	0.8314	-1.0085
1.0	0.25	296.14	4142.1	0.6522	0.5650
1.0	-0.25	388.64	-5435.8	0.8559	-0.7415
1.0	0.1	415.11	2322.4	0.9142	0.3168
1.0	-0.1	422.93	-2366.2	0.9314	-0.3228
1.0	0.05	470.38	1315.8	1.0359	0.1795
1.0	-0.05	452.89	-1266.9	0.9974	-0.1728
1.0	0.03	464.82	780.16	1.0237	0.1064
1.0	-0.03	450.89	-756.78	0.9930	-0.1032
1.0	0.01	455.08	254.61	1.0022	0.0347
1.0	-0.01	449.31	-251.38	0.9895	-0.0343
1.0	0.005	455.81	127.51	1.0038	0.0174
1.0	-0.005	473.07	-132.33	1.0418	-0.0181
1.0	0.001	455.19	25.467	1.0024	0.0035

BUCKLING LOADS AS PREDICTED BY WU PROGRAM

Tube No: 13 Laminate: $[0/\pm45/90]_s$ Material: B/E

Length (in): L = 20.062 Avg. Radius (in): R = 2.9760 Thickness (in): t = 0.0400

Max Torque: T* = 25179.0 Max Axial Load/cir.: P* = 2505.3 Max Axial Load: $2\pi RP^*$ = 46846.00

Given Load Ratios		Predicted Buckling Loads		Buckling Ratios	
P	T	P(lbs/in)	T(in-lbs)	P/P*	T/T*
0.0	1.0	0.0	25179.0	0.0	1.0
0.0	-1.0	0.0	-21116.0	0.0	-0.8386
1.0	0.0	2505.3	0.0	1.0	0.0
1.0	1.0	409.63	22795.0	0.1635	0.9053
1.0	-1.0	339.47	-18891.0	0.1355	-0.7503
1.0	0.75	525.61	21937.0	0.2098	0.8712
1.0	-0.75	433.96	-18112.0	0.1732	-0.7193
1.0	0.5	728.83	20279.0	0.2906	0.8054
1.0	-0.5	599.83	-16689.0	0.2394	-0.6628
1.0	0.35	952.12	18544.0	0.3800	0.7365
1.0	-0.35	786.15	-15312.0	0.3138	-0.6081
1.0	0.25	1208.3	16810.0	0.4823	0.6676
1.0	-0.25	989.20	-13762.0	0.3948	-0.5466
1.0	0.1	1941.2	10802.0	0.7748	0.4290
1.0	-0.1	1600.8	-8907.9	0.6390	-0.3538
1.0	0.05	2415.3	6720.2	0.9641	0.2669
1.0	-0.05	1967.7	-5474.9	0.7854	-0.2174
1.0	0.03	2656.3	4434.6	1.0603	0.1761
1.0	-0.03	2153.9	-3595.7	0.8597	-0.1428
1.0	0.01	2612.8	1453.9	1.0429	0.0577
1.0	-0.01	2373.8	-1321.0	0.9475	-0.0525
1.0	0.005	2560.9	7125.3	1.022	0.2830
1.0	-0.005	2434.2	-676.78	0.9716	-0.0269
1.0	-0.001	2502.9	139.28	0.9990	0.0055

BUCKLING LOADS AS PREDICTED BY WU PROGRAM

Tube No: 14	Laminate: $[-45_2/45_2]_s$	Material: Gr/E
Length (in): L = 20.063	Avg. Radius (in): R = 2.9755	Thickness (in): t = 0.0500
Max Torque: T* = 23344.0	Max Axial Load/cir.: P* = 1854.4	Max Axial Load: $2\pi RP^*$ = 34669.15

Given Load Ratios		Predicted Buckling Loads		Buckling Ratios	
P	T	P(lbs/in)	T(in-lbs)	P/P*	T/T*
0.0	1.0	0.0	23344.0	0.0	1.0
0.0	-1.0	0.0	-46613.0	0.0	-1.9968
1.0	0.0	1854.4	0.0	1.0	0.0
1.0	1.0	359.11	19977.0	0.1937	0.8558
1.0	-1.0	702.64	-39087.0	0.3789	-1.6744
1.0	0.75	455.43	19001.0	0.2456	0.8140
1.0	-0.75	895.97	-37381.0	0.4832	-1.6013
1.0	0.5	626.72	17432.0	0.3380	0.7467
1.0	-0.5	1207.3	-33580.0	0.6510	-1.4385
1.0	0.35	801.55	15606.0	0.4322	0.6685
1.0	-0.35	1519.6	-29587.0	0.8195	-1.2674
1.0	0.25	988.16	13743.0	0.5329	0.5887
1.0	-0.25	1825.8	-25392.0	0.9846	-1.0877
1.0	0.1	1474.6	8203.3	0.7952	0.3514
1.0	-0.1	1923.8	-10702.0	1.0374	-0.4584
1.0	0.05	1760.4	4896.5	0.9493	0.2098
1.0	-0.05	1886.8	-5248.1	1.0175	-0.2248
1.0	0.03	1885.9	3147.3	1.0170	0.1348
1.0	-0.03	1880.0	-3137.5	1.0138	-0.1344
1.0	0.01	1841.5	1024.4	0.9930	0.0439
1.0	-0.01	1861.8	-1035.7	1.0040	-0.0444
1.0	0.005	1846.1	513.47	0.9955	0.0220
1.0	-0.005	1850.1	-514.60	0.9977	-0.0220
1.0	0.001	1852.7	103.06	0.9991	0.0044

BUCKLING LOADS AS PREDICTED BY WU PROGRAM

Tube No: 15	Laminate: $[0/\pm45/90]_s$	Material: Gr/E
Length (in): L = 20.063	Avg. Radius (in): R = 2.9755	Thickness (in): t = 0.0400
Max Torque: T* = 23143.0	Max Axial Load/cir.: P* = 2225.7	Max Axial Load: $2\pi RP^*$ = 4160.84

Given Load Ratios		Predicted Buckling Loads		Buckling Ratios	
P	T	P(lbs/in)	T(in-lbs)	P/P*	T/T*
0.0	1.0	0.0	23143.0	0.0	1.0
0.0	-1.0	0.0	-18647.0	0.0	-0.8057
1.0	0.0	2225.7	0.0	1.0	0.0
1.0	1.0	372.14	20702.0	0.1672	0.8945
1.0	-1.0	298.39	-16599.0	0.1341	-0.7172
1.0	0.75	476.26	19870.0	0.2140	0.8586
1.0	-0.75	385.55	-16086.0	0.1732	-0.6951
1.0	0.5	663.60	18458.0	0.2982	0.7976
1.0	-0.5	532.78	-14819.0	0.2394	-0.6403
1.0	0.35	868.19	16904.0	0.3901	0.7304
1.0	-0.35	705.08	-13728.0	0.3168	-0.5932
1.0	0.25	1096.1	15243.0	0.4925	0.6586
1.0	-0.25	881.97	-12266.0	0.3963	-0.5300
1.0	0.1	1773.0	9862.9	0.7966	0.4262
1.0	-0.1	1402.0	-7799.1	0.6299	-0.3370
1.0	0.05	2219.6	6173.7	0.9973	0.2668
1.0	-0.05	1731.6	-4816.4	0.7780	-0.2081
1.0	0.03	2472.2	4125.8	1.1108	0.1783
1.0	-0.03	1929.0	-3219.3	0.8667	-0.1391
1.0	0.01	2345.1	1304.5	1.0536	0.0564
1.0	-0.01	2121.5	-1180.2	0.9532	-0.0510
1.0	0.005	2299.5	639.60	1.0332	0.0276
1.0	-0.005	2172.5	-604.28	0.9761	-0.0261
1.0	0.001	2244.5	124.86	1.0084	0.0054
1.0	-0.001	2217.5	-123.36	0.9963	-0.0554
1.0	0.003	2269.3	378.71	1.0196	0.0164

BUCKLING LOADS AS PREDICTED BY WU PROGRAM

Tube No: 16	Laminate: $[-45/45]_s$	Material: Gr/E
Length (in): L = 18.938	Avg. Radius (in): R = 2.988	Thickness (in): t = 0.025
Max Torque: T* = 4988.0	Max Axial Load/cir.: P* = 460.82	Max Axial Load: $2\pi RP^*$ = 8651.5074

Given Load Ratios		Predicted Buckling Loads		Buckling Ratios	
P	T	P(lbs/in)	T(in-lbs)	P/P*	T/T*
0.0	1.0	0.0	4988.0	0.0	1.0
0.0	-1.0	0.0	-9045.9	0.0	-1.8135
1.0	0.0	460.82	0.0	1.0	0.0
1.0	1.0	77.497	4347.4	0.1682	0.8716
1.0	-1.0	139.67	-7834.9	0.3031	-1.5707
1.0	0.75	99.404	4182.2	0.2157	0.8385
1.0	-0.75	177.58	-7471.1	0.3854	-1.4978
1.0	0.5	137.00	3842.6	0.2973	0.7704
1.0	-0.5	247.11	-6931.1	0.5362	-1.3896
1.0	0.35	177.78	3490.5	0.3858	0.6998
1.0	-0.35	320.02	-6283.2	0.6945	-1.2597
1.0	0.25	221.01	3099.5	0.4796	0.6214
1.0	-0.25	397.5	-5574.7	0.8626	-1.1176
1.0	0.1	343.22	1925.4	0.7448	0.3860
1.0	-0.1	479.49	-2689.8	1.0405	-0.5393
1.0	0.05	417.84	1172.0	0.9067	0.2350
1.0	-0.05	495.12	-1388.8	1.0744	-0.2784
1.0	0.03	454.11	764.23	0.9854	0.1532
1.0	-0.03	467.35	-786.52	1.0142	-0.1577
1.0	0.01	458.65	257.29	0.9953	0.0516
1.0	-0.01	474.70	-266.30	1.0301	-0.0534
1.0	0.005	468.11	131.30	1.0158	0.0263
1.0	-0.005	460.87	-129.27	1.0001	-0.0259
1.0	0.001	460.37	25.826	0.9990	0.0052

BUCKLING LOADS AS PREDICTED BY WU PROGRAM

Tube No: 17 Laminate: [-82.5/30/20/-82.5] Material: B/E

Length (in): L = 20.125 Avg. Radius (in): R = 2.9865 Thickness (in): t = 0.0210

Max Torque: T* = 7327.0 Max Axial Load/cir.: P* = 458.33 Max Axial Load: $2\pi RP^*$ = 8600.44

Given Load Ratios		Predicted Buckling Loads		Buckling Ratios	
P	T	P(lbs/in)	T(in-lbs)	P/P*	T/T*
0.0	1.0	0.0	7327.0	0.0	1.0
0.0	-1.0	0.0	-13838.0	0.0	-1.8886
1.0	1.0	111.14	6228.6	0.2425	0.8501
1.0	-1.0	216.23	-12117.0	0.4718	-1.6537
1.0	0.0	458.33	0.0	1.0	0.0
1.0	0.75	139.96	5882.8	0.3054	0.8029
1.0	-0.75	277.76	-11675.0	0.6060	-1.5934
1.0	0.5	189.57	5311.8	0.4136	0.7250
1.0	-0.5	337.41	-9454.3	0.7362	-1.2903
1.0	0.35	241.36	4734.2	0.5266	0.6461
1.0	-0.35	359.60	-7053.3	0.7846	-0.9626
1.0	0.25	294.21	4121.9	0.6419	0.5626
1.0	-0.25	393.98	-5519.8	0.8596	-0.7534
1.0	0.1	415.46	2328.3	0.9065	0.3178
1.0	-0.01	449.17	-251.72	0.9800	-0.0344
1.0	0.05	476.40	1334.9	1.0394	0.1822
1.0	-0.05	438.73	-1229.3	0.9572	-0.1678
1.0	0.03	462.73	777.96	1.0096	0.1062
1.0	-0.03	442.95	-744.71	0.9664	-0.1016
1.0	0.01	476.10	266.81	1.0388	-0.0364
1.0	0.005	455.72	127.69	0.9943	0.0174
1.0	-0.005	450.42	-126.21	0.9827	-0.0172
1.0	0.001	454.59	25.476	0.9918	0.0035

BUCKLING LOADS AS PREDICTED BY WU PROGRAM

Tube No: 18 | Laminate: $[-45_2/45_2]$ | Material: Gr/E

Length (in): L = 20.937 | Avg. Radius (in): R = 2.9725 | Thickness (in): t = 0.054

Max Torque: T* = 26931.0 | Max Axial Load/cir.: P* = 2154.1 | Max Axial Load: $2\pi RP^*$ = 40231.63

Given Load Ratios		Predicted Buckling Loads		Buckling Ratios	
P	T	P(lbs/in)	T(in-lbs)	P/P*	T/T*
0.0	1.0	0.0	26931.0	0.0	1.0
0.0	-1.0	0.0	-52496.0	0.0	-1.9493
1.0	0.0	2154.1	0.0	1.0	0.0
1.0	1.0	413.53	22958.0	0.1920	0.8525
1.0	-1.0	791.12	-43921.0	0.3673	-1.6309
1.0	0.75	522.72	21765.0	0.2427	0.8082
1.0	-0.75	999.15	-41602.0	0.4638	-1.5448
1.0	0.5	717.11	19906.0	0.3329	0.7391
1.0	-0.5	1344.9	-37333.0	0.6243	-1.3862
1.0	0.35	920.33	17883.0	0.4272	0.6640
1.0	-0.35	1708.1	-33190.0	0.7930	-1.2324
1.0	0.25	1128.6	15664.0	0.5239	0.5816
1.0	-0.25	2064.4	-28652.0	0.9584	-1.0639
1.0	0.1	1713.9	9514.8	0.7956	0.3533
1.0	-0.1	2237.7	-12423.0	1.0388	-0.4613
1.0	0.05	2067.0	5737.6	0.9596	0.2130
1.0	-0.05	2222.6	-6169.6	1.0318	-0.2291
1.0	0.03	2121.0	3532.5	0.9846	0.1312
1.0	-0.03	2203.9	-3670.5	1.0231	-0.1363
1.0	0.01	2144.8	1190.7	0.9957	0.0442
1.0	-0.01	2160.2	-1199.3	1.0028	-0.0445
1.0	0.005	2154.7	598.12	1.0003	0.0222
1.0	-0.005	2154.8	-598.13	1.0003	-0.0222
1.0	0.001	2152.1	119.47	0.9991	0.0044

BUCKLING LOADS AS PREDICTED BY WU PROGRAM

Tube No: 19	Laminate: $[-45_2/45_2]_s$	Material: B/E
Length (in): L = 20.063	Avg. Radius (in): R = 2.9785	Thickness (in): t = 0.038
Max Torque: T* = 15764.0	Max Axial Load/cir.: P* = 1447.8	Max Axial Load: $2\pi RP^*$ = 27094.806

Given Load Ratios		Predicted Buckling Loads		Buckling Ratios	
P	T	P(lbs/in)	T(in-lbs)	P/P*	T/T*
0.0	1.0	0.0	15764.0	0.0	1.0
1.0	-1.0	413.09	-23026.0	0.2853	-1.4607
1.0	0.0	1447.8	0.0	1.0	0.0
1.0	1.0	242.17	13499.0	0.1763	0.8563
1.0	0.75	312.07	13046.0	0.2155	0.8276
1.0	-0.75	527.71	-22061.0	0.3645	-1.3995
1.0	0.5	428.53	11943.0	0.2960	0.7576
1.0	-0.5	720.20	-20072.0	0.4973	-1.2733
1.0	0.35	552.99	10788.0	0.3820	0.6843
1.0	-0.35	938.22	-18304.0	0.6840	-1.1611
1.0	0.25	876.01	12207.0	0.6051	0.7744
1.0	-0.25	1172.8	-16343.0	0.8101	-1.0367
1.0	0.1	1069.8	5963.3	0.7389	0.3783
1.0	-0.1	1521.4	-8480.6	1.0508	-0.5380
1.0	0.05	1306.2	3640.6	0.9022	0.2309
1.0	-0.05	1461.2	-4072.3	1.0093	-0.2583
1.0	0.03	1423.9	2381.1	0.9835	0.1510
1.0	-0.03	1452.9	-2429.5	1.0035	-0.1541
1.0	0.01	1447.3	806.72	0.9997	0.0512
1.0	-0.01	1436.3	-800.61	0.9921	-0.0508
1.0	0.005	1450.9	404.37	1.0021	0.0257

BUCKLING LOADS AS PREDICTED BY WU PROGRAM

Tube No: 20 | Laminate: $[-45_2/45_2]$ | Material: Gr/E

Length (in): L = 20.937 | Avg. Radius (in): R = 2.975 | Thickness (in): t = 0.052

Max Torque: T* = 24765.0 | Max Axial Load/cir.: P* = 2000.3 | Max Axial Load: $2\pi RP^*$ = 37390.56

Given Load Ratios		Predicted Buckling Loads		Buckling Ratios	
P	T	P(lbs/in)	T(in-lbs)	P/P*	T/T*
0.0	1.0	0.0	24765.0	0.0	1.0
0.0	-1.0	0.0	-48914.0	0.0	-1.9751
1.0	0.0	2000.3	0.0	1.0	0.0
1.0	1.0	379.55	21107.0	0.1897	0.8523
1.0	-1.0	724.46	-40287.0	0.3622	-1.6268
1.0	0.75	481.17	20068.0	0.2405	0.8103
1.0	-0.75	920.75	-38402.0	0.4603	-1.5507
1.0	0.5	661.27	18387.0	0.3306	0.7425
1.0	-0.5	1247.8	-34694.0	0.6238	-1.4009
1.0	0.35	845.03	16447.0	0.4225	0.6641
1.0	-0.35	1575.7	-30668.0	0.7877	-1.2384
1.0	0.25	1038.9	14443.0	0.5194	0.5832
1.0	-0.25	1915.7	-26634.0	0.9577	-1.0755
1.0	0.1	1587.8	8829.5	0.7938	0.3565
1.0	-0.1	2122.6	-11804.0	1.0611	-0.4766
1.0	0.05	1893.0	5263.6	0.9464	0.2125
1.0	-0.05	2036.4	-5662.1	1.0180	-0.2286
1.0	0.03	1967.6	3282.5	0.9837	0.1325
1.0	-0.03	2023.2	-3375.3	1.0114	-0.1363
1.0	0.01	1984.7	1103.7	0.9922	0.0446
1.0	-0.01	2014.1	-1120.0	1.0069	-0.0452
1.0	0.005	1994.0	554.43	0.9969	0.0224
1.0	-0.005	1994.0	-554.43	0.9969	-0.0224
1.0	0.001	1998.4	111.13	0.9991	0.0045

BUCKLING LOADS AS PREDICTED BY WU PROGRAM

Tube No: 21 | Laminate: $[-45_2/45_2]$ | Material: Gr/E

Length (in): L = 16.937 | Avg. Radius (in): R = 2.9745 | Thickness (in): t = 0.051

Max Torque: T* = 27004.0 | Max Axial Load/cir.: P* = 2017.0 | Max Axial Load: $2\pi RP^*$ = 37696.39

Given Load Ratios		Predicted Buckling Loads		Buckling Ratios	
P	T	P(lbs/in)	T(in-lbs)	P/P*	T/T*
0.0	1.0	0.0	27004.0	0.0	1.0
0.0	-1.0	0.0	-53758.0	0.0	-1.9907
1.0	0.0	2017.0	0.0	1.0	0.0
1.0	1.0	410.29	22809.0	0.2034	0.8447
1.0	-1.0	805.47	-44777.0	0.3993	-1.6582
1.0	0.75	520.33	21694.0	0.2580	0.8034
1.0	-0.75	1020.9	-42567.0	0.5061	-1.5763
1.0	0.5	701.95	19511.0	0.3480	0.7225
1.0	-0.5	1396.4	-38813.0	0.6923	-1.4373
1.0	0.35	901.07	17532.0	0.4467	0.6492
1.0	-0.35	1787.4	-34778.0	0.8862	-1.2879
1.0	0.25	1101.2	15304.0	0.5460	0.5667
1.0	-0.25	2129.9	-29602.0	1.0560	-1.0962
1.0	0.1	1634.1	9084.4	0.8102	0.3364
1.0	-0.1	2137.4	-11882.0	1.0597	-0.4400
1.0	0.05	1951.8	5425.1	0.9677	0.2009
1.0	-0.05	1960.6	-5449.5	0.9720	-0.2018
1.0	0.03	1978.3	3299.3	0.9808	0.1222
1.0	-0.03	2025.8	-3378.5	1.0044	-0.1251
1.0	0.01	1915.6	1064.9	0.9497	0.0394
1.0	-0.01	1933.4	-1074.8	0.9586	-0.0398
1.0	0.005	1935.1	537.89	0.9594	0.0199
1.0	-0.005	1924.5	534.92	0.9541	0.0198
1.0	0.001	2015.1	112.02	0.9991	0.0041

BUCKLING LOADS AS PREDICTED BY WU PROGRAM

Tube No: -

Laminate: $[-45_2/45_2/-45_2/45_2]$

Material: B/E

Length (in): L = 20.063

Avg. Radius (in): R = 2.9785

Thickness (in): t = 0.038

Max Torque: T* = 21811.0

Max Axial Load/cir.: P* = 1761.5

Max Axial Load: $2\pi RP^*$ = 32965.53

Given Load Ratios		Predicted Buckling Loads		Buckling Ratios	
P	T	P(lbs/in)	T(in-lbs)	P/P*	T/T*
0.0	1.0	0.0	21811.0	0.0	1.0
1.0	-1.0	339.33	-18914.0	0.1926	-0.8672
1.0	0.0	1761.5	0.0	1.0	0.0
1.0	1.0	339.33	18914.0	0.1926	0.8672
1.0	0.75	432.53	18082.0	0.2455	0.8290
1.0	-0.75	432.53	-18082.0	0.2455	-0.8290
1.0	0.5	599.48	16708.0	0.3403	0.7660
1.0	-0.5	599.48	-16708.0	0.3403	-0.7660
1.0	0.35	768.40	14991.0	0.4362	0.6873
1.0	-0.35	768.40	-14991.0	0.4362	-0.6873
1.0	0.25	951.30	13257.0	0.5401	0.6078
1.0	-0.25	951.30	-13257.0	0.5401	-0.6078
1.0	0.1	1505.9	8394.3	0.8549	0.3849
1.0	-0.1	1505.9	-8394.3	0.8549	-0.3849
1.0	0.05	1736.3	4839.3	0.9857	0.2219
1.0	-0.05	1736.3	-4839.3	0.9857	-0.2219
1.0	0.03	1716.6	2870.6	0.9745	0.1316
1.0	-0.03	1716.6	-2870.6	0.9745	-0.1316
1.0	0.01	1734.0	966.57	0.9844	0.0443
1.0	-0.01	1734.0	-966.57	0.9844	-0.0443
1.0	0.005	1785.1	497.52	1.0134	0.0228

BUCKLING LOADS AS PREDICTED BY WU PROGRAM

Tube No: -	Laminate: $[\pm 45]_s$	Material: B/E
Length (in): L = 20.062	Avg. Radius (in): R = 2.987	Thickness (in): t = 0.022
Max Torque: T* = 7592.7	Max Axial Load/cir.: P* = 479.37	Max Axial Load: $2\pi RP^*$ = 8996.76

Given Load Ratios		Predicted Buckling Loads		Buckling Ratios	
P	T	P(lbs/in)	T(in-lbs)	P/P*	T/T*
0.0	1.0	0.0	7592.7	0.0	1.0
0.0	-1.0	0.0	-4636.7	0.0	-0.6107
1.0	0.0	479.37	0.0	1.0	0.0
1.0	1.0	120.40	6749.4	0.2512	0.8889
1.0	-1.0	72.133	-4043.7	0.1505	-0.5326
1.0	0.75	154.14	6480.9	0.3215	0.8536
1.0	-0.75	92.957	-3908.4	0.1939	-0.5148
1.0	0.5	215.20	6031.9	0.4489	0.7944
1.0	-0.5	128.95	-3614.3	0.2690	-0.4760
1.0	0.35	279.31	5480.2	0.5827	0.7218
1.0	-0.35	167.08	-3278.2	0.3485	-0.4318
1.0	0.25	351.69	4928.9	0.7337	0.6492
1.0	-0.25	210.85	-2955.0	0.4398	-0.3892
1.0	0.1	503.23	2821.1	1.0498	0.3716
1.0	-0.1	335.44	-1880.5	0.6998	-0.2477
1.0	0.05	489.26	1371.4	1.0206	0.1806
1.0	-0.05	412.50	-1156.2	0.8605	-0.1523
1.0	0.03	489.81	823.76	1.0218	0.1085
1.0	-0.03	456.04	-766.96	0.9513	-0.1010
1.0	0.01	493.43	276.61	1.0293	0.0364
1.0	-0.01	477.33	-267.59	0.9957	-0.0352
1.0	0.005	478.89	134.23	0.9990	0.0177
1.0	-0.005	482.28	-135.18	1.0061	-0.0178
1.0	0.001	478.90	26.847	0.9990	0.0035

BUCKLING LOADS AS PREDICTED BY WU PROGRAM

Tube No: Av. Size Laminate: [-82.5/30/20/-82.5] Material: B/E

Length (in): L = 20.063 Avg. Radius (in): R = 3.00 Thickness (in): t = 0.0212

Max Torque: T* = 11633.0 Max Axial Load/cir.: P* = 663.82 Max Axial Load: $2\pi RP^*$ = 12512.71

Given Load Ratios		Predicted Buckling Loads		Buckling Ratios	
P	T	P(lbs/in)	T(in-lbs)	P/P*	T/T*
0.0	1.0	0.0	11633.0	0.0	1.0
0.0	-1.0	0.0	-12958.0	0.0	-1.1139
1.0	0.0	663.82	0.0	1.0	0.0
1.0	1.0	180.20	10190.0	0.2715	0.8760
1.0	-1.0	200.14	-11318.0	0.3015	-0.9729
1.0	0.75	228.70	9699.7	0.3445	0.8338
1.0	-0.75	257.60	-10925.0	0.3881	-0.9391
1.0	0.5	319.39	9030.6	0.4811	0.7763
1.0	-0.5	356.28	-10074.0	0.5367	-0.8660
1.0	0.35	411.90	8152.3	0.6205	0.7008
1.0	-0.35	460.32	-9110.6	0.6934	-0.7832
1.0	0.25	506.47	7160.0	0.7630	0.6155
1.0	-0.25	569.77	-8054.9	0.8583	-0.6924
1.0	0.1	641.59	3628.1	0.9665	0.3119
1.0	-0.1	610.52	-3452.4	0.9197	-0.2968
1.0	0.05	667.71	1887.9	1.0059	0.1623
1.0	-0.05	635.12	-1795.8	0.9568	-0.1544
1.0	0.03	674.75	1144.7	1.0165	0.0984
1.0	-0.03	648.55	-1100.2	0.9770	-0.0946
1.0	0.01	671.81	379.90	1.0120	0.0327
1.0	-0.01	653.36	-369.47	0.9842	-0.0318
1.0	0.005	698.76	197.57	1.0526	0.0170
1.0	-0.005	663.12	-187.49	0.9989	-0.0161
1.0	0.003	698.60	118.52	1.0524	0.0102
1.0	-0.003	656.74	-111.41	0.9893	-0.0096
1.0	0.001	667.62	37.753	1.0057	0.0032
1.0	-0.001	660.69	-37.361	0.9953	-0.0032

BUCKLING LOADS AS PREDICTED BY WU PROGRAM

Tube No: Av. Size Laminate: [-82.5/30/20/-82.5] Material: Gr/E

Length (in): L = 20.041 Avg. Radius (in): R = 3.006 Thickness (in): t = 0.022

Max Torque: T* = 12234.0 Max Axial Load/cir.: P* = 637.68 Max Axial Load: $2\pi RP^*$ = 12044.02

Given Load Ratios		Predicted Buckling Loads		Buckling Ratios	
P	T	P(lbs/in)	T(in-lbs)	P/P*	T/T*
0.0	1.0	0.0	12234.0	0.0	1.0
0.0	-1.0	0.0	-13745.0	0.0	-1.1235
1.0	0.0	637.68	0.0	1.0	0.0
1.0	1.0	186.31	10578.0	0.2922	0.8646
1.0	-1.0	209.72	-11907.0	0.3289	-0.9733
1.0	0.75	236.91	10088.0	0.3715	0.8246
1.0	-0.75	267.64	-11396.0	0.4197	-0.9315
1.0	0.5	330.48	9381.5	0.5183	0.7668
1.0	-0.5	368.52	-10461.0	0.5779	-0.8551
1.0	0.35	424.18	8429.0	0.6652	0.6890
1.0	-0.35	482.72	-9592.2	0.7570	-0.7841
1.0	-0.25	515.56	-7317.8	0.8085	-0.5982
1.0	0.25	505.58	7176.1	0.7928	0.5866
1.0	0.1	623.65	3540.8	0.9780	0.2894
1.0	-0.1	573.18	-3254.3	0.8989	-0.2660
1.0	-0.05	591.79	-1680.0	0.9280	-0.1373
1.0	0.05	648.33	1840.5	1.0167	0.1504
1.0	0.03	628.33	1070.2	0.9853	0.0875
1.0	-0.03	610.28	-1039.5	0.9570	-0.0850
1.0	-0.01	653.20	-370.85	1.0243	-0.0303
1.0	0.01	622.33	353.33	0.9759	0.0289
1.0	0.005	620.33	176.10	0.9728	0.0144
1.0	-0.005	618.45	-175.56	0.9698	-0.0144
1.0	-0.003	633.06	-107.83	0.9928	-0.0088
1.0	0.003	623.19	106.15	0.9773	0.0087
1.0	0.001	586.74	33.312	0.9201	0.0027
1.0	-0.001	618.23	-35.100	0.9695	-0.0029

BUCKLING LOADS AS PREDICTED BY WU PROGRAM

Tube No: Av. Size Laminate: $[-45_2/45_2]_s$ Material: B/E

Length (in): L = 20.0 Avg. Radius (in): R = 2.997 Thickness (in): t = 0.038

Max Torque: T* = 15821.0 Max Axial Load/cir.: P* = 1439.3 Max Axial Load: $2\pi RP^*$ = 27103.04

Given Load Ratios		Predicted Buckling Loads		Buckling Ratios	
P	T	P(lbs/in)	T(in-lbs)	P/P*	T/T*
0.0	-1.0	0.0	-26646.0	0.0	-1.6842
0.0	1.0	0.0	15821.0	0.0	1.0
1.0	0.0	1439.3	0.0	1.0	0.0

BUCKLING LOADS AS PREDICTED BY WU PROGRAM

Tube No: Appx. Size Laminate: [-82.5/30/20/-82.5] Material: B/E

Length (in): L = 20.0 Avg. Radius (in): R = 2.997 Thickness (in): t = 0.021

Max Torque: T* = 7350.0 Max Axial Load/cir.: P* = 456.95 Max Axial Load: $2\pi RP^*$ = 8604.69

Given Load Ratios		Predicted Buckling Loads		Buckling Ratios	
P	T	P(lbs/in)	T(in-lbs)	P/P*	T/T*
0.0	-1.0	0.0	-13832.0	0.0	-1.8819
0.0	1.0	0.0	7350.0	0.0	1.0
1.0	0.0	456.95	0.0	1.0	0.0

DISTRIBUTION LIST

Professor Donald F. Adams
Dept. of Mechanical Engineering
University of Wyoming
Larmie, WY 82070

Dr. N. R. Adsit
General Dynamics Convair
P.O. Box 80837
San Diego, CA. 92138

Dr. Clifford J. Astill
Solid Mechanics Program
National Science Foundation
Washington, D. C. 20550

Dr. J. A. Bailie
D81-12, Bldg. 154
Lockheed Missiles & Space Co., Inc.
1111 Lockheed Way
Sunnyvale, CA. 94088

Mr. Henry W. Bergner, Jr.
The Boeing Company
Mail Stop 3001
P.O. Box 3707
Seattle, WA. 98124

Dr. Charles W. Bert, Director
School of Aerospace, Mechanical
& Nuclear Engineering
The University of Oklahoma
Norman, Oklahoma 73069

Mr. Richard Boitnott
ESM Dept.
VPI & SU
Blacksburg, VA. 24061

Dr. H. F. Brinson
ESM Dept.
VPI & SU
Blacksburg, VA. 24061

Dr. Michael F. Card
Mail Stop 190
NASA-Langley Research Center
Hampton, VA. 23665

Dr. Paul A. Cooper
Mail Stop 208
NASA-Langley Research Center
Hampton, VA. 23665

Dr. Frank Crossman
Lockheed Research Lab
Org. 52-41, Bldg. 204
3251 Hanover Street
Palo Alto, CA. 94034

Dr. I. M. Daniel, Manager
IIT Research Institute
10 West 35 Street
Chicago, IL. 60616

Dr. John R. Davidson
Mail Code 188E
MD-Structural Integrity Branch
Langley Research Center
Hampton, VA. 23665

Dr. John G. Davis, Jr.
Mail Code No. 188A
Langley Research Center
Hampton, VA. 23665

Mr. Jerry W. Deaton
Mail Stop 188A
NASA-Langley Research Center
Hampton, VA. 23665

Mr. H. Benson Dexter
Mail Stop 188A
NASA-Langley Research Center
Hampton, VA. 23665

Mr. O. Earl Dhonau
Section 2-53400
Vought Corp.
P.O. Box 5907
Dallas, TX. 75222

Dr. S. C. Dixon
Mail Stop 395
NASA-Langley Research Center
Hampton, VA. 23665

Dr. J. E. Duberg
Mail Stop 103
NASA-Langley Research Center
Hampton, VA. 23665

Dr. Wolf Elber
Mail Stop 188E
NASA-Langley Research Center
Hampton, VA. 23665

Mr. Gary L. Farley
Mail Stop 188A
NASA-Langley Research Center
Hampton, VA. 23665

Dr. R. L. Foye
USAMRDL
SAUDLAS (207-5)
Moffett Field, CA. 94035

Dr. D. Frederick
ESM Dept.
VPI & SU
Blacksburg, VA. 24061

Mr. Samuel P. Garbo
McDonnell Aircraft Co.
Bldg. 34, Post 350
St. Louis, MO. 63166

Mr. Ramon Garcia
Mail Stop 190, Bldg. 1148
NASA-Langley Research Center
Hampton, VA. 23665

Dr. Longin B. Greszczuk
McDonnell Douglass Astronautics Co.
5301 Bolas Avenue
Huntington Beach CA. 92647

Mr. Glen C. Grimes, Engr. Specialist
Structures R & T, Dept. 3780/62
Northrop Corp., Aircraft Div.
3901 W. Broadway
Hawthorne, CA 90250

Dr. H. T. Hahn
Nonmetallic Materials Div.
Air Force Materials Laboratory
Wright-Patterson Air Force Base
Ohio 45433

Dr. J. C. Halpin
Flight Dynamics Lab.
Wright-Patterson Air Force Base
OH. 45433

Professor S. Hashin
Metallurgical & Materials Science
Univ. of Pennsylvania
Philadelphia, PA. 19174

Dr. R. A. Heller
ESM Dept.
VPI & SU
Blacksburg, VA. 24061

Dr. E. G. Henneke
ESM Dept.
VPI & SU
Blacksburg, VA. 24061

Professor Phil Hodge
107 Aeronautical Engr. Bldg.
University of Minnesota
Minneapolis, MN 55455

Mr. Edward L. Hoffman
Mail Stop 188A
NASA-Langley Research Center
Hampton, VA. 23665

Dr. Peter W. Hsu
2195 Rockdell Dr., Apt. #6
Fairborn, OH. 45324

Mr. Edward A. Humphreys
McDonnell Douglas Astronautics
Co-East
P.O. Box 516
Bldg. 106, Level 3, Post D-7
St. Louis, MO. 63166

Dr. Donald E. Johnson
AVCO
Systems Division
Subsystems & Methodology Structures Dept.
201 Lowell Street
Wilmington, MA. 01887

Dr. Eric R. Johnson
116 Lake One Dr.
Hampton, VA. 23666

Dr. N. J. Johnson
Mail Stop 226
NASA-Langley Research Center
Hampton, VA. 23665

Dr. M. P. Kamat
ESM Dept.
VPI & SU
Blacksburg, VA. 24061

Dr. Keith T. Kedward
1768 Granite Hills Dr.
El Cajon, CA. 92021

Mr. John M. Kennedy
Mail Stop 188E
NASA-Langley Research Center
Hampton, VA. 23665

Mr. James F. Knauss
Section 253400, B. Jordan
Vought Corp.
P.O. Box 5907
Dallas, TX 75222

Mr. Ronald D. Kriz
Mail Stop 188B
NASA-Langley Research Center
Hampton, VA. 23665

Dr. S. V. Kulkarni
Materials Sciences Corporation
Blue Bell Office Campus
Blue Bell, PA. 19422

Dr. M. R. Louthan
Materials Engineering
VPI & SU
Blacksburg, VA. 24061

Mr. Larry R. Markham
Lockheed-California
Dept. 7572, Bldg. 63, Plant A1
P.O. Box 551
Burbank, CA. 91520

Mr. Vic Mazzio
General Electric Co.
P.O. Box 8555
Bldg. 100, Rm. M4018
Philadelphia, PA. 19101

Mr. Robert R. McWithey
Mail Stop 190
NASA-Langley Research Center
Hampton, VA. 23665

Mr. Martin M. Mikulas
Mail Stop 190
NASA-Langley Research Center
Hampton, VA. 23665

Mr. J. Steve Mills
Mail Stop 188A
NASA-Langley Research Center
Hampton, VA. 23665

Dr. D. H. Morris
ESM Dept.
VPI & SU
Blacksburg, VA. 24061

NASA Scientific and Technical
Information Facility
P.O. Box 8757
Baltimore/Washington International
Airport
Baltimore, MD. 21240

Newman Library - VPI & SU

Mr. David A. O'Brien OCUI-2, USNR
Section L - 78200
NOCS, NETC
Newport, R.I. 02840

Dr. Donald W. Oplinger
Army Materials & Mechanics Research
Center
Department of the Army
Watertown, MA. 02172

Dr. Nicholas J. Pagano
WPAFB/MBM
Wright Patterson Air Force Base
OH. 45433

Dr. Nicholas Perrone, Director
Structural Mechanics Program
Department of the Navy
Office of Naval Research
Arlington, VA. 22217

Mr. Marek Pindera
Mail Stop 188A
NASA-Langley Research Center
Hampton, VA. 23665

Dr. R. Byron Pipes
Dept. of Mechanical & Aerospace Engr.
107 Evans Hall
University of Delaware
Newark, DE. 19711

Dr. K. L. Reifsnider
ESM Dept.
VPI & SU
Blacksburg, VA. 24061

Dr. Gary D. Renieri
McDonnell Douglas Astronautics Co-East
P.O. Box 516
Bldg. 106, Level 4, Post C-5
St. Louis, MO. 63166

Dr. Michael P. Renieri
McDonnell Aircraft Co.
Bldg. 34, Post 350
St. Louis, MO. 63166

Dr. Larry Roderick
Langley Research Center
Mail Stop 188E
Hampton, VA. 23665

Dr. B. W. Rosen
Materials Science Corporation
Blue Bell Office Campus
Blue Bell, PA. 19422

Dr.Professor R. E. Rowlands
Dept. of Engineering Mechanics
University of Wisconsin
Madison, WI. 53706

Dr. Edmund F. Rybicki
Battelle
Columbus Laboratories
505 King Avenue
Columbus, OH. 43201

Dr. George P. Sendeckyj
Structures Division
Air Force Flight Dynamics Lab.
Wright-Patterson Air Force Base
OH. 45433

Mr. Mark J. Shuart
Mail Stop 188A
NASA-Langley Research Center
Hampton, VA. 23665

Dr. James H. Starnes, Jr.
Mail Stop 190
NASA-Langley Research Center
Hampton, VA. 23665

Dr. W. W. Stinchcomb
ESM Dept.
VPI & SU
Blacksburg, VA. 24061

Dr. Darrel R. Tenney
Mail Code 188M
MD-Materials Research Branch
Langley Research Center
Hampton, VA. 23665

Dr. S. W. Tsai
Nonmetallic Materials Division
Air Force Materials Laboratory
Wright-Patterson Air Force Base
OH. 45433

Dr. J. R. Vinson
6242 Urey Hall
Applied Mechanics & Science Dept.
University of California-San Diego
La Jolla, CA. 92037

Dr. J. R. Vinson
6242 Urey Hall
Applied Mechanics & Science Dept.
University of California-San Diego
La Jolla, CA. 92037

Mr. M. E. Waddoups
General Dynamic Corp.
Fort Worth, TX. 76101

Dr. T. A. Weisshaar
Aero & Ocean Engr. Dept.
VPI & SU
Blacksburg, VA. 24061

Dr. J. M. Whitney
Nonmetallic Materials Division
Air Force Materials Laboratory
Wright-Patterson Air Force Base
OH. 45433

Dr. Carl H. Zweben
Textile Fibers Dept.
E. I. DuPont de Nemours & Co., Inc.
Experimental Station/B262
Wilmington, DE. 19898

BIBLIOGRAPHIC DATA SHEET	1. Report No. VPI-E-78-14	2.	3. Recipient's Accession No.

4. Title and Subtitle
THEORETICAL-EXPERIMENTAL CORRELATION FOR BUCKLING OF COMPOSITE CYLINDERS UNDER COMBINED COMPRESSION AND TORSION

5. Report Date
July, 1978

6.

7. Author(s)
Carl T. Herakovich

8. Performing Organization Rept. No. VPI-E-78-14

9. Performing Organization Name and Address
Virginia Polytechnic Institute and State University
Engineering Science and Mechanics
Blacksburg, Virginia 24061

10. Project/Task/Work Unit No.

11. Contract/Grant No.
NASA NAS1-13175 Task 17

12. Sponsoring Organization Name and Address
National Aeronautics & Space Administration
Langley Research Center
Hampton, Virginia 23665

13. Type of Report & Period Covered

14.

15. Supplementary Notes

16. Abstracts
see page ii

17. Key Words and Document Analysis. 17a. Descriptors
composites, buckling, compression, torsion, graphite-epoxy, boron-epoxy

17b. Identifiers/Open-Ended Terms

17c. COSATI Field/Group

18. Availability Statement	19. Security Class (This Report)	21. No. of Pages
Distribution Unlimited	UNCLASSIFIED	
	20. Security Class (This Page) UNCLASSIFIED	22. Price

SECURITY CLASSIFICATION OF THIS PAGE (When Data Entered)

REPORT DOCUMENTATION PAGE		READ INSTRUCTIONS BEFORE COMPLETING FORM
1. REPORT NUMBER VPI-E-78-14	2. GOVT ACCESSION NO.	3. RECIPIENT'S CATALOG NUMBER
4. TITLE (and Subtitle) THEORETICAL-EXPERIMENTAL CORRELATION FOR BUCKLING OF COMPOSITE CYLINDERS UNDER COMBINED COMPRESSION AND TORSION		5. TYPE OF REPORT & PERIOD COVERED 6. PERFORMING ORG. REPORT NUMBER VPI-E-78-14
7. AUTHOR(s) Carl T. Herakovich		8. CONTRACT OR GRANT NUMBER(s) NASA NAS1-13175 Task 17
9. PERFORMING ORGANIZATION NAME AND ADDRESS Virginia Polytechnic Institute & State University Engineering Science & Mechanics Blacksburg, Virginia 24061		10. PROGRAM ELEMENT, PROJECT, TASK AREA & WORK UNIT NUMBERS
11. CONTROLLING OFFICE NAME AND ADDRESS National Aeronautics & Space Administration Langley Research Center Hampton, Virginia 23665		12. REPORT DATE July, 1978 13. NUMBER OF PAGES
14. MONITORING AGENCY NAME & ADDRESS(if different from Controlling Office) Virginia Polytechnic Institute & State University Engineering Science & Mechanics Blacksburg, Virginia 24061		15. SECURITY CLASS. (of this report) Unclassified 15a. DECLASSIFICATION/DOWNGRADING SCHEDULE

16. DISTRIBUTION STATEMENT (of this Report)

Approved for public release; distribution unlimited.

17. DISTRIBUTION STATEMENT (of the abstract entered in Block 20, if different from Report)

Approved for public release; distribution unlimited.

18. SUPPLEMENTARY NOTES

19. KEY WORDS (Continue on reverse side if necessary and identify by block number)

composites, buckling, compression, torsion, graphite-epoxy, boron-epoxy

20. ABSTRACT (Continue on reverse side if necessary and identify by block number)

see page ii

DD FORM 1 JAN 73 1473 EDITION OF 1 NOV 65 IS OBSOLETE

SECURITY CLASSIFICATION OF THIS PAGE (When Data Entered)